RHYTHM GENERATORS IN THE SEPTOHIPPOCAMPAL NETWORK AND THEIR ROLE IN HIPPOCAMPAL THETA RHYTHM

You Lim Huh

Department of Neurology and Neurosurgery
McGill University, Montréal

June, 2012

A thesis submitted to McGill University in partial fulfilment of the requirements of the degree of Doctor of Philosophy

Acknowledgements

First and foremost, I would like to thank my supervisor, Sylvain Williams, Ph.D., for all the genuine and incredibly generous support, understanding and patience he has shown me over the past eight years. Sylvain, I really appreciate how you never laughed at my naïve questions from day one and for all the advice and help you have given me over the years. I hope that I can count on more invaluable wisdom and guidance from you in the future. You have not only taught me the knowledge and skills of an electrophysiologist but also set an example for the type of scientist I hope to be someday: respectful, open-minded and always enthusiastic about new ideas and working with new people.

Secondly but equally as important, I would like to thank my boyfriend, John Peach, for his generous love, support and help over the years. Thank you, John, for teaching me to drive all over again in the rough streets of Montréal, inspiring me to scuba-dive, helping me grow as a person and sticking by my side through all the fun and difficult times. You must be the only boyfriend in the world that constructed a Faraday cage for his sweetheart, all from the initial engineering design to the final shiny product! I hope that someday I can be as good of a person you have been to me all these years and I look forward to sharing more amazing moments with you in the future.

Thirdly, I would like to thank my fellow Williams labmates, past and present. Thank you, Marc Danik, Ph.D., for showing me great warmth when I first arrived in Montréal, for instilling in me the idea that the lab should be kept 'clean', and for teaching me how to culture lonely neurons on microislands. I would also like to thank Germaine Lowe, Ph.D., who was not only a fellow graduate student and showed me the ropes at the beginning but remains to this day a great friend. Many thanks also go out to Frédéric Manseau, Ph.D., for all his advice and help with electrophysiology and for writing the French abstract of this Thesis. Thank you so much, Bénédicte Amilhon, Ph.D., for the second project of my Ph.D.

would not have been possible without your help with animal colonies, transgenic mice characterizations, optogenetic techniques among other things that are too numerous to mention here. I am also thankful to Stephanie Scodras for the anatomical characterization of the mice. I would also like to thank Romain Goutagny, Ph.D., and Jesse Jackson for their seminal work upon which my second project is based and for all their help and advice on Matlab, analyses and science in general. Special thanks go out to the rest of the Team Williams, including Guillaume Ducharme, Ning Gu, Ph.D., Jennifer Robinson, Richard Boyce, Siddhartha Mondragon, Ph.D., Lina Marsan and Youssouf Cisse, Ph.D. for the fruitful discussions and fun times we have shared together. Also thanks everyone for putting up with my 'clean' notes.

Fourthly, I would like to thank my Ph.D. committee members, Tak Pan Wong, Ph.D. and Salah El Mestikawy, Ph.D., and my mentor Naguib Mechawar, Ph.D. Your honest input and helpful advice have shaped the progress of my projects and have informed the journey I have taken as a graduate student. Thanks for writing me the reference letters, Tak Pan and Naguib! I would also like to thank Edward Ruthazer, Ph.D. at the MNI, for the neuroplasticity course that he taught, which helped inspire me to go explore the potential of adult neuroplasticity during my postdoc. As well, I would like to send sincere thanks to Robert Hess, Ph.D. at the McGill Vision Research Unit and his team for giving me the opportunity to get involved in their research and learn a great deal about amblyopia. Thank you, Drs. Mullen and Kingdom also at McGill Vision Research, for letting me audit the visual perception course.

Fifthly, I would also like to thank my collaborators, past and present. Thanks so much, Katie A. Ferguson at the University of Toronto, for helping me with a tricky part of Matlab analyses for the interneuron project. I would also like to thank her supervisor, Frances K. Skinner, Ph.D. for the opportunity to collaborate. Special thanks also go out to Louis-Eric Trudeau, Ph.D. at Université de Montréal for his always insightful advice and his team for sharing culture

protocols and lending me equipment and mice when I needed them. Thank you, Antoine Adamantidis, Ph.D. and his team for the advice and know-how for the optogenetic project. I would like to mention special thanks to the Wong lab for sharing lab protocols, equipments and reagents. I would also like to acknowledge the support of the colleagues and friends here at the Douglas, whom I have had the good fortune to share many interesting discussions and laughs with, both in and out of the lab, including Melissa Burt, Leora Yetnikoff, Ph.D., Julio Morales, Ph.D., Argel Aguilar, Ph.D., Wataru Inoue, Ph.D., Chung Tse, Ph.D., Gaby (Susana) Torres-Platas, Gregory Dal Bo, Ph.D., Caroline Fasano, Ph.D. and Suna Jung, among many others. I would also like to thank dear friends at Montréal Korean Language and Culture Club, for the unforgettable events and workshops that I have had the amazing opportunity to help organize and take part in.

Big thanks also go out to Natural Sciences and Engineering Research Council of Canada (NSERC) for the generous financial support during my doctoral studies. Also, I would like to thank the Douglas Institute, the Integrated Program in Neuroscience (IPN) and McGill University for honouring me with various awards and recognitions over the years.

Last but not least, I would like to thank my family. I want to express the deep gratitude I feel for my parents by dedicating this Thesis to them. Thank you, Mom (Mee Yun Ham) and Dad (Bong Sam Huh), for your unconditional love and support. Knowing that you believe in me and that you are always rooting for me gives me strength. I would like to thank my brother (Jung Lim), my sister-in-law (Ji Yun) and my brand-new niece (Ju Eun) for the love and support. I would also like to thank my big uncle (Yong Sam Huh), the rest of the extended family in Korea as well as my relatives in Canada, USA and Australia for all their constant support and encouragements. I would like to express special thanks to my grandparents who passed away in recent years and my maternal grandmother in Washington D.C., for always keeping me in their thoughts, hearts and prayers.

Table of contents

Abstract

Hippocampal theta rhythm is an oscillatory activity in the range of 3 – 12 Hz, prominently observed in hippocampal extracellular field recordings *in vivo*. Hippocampal theta rhythm has been closely associated with episodic memory and spatial learning in both humans and animals. Here, I describe two research projects I carried out in the course of my Ph.D., exploring several different types of neurons that could serve as potential rhythm generators for hippocampal theta rhythm. The medial septum and diagonal band of Broca (MS-DBB) has long been known to provide crucial inputs for the generation of hippocampal theta rhythm *in vivo*. The 'septohippocampal network' thus refers to the hippocampal formation, the MS-DBB and the connections between the two structures. While there has been many studies investigating the contributions of cholinergic and GABAergic MS-DBB neurons, the role of the recently described glutamatergic MS-DBB neurons in the septohippocampal network and theta rhythm generation remains unknown. In order to address this issue, for my first project, I investigated the electrophysiological properties of the glutamatergic MS-DBB neurons and examined their functional role in the septohippocampal network. Recently, a study using a complete hippocampal preparation *in vitro* demonstrated that the CA1 region of the hippocampal formation can generate its own theta oscillations independently of external inputs. It is unknown which CA1 interneuron subtype plays a key role in generating this intrinsic CA1 theta rhythm. During *in vivo* theta rhythm, parvalbumin (PV)- and somatostatin (SOM)-expressing interneurons fire strongly phase-locked to field theta rhythm, indicating that they may be good candidates for potential theta rhythm generators. Thus, for my second project, I explored the intrinsic properties of PV and SOM interneurons and examined their cellular behaviour during *in vitro* CA1 theta rhythm. Furthermore, I investigated the causal role of these interneurons in CA1 field theta oscillations using optogenetic silencing methods. Results from the first project illustrate that in addition to the well-known cholinergic and GABAergic septohippocampal pathway, the glutamatergic MS-DBB neurons provide a functional excitatory synaptic input to hippocampal neurons that may contribute to theta rhythm generation and synchronization across the septohippocampal network. Results from the second project demonstrate that both synaptic and intrinsic factors determine the interneurons' firing patterns during theta rhythm and that PV interneurons, with their highly synchronous and powerful inhibitory outputs onto pyramidal cells, appear to play an important role in generating the field theta signal. These findings provide new information about the potential role of several different neuronal classes in the septohippocampal network in relation to theta rhythm generation. It is my hope that a greater understanding of this matter will bring new insights into the mechanisms with which neural oscillations contribute to essential operations of the brain such as learning and memory.

Résumé

Le rythme thêta de l'hippocampe est une activité neuronale oscillatoire dans la gamme de 3 - 12 hertz, pouvant être primordialement observée durant les enregistrements extracellulaires de champ hippocampal *in vivo*. Le rythme thêta hippocampal a été étroitement associé à la mémoire épisodique et à l'exploration spatiale chez les humains et les animaux. Dans cette thèse, je décris deux projets de recherche mis à exécution au cours de mon Ph.D. et explorant différents types de neurones qui pourraient potentiellement servir de générateurs pour les rythmes thêta de l'hippocampe. Le septum médian et la bande diagonale de Broca (MS-DBB) ont été longtemps reconnus comme les zones principales fournissant les entrées cruciales pour la génération du rythme thêta de l'hippocampe *in vivo*. Le « réseau septohippocampal » se rapporte ainsi à la formation hippocampale, au MS-DBB et aux raccordements entre les deux structures. Bien qu'un grand nombre d'études ait déjà exploré la contribution des neurones cholinergiques et GABAergic du MS-DBB dans le réseau septohippocampal et dans la génération des rythmes thêta, le rôle d'une population de neurones glutamatergiques nouvellement découverte au niveau du MS-DBB, reste pour l'instant inconnu. Afin d'aborder cette question, pour mon premier projet, j'ai étudié les propriétés électrophysiologiques des neurones glutamatergiques du MS-DBB et j'ai examiné leur rôle fonctionnel dans le réseau septohippocampal. Récemment, une étude utilisant une préparation hippocampale complète *in vitro* a par ailleurs démontré que la région CA1 de la formation hippocampale peut produire ses propres oscillations thêta, indépendamment des entrées externes. L'identité des sous-types d'interneurones qui sont impliquées dans la production de ce rythme thêta intrinsèque à CA1 est pour l'instant inconnue. Pendant le rythme thêta *in vivo*, les interneurones qui expriment la parvalbumin (PV) - ou la somatostatin (SOM) - déchargent fortement et à phase-verrouillé sur le rythme extracellulaire, indiquant qu'elles pourraient être de bons candidats de générateurs pour le rythme thêta. Ainsi, pour mon deuxième projet, j'ai exploré les propriétés intrinsèques des interneurones PV et SOM et j'ai examiné leur comportement cellulaire au cours du rythme thêta enregistré *in vitro* dans la région CA1. En outre, j'ai examiné le rôle causal de ces interneurones dans la thêta de champ en utilisant des méthodes optogénétiques pour contrôler l'activité neuronale. Les résultats du premier projet illustrent qu'en plus des voies septohippocampales cholinergiques et GABAergiques bien connues, les neurones glutamatergiques du MS-DBB fournissent une entrée synaptique excitatrice fonctionnelle aux neurones de l'hippocampe. Ces neurones pourraient ainsi contribuer à la génération et à la synchronisation des rythmes thêta à travers le réseau septohippocampal. Les résultats du deuxième projet démontrent; 1) que plusieurs facteurs synaptiques et intrinsèques déterminent les modes de mise à feu des interneurones pendant le rythme thêta et ; 2) que les interneurones PV, avec leurs sorties inhibitrices

fortement synchrones et puissantes sur les cellules pyramidales, semblent jouer un rôle prépondérant dans le contrôle du signal thêta de champ. Ces résultats fournissent de nouvelles informations au sujet du rôle potentiel de différentes classes neuronales du réseau septohippocampal par rapport à la génération du rythme thêta. J'ai grand espoir que ces travaux mèneront à une meilleure compréhension des mécanismes avec lesquels les oscillations neurales contribuent aux opérations essentielles du cerveau telles que l'apprentissage et la mémoire.

List of figures

List of tables

Chapter I: Introduction

I.1. Role of the septohippocampal network in learning and memory

1.1. The hippocampal formation

Ever since Scoville and Milner (1957) described the famous case of the epileptic patient H.M., who underwent a bilateral resection of the medial temporal lobe (MTL) and subsequently developed amnesia, much research has been done to better understand the role of this brain area in memory. While H.M. was severely impaired in forming new episodic memories (anterograde amnesia), his ability to recall distant events that occurred prior to the surgery was largely spared (relative lack of retrograde amnesia), as were implicit forms of learning (*e.g.*, motor learning and perceptual priming) (Corkin, 1968; Milner et al., 1968). These studies supported the notion that there are multiple, physiologically separate memory systems in the brain. Careful lesion studies in animals have since confirmed that the MTL, especially the hippocampal formation, is indeed crucial for the generation of declarative memory that is relational and context-dependent (*e.g.*, episodic and spatial memory) in the rat (Morris et al., 1982) and the monkey (Zola-Morgan et al., 1989).

The role of the hippocampus in the long-term storage of these memories, however, remains more contentious. It was initially observed in H.M. and other patients with hippocampal lesions that some retrograde amnesia was present for memories proximal to the time of the surgery (Scoville and Milner, 1957). Animal lesion studies have also demonstrated that retrograde amnesia due to hippocampal damage is temporally graded such that the memory loss is greater for recent memories and less for remote ones (Zola-Morgan and Squire, 1990; Kim and Fanselow, 1992). Thus, it has been suggested that the hippocampus-dependent consolidation process takes place gradually, so that recent memories that have not had the time to completely consolidate at the time of hippocampal damage is lost.

What happens to memories as they are consolidated? Memory consolidation can be conceptualized both at the cellular level and at the systems level. The cellular process refers to functional and structural changes made at the level of the synapses. Through systems-level consolidation, memories are thought to be converted from a more labile, hippocampus-dependent form into a more permanent form that is stored in distributed neocortical networks, a process that can take days, weeks or even months (Squire and Alvarez, 1995). However, an observation that the already consolidated memory trace can be reactivated and turned back into a hippocampus-dependent form (Debiec and LeDoux, 2002) has challenged the notion that the hippocampus has a time-limited role in the consolidation process (Winocur et al., 2010). Therefore, the hippocampus plays an essential role for the formation of certain type of memories such as episodic and spatial memory and it may have additional roles in the consolidation, storage and recall of these memories.

How does the hippocampus perform these functions? Anatomically, the hippocampus is intricately connected via intrinsic connections as well as extrinsic connections with both cortical and subcortical regions. For clarity and unity, I would like to define the limits of the 'hippocampal formation' here by including the hippocampus proper (CA1, CA2, CA3), the dentate gyrus (DG) and the subiculum, following a previous convention (Van Strien et al., 2009). Though overly simplified, the well-known trisynaptic circuit describes the information flow through the hippocampal formation in terms of three major excitatory synapses, from the entorhinal cortex to DG via the perforant pathway, from DG to CA3 via mossy fibers, and from CA3 to CA1 via Schaffer collaterals. However, in actuality all sub-structures of the hippocampal formation receive direct inputs from the entorhinal cortex, which serves as a gateway through which most neocortical inputs arrive at the hippocampal formation (Steward and Scoville, 1976; Witter et al., 2006), although direct monosynaptic connections from some cortical areas to the hippocampal formation have also been noted (Naber et al.,

2001). Cortical inputs to the entorhinal cortex arise from several areas of the cortex, including the piriform cortex (olfactory), the perirhinal and postrhinal cortices (multisensory), the insular cortex, the medial prefrontal region, the anterior cingulate and retrosplenial cortices (multisensory, associational areas) (Burwell and Amaral, 1998a, 1998b). As for subcortical afferents, the hippocampal formation receives direct inputs from the medial septum, the amygdala, parts of the hypothalamus and the thalamus as well as midbrain inputs from the ventral tegmental area (dopaminergic), raphe nuclei (serotonergic) and locus coeruleus (noradrenergic) (Herkenham, 1978; Moore et al., 1978; Swanson and Cowan, 1979; Wyss et al., 1979; Maglóczky et al., 1994; Pikkarainen et al., 1999). While cortical inputs are thought to carry sensory and cognitive information, subcortical inputs likely convey information about the emotional, motivational and arousal state of the animal. Some of the above-mentioned cortical and subcortical areas receive inputs back from the hippocampal formation, thus the outcome of hippocampal information processing is thought to be projected back, closing the loop. The major output structures of the hippocampal formation are the CA1 and subiculum (Swanson and Cowan, 1975, 1977; Swanson et al., 1981). It is hypothesized that the information flowing through these extensive connections both within the hippocampal formation and with other brain structures underlies how episodic and spatial memories are formed, stored and updated.

1.2. The septohippocampal network

Among many subcortical structures that send projections to the hippocampal formation, the best studied is the medial septum and diagonal band of Broca (MS-DBB). Thus, the 'septohippocampal network' refers to the hippocampal formation, the MS-DBB and the fiber system that connects the two

structures, the fimbria-fornix. Shaped like an inverted Y, the MS-DBB is situated in the medial and caudal part of the septal area. The septal area refers to an anterior and medial part of the basal forebrain. In rodents, the septal area is divided into four sub-regions: the MS-DBB, lateral septum, posterior septum and bed nuclei of the stria terminalis.

Since the claim that cholinergic basal forebrain neurons are selectively degenerated in Alzheimer's disease (AD) (Bartus et al., 1982; Coyle et al., 1983; McGeer et al., 1984; Whitehouse, 1998), the MS-DBB and its functions have been intensively investigated. As part of the basal forebrain, the MS-DBB serves as the sole provider of cholinergic input to the hippocampal formation, whereas the cortex is innervated by cholinergic fibers from other basal forebrain areas, including parts of the DBB, preoptic nuclei, substantia innominata and globus pallidus, collectively referred to as the nucleus basalis magnocellularis (Bigl et al., 1982; Mesulam et al., 1983). In AD patients, levels of cholinergic markers such as choline acetyltransferase (ChAT) are dramatically reduced in the hippocampus, cortex and the MS-DBB, compared to age-matched controls (Bowen et al., 1976; Perry et al., 1977; Henke and Lang, 1983). In animal models of AD, intraseptal injections of beta-amyloid (Aβ) peptide damage mostly cholinergic neurons with minor effects on GABAergic neurons (Harkany et al., 1995). Intraventricular Aβ injections were also found to cause reductions in ChAT activity in the MS-DBB, cortex and the hippocampus and lead to deficits in spatial learning (Yamaguchi and Kawashima, 2001). Therefore, much emphasis has been placed on trying to understand how the MS-DBB, particularly the septohippocampal cholinergic neurons, affect hippocampus-related functions.

It is well established that MS-DBB lesions cause impairments in Morris water maze, radial arm maze and other hippocampus-mediated spatial learning tasks (Winson, 1978; Mitchell et al., 1982; Hagan et al., 1988; Kelsey and Vargas, 1993; McAlonan et al., 1995). The dominant thinking in the field for decades has been that the MS-DBB contributes to hippocampal function by providing the

pacemaker input necessary to generate the hippocampal theta rhythm (Petsche et al., 1962; Stewart and Fox, 1990). Theta rhythm is thought to represent the on-line state of the hippocampus (Buzsaki, 2002). The belief that the MS-DBB acts as the theta rhythm generator stems from a large body of evidence showing that septal or fimbria-fornix lesions virtually abolish hippocampal theta rhythm (Green and Arduini, 1954; Winson, 1978; Rawlins et al., 1979; Mitchell et al., 1982). However, this long-standing view of the MS-DBB as the pacemaker requires re-examination in light of the recent evidence that the hippocampal formation is able to generate its own theta rhythm, albeit with a smaller amplitude (Goutagny et al., 2009). Thus, the role of the MS-DBB may be to modulate and amplify hippocampal theta rhythm rather than to generate it. It is clear that the MS-DBB plays an important role in hippocampus-related functions, but the mechanisms of its action and its exact role in hippocampal theta rhythm generation remain to be clarified.

In terms of connectivity, the MS-DBB has robust intrinsic connections as well as extrinsic connections with numerous other brain areas. The MS-DBB receives inputs from the hippocampal formation, the entorhinal cortex, several hypothalamic and thalamic nuclei, some midbrain structures and the lateral septum (Swanson and Cowan, 1979; Alonso and Köhler, 1982, 1984; Vertes, 1992; Vertes et al., 1995). Conversely, the MS-DBB provides inputs to the hippocampal formation, the entorhinal cortex, the olfactory bulb, some hypothalamic and thalamic nuclei, as well as parts of the midbrain such as the ventral tegmental area and raphe nuclei (Meibach and Siegel, 1977; Swanson and Cowan, 1979; Alonso and Köhler, 1984; Gaykema et al., 1990).

I.2. Role of theta rhythm in learning and memory

2.1. Hippocampal theta rhythm

Hippocampal theta rhythm is an oscillatory activity in the range of 3 – 12 Hz, prominently observed in hippocampal extracellular field recordings *in vivo* (Green and Arduini, 1954). It reflects synchronous oscillations in the somatodendritic membrane of principal cells, produced by transmembrane currents due to afferent synaptic inputs as well as intrinsic ionic conductances of neurons (Buzsaki, 2002). Hippocampal theta rhythm occurs during specific behaviours and states of consciousness, and it has been associated with an extensive list of behaviours and functions: arousal, attention, exploratory behaviour, voluntary motor control, spatial learning and memory, REM sleep and sensory motor integration. Green and Arduini (1954) reported that when a resting, unanesthetized rabbit or cat shifts from a drowsy state to an alert state due to sensory stimulation (*e.g.*, a tail pinch), field recordings in the hippocampus show the occurrence of large-amplitude oscillations in the theta frequency band. Hippocampal theta activity has been categorized into two types according to behavioural and pharmacological criteria (Kramis et al., 1975). Type 1 theta (peak frequency of 6 – 10 Hz) is observed when an animal is engaged in active, exploratory movements and is resistant to high doses of atropine, a muscarinic cholinergic receptor antagonist. Type 2 theta (peak frequency of 4 – 6 Hz) is present during immobility, urethane anaesthesia and movements and is abolished by atropine, thus it is thought to be mediated by muscarinic activity. Type 1 theta can vary systematically with parameters of voluntary movement such as speed and magnitude of movement (Vanderwolf, 1969).

The potential role of hippocampal theta rhythm in memory and learning has been particularly well studied. In humans, increased hippocampal theta power

is associated with spatial navigation and working memory tasks in EEG and MEG studies (Kahana et al., 1999; Tesche and Karhu, 2000; Cornwell et al., 2008). Enhanced hippocampal theta power during the encoding phase of a word recognition task has been shown to predict later successful recall of the items (Fell et al., 2011). The strength of human memory has also been linked with the extent of phase-locking shown by single hippocampal neurons to network theta oscillations (Rutishauser et al., 2010). In animals, manipulations that drastically reduce the power of hippocampal theta such as MS-DBB lesion or inactivation have been shown to severely impair spatial learning (Winson, 1978; Mizumori et al., 1989). It is thought that the mechanism with which theta rhythm contributes to mnemonic processes is by facilitating synaptic plasticity. Electrophysiological studies have demonstrated that bursts of high-frequency electrical stimulation given to the Schaffer collateral pathway on the positive phase (peak) of ongoing theta rhythm induce long-term potentiation (LTP) of the relevant synapses, while bursts given on the negative phase (trough) of theta lead to de-potentiation of previously established LTP *in vivo* and *in vitro* (Huerta and Lisman, 1993, 1995; Hölscher et al., 1997). Thus, it may be that theta oscillations act as a powerful regulator of synaptic plasticity, providing the neural network with alternating states of excitation and inhibition whereby synaptic weights can be properly adjusted and updated.

Furthermore, evidence suggests that theta rhythm may also provide a temporal framework along which spatial information can be represented. Recordings in freely moving rats have revealed that information about the animal's location in space is encoded in single-unit activities of hippocampal cells. Pyramidal cells ('place cells') display a sharp increase in firing rate as the animal moves through a certain location in a given environment (the cell's 'place field') (O'Keefe and Dostrovsky, 1971). Place fields develop quickly within minutes of exploring the environment (Bostock et al., 1991) and they can remain stable for long periods of time (weeks - months) upon repeated testing in the same

environment (Muller and Kubie, 1987; Thompson and Best, 1990). As an animal moves through a place field, the corresponding place cell fires at progressively earlier phases of ongoing theta in a phenomenon known as 'phase precession', and the phase advancement can be as great as a full theta cycle (O'Keefe and Recce, 1993). While theta rhythm reflects the dominant synaptic currents and membrane oscillations of the majority of cells in the network, phase precession arises due to the most strongly activated few being driven to fire faster than the network rhythm (Harvey et al., 2009). It is hypothesized that phase precession can promote place cells with overlapping, neighbouring place fields to fire closer together in time, providing a mechanism for spatiotemporal binding of cell assemblies (O'Keefe and Recce, 1993; Skaggs et al., 1996). Thus, spatial information may be represented not only in the firing rate of the cell (rate code) but also in the timing of the spikes in relation to the theta oscillation (phase code).

Then, is theta rhythm required for encoding of spatial information? Evidence indicates that significantly reducing hippocampal theta via MS-DBB inactivation does not abolish CA1 place cell activity and the formation of place fields *per se* (Mizumori et al., 1989; Koenig et al., 2011). However, under theta rhythm reduction, place cell firing becomes much slower and it is likely that proper synchronization of place cell activity and appropriate formation of cell assemblies do not occur without normal hippocampal theta, although this needs to be tested directly (Leutgeb and Mizumori, 1999). For spatial information, more accurate information may be encoded if place cell activity is organized into cell assemblies, compared to representation by rate code alone (Harris et al., 2003) Interestingly, place field stabilization and maintenance, but not initial formation, depend on long-term synaptic plasticity mechanisms (McHugh et al., 1996; Rotenberg et al., 1996; Kentros et al., 1998; Nakazawa et al., 2003). Disrupting synaptic plasticity, much like inhibiting theta rhythm, leads to impairments in hippocampus-dependent learning and memory (Morris, 1989; Nakazawa et al., 2003).

Therefore, theta rhythm may represent the optimal mode of operation for the hippocampal formation. It may enable proper encoding of spatial and episodic information by hippocampal neurons. Theta rhythm may also aid long-term storage of memories via its facilitative effects on synaptic plasticity. Finally, synchronized theta oscillations may provide a mechanism with which nearby and distant neural circuits can become functionally coupled, allowing information transfer and systems-level consolidation to occur. Given the importance of theta rhythm for hippocampal functions, it is perhaps not surprising that some neurological disorders with hippocampal deficits, such as AD and schizophrenia, are also characterized by abnormalities in neural oscillations and synchrony (Montez et al., 2009; Uhlhaas and Singer, 2010).

2.2. Septohippocampal circuitry

For many years, the MS-DBB was known to contain only two neuronal populations: neurons that release acetylcholine and those that release gamma-aminobutyric acid (GABA). Cholinergic MS-DBB neurons have relatively large cell bodies (diameter of ~22 μm in the rat) and are located mostly in the DBB and the lateral region of the medial septum (Kimura et al., 1980; Brashear et al., 1986; Brauer et al., 1999). GABAergic neurons of the MS-DBB have small- to medium-sized somata (10 - 20 μm), located close to the midline of the MS-DBB (Panula et al., 1984; Onteniente et al., 1987) and they express both isoforms of glutamic acid decarboxylase, GAD65 and GAD67 (Castañeda et al., 2005). Distinct populations of GABAergic MS-DBB neurons contain different calcium-binding proteins including parvalbumin (PV) (Kiss et al., 1997) and some evidence suggests that PV may be preferentially expressed by GABAergic MS-DBB neurons that project to the hippocampus (Freund, 1989).

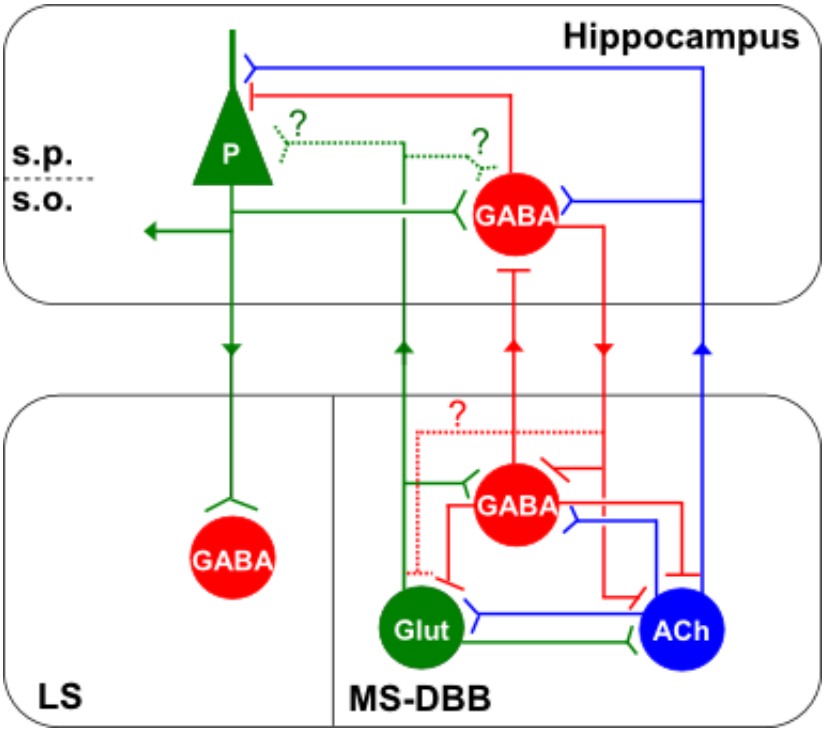

Figure 1. Schematic of the septohippocampal circuitry. GABAergic MS-DBB neurons specifically target inhibitory interneurons in the hippocampus while cholinergic MS-DBB neurons innervate both pyramidal cells and interneurons. Conversely, hippocampal inhibitory neurons with septal projections innervate both cholinergic and GABAergic MS-DBB neurons. Pyramidal cells seldom send projections to the MS-DBB but heavily innervate the lateral septum. Glutamatergic septohippocampal neurons have also been described but it remains unknown which hippocampal cell types they target and whether they receive any input from the hippocampus. Within the MS-DBB, there are mutual connections among the three neuronal types.

However, there has been mounting evidence for the presence of glutamatergic neurons in the MS-DBB. First, retrograde labelling and immunohistochemical studies reported the presence of a population of basal forebrain neurons, some of which project to the cortex or hippocampus, that could not be identified with either cholinergic or GABAergic markers (Gritti et al., 1997; Kiss et al., 1997). Secondly, MS-DBB neurons were labelled with glutamate, phosphate-activated glutaminase (PAG, an enzyme for synthesizing glutamate) and [^{3}H]aspartate, indirect indicators of glutamate being used as a neurotransmitter (Gonzalo-Ruiz and Morte, 2000; Manns et al., 2001, 2003; Kiss et al., 2002; Gritti et al., 2006). Thirdly, a single-cell reverse transcriptase polymerase chain reaction (sc-RT-PCR) analysis showed that a significant proportion (about 27%) of MS-DBB neurons expressed messenger ribonucleic acids (mRNAs) for vesicular glutamate transporters type 1 and/or 2 (VGLUT1/2) (Danik et al., 2003, 2005; Sotty et al., 2003). The VGLUT markers have been demonstrated to reliably indicate a cell's capacity to use glutamate as a neurotransmitter (Herzog et al., 2001; Moriyama and Yamamoto, 2004). Sotty and colleagues (2003) further showed that a proportion of these VGLUT1/2-positive MS-DBB cells project to the hippocampus, as they were labelled with a retrograde tracer injected into the hippocampus. Consistent with this, other groups have also reported the expression of mRNAs for VGLUT2 transcripts in the MS-DBB (Hisano et al., 2000; Fremeau et al., 2001; Lin et al., 2003) and VGLUT2 proteins in the cell bodies of some MS-DBB neurons after treatment with colchicine, an axonal transport blocker (Lin et al., 2003; Hajszan et al., 2004). Colom and colleagues (2005) revealed that out of all MS-DBB neurons labelled with ChAT, GAD or glutamate antibodies, 25% were positive for glutamate, an estimate consistent with that reported by Sotty et al. (27%). Glutamatergic MS-DBB neurons are mostly small- to medium-sized neurons (5 - 21 μm), concentrated in the MS-DBB but also present in the lateral septum at a lower

density (Colom et al., 2005). Putatively glutamatergic MS-DBB neurons have been found to express calcium-binding proteins such as calretinin and calbindin (Gritti et al., 2003). Colom and colleagues estimated that glutamatergic MS-DBB neurons provide 23% of the septohippocampal projection, but a recent study by Henderson et al. using VGLUT2-eGFP transgenic mice gave a much lower estimate of 4% (Colom et al., 2005; Henderson et al., 2010). Variability in the estimates given by these studies may be due to differences in the species (rat *vs.* mouse) and experimental procedures used. Taken together, there is sufficient evidence for the idea that a sizable portion of MS-DBB neurons are glutamatergic and that some of these neurons send projections to the hippocampus.

Within the MS-DBB, there are numerous mutual connections among cholinergic, GABAergic and glutamatergic neurons. GAD-positive terminals have been found to innervate ChAT-positive dendrites in the MS-DBB and conversely, ChAT-positive terminals make synaptic contacts on GAD-expressing cell bodies and proximal dendrites (Leranth and Frotscher, 1989). VGLUT2-postive puncta have been found in close proximity to ChAT-, GAD67-, PV- and VGLUT2-positive neurons in the MS-DBB (Hajszan et al., 2004; Manseau et al., 2005). In turn, ChAT- and GAD67-positive puncta have also been found close to VGLUT2/glutamate-positive neurons (Colom et al., 2005). Recent electrophysiological studies provided evidence that local synapses made by these glutamatergic neurons are indeed functional and that they play a role in the MS-DBB network activity. Wu and colleagues (2003) found that rapid excitatory effects of nicotine on septohippocampal GABAergic neurons require the action of endogenously released glutamate on group 1 metabotropic glutamate receptors. Manseau and colleagues (2005) showed that disinhibited glutamatergic MS-DBB neurons can provide spontaneous, large-amplitude excitatory postsynaptic potentials (EPSPs) to electrophysiologically identified putatively cholinergic, GABAergic and glutamatergic MS-DBB neurons, demonstrating that the glutamatergic neurons form a functional network within the MS-DBB. They

further determined using organotypic cultures of MS-DBB mini-slices, that the glutamatergic EPSPs originated from within the MS-DBB. Therefore, an extensive, mutual and functional synaptic network exists among cholinergic, GABAergic and glutamatergic neuronal populations within the MS-DBB.

The MS-DBB and the hippocampus are reciprocally linked via the fimbria-fornix fibers. Afferents from the MS-DBB are found in all subregions and layers of the hippocampus with the strongest innervation in CA3, DG, subiculum and a weaker innervation to CA1 (Swanson and Cowan, 1979). Conversely, the MS-DBB receives afferent inputs from CA1, CA3, DG and subiculum (Tóth and Freund, 1992; Toth et al., 1993). As shown in the schematic in **Figure 1**, GABAergic MS-DBB neurons specifically target inhibitory interneurons in CA1 and CA3, mostly located in stratum oriens and pyramidale (Freund and Antal, 1988) whereas cholinergic MS-DBB neurons innervate both principal cells and interneurons (Frotscher and Leranth, 1985; Frotscher et al., 1992). Conversely, septally-projecting hippocampal inhibitory neurons target both cholinergic and GABAergic MS-DBB neurons, and pyramidal cells seldom send projections to the MS-DBB but heavily innervate the lateral septum (Toth et al., 1993; Linke et al., 1995). As described above, glutamatergic MS-DBB neurons have also been described to send projections to the hippocampus (Sotty et al., 2003; Colom et al., 2005; Henderson et al., 2010). A preliminary report showed that numerous VGLUT2-positive septohippocampal puncta are found in close apposition with the soma and proximal dendrites of CA1 and CA3 pyramidal cells and interneurons (Hernandez et al., 2009). However, it remains unknown which specific hippocampal cell types they target and whether they receive any input back from the hippocampus.

2.3. Rhythm generators in the MS-DBB

The neural pathway that gives rise to hippocampal theta rhythm, known as the 'ascending brainstem hippocampal synchronizing pathway', includes the brainstem rostral pontine region, the supramammillary and posterior hypothalamic nuclei and the MS-DBB (Bland and Colom, 1993). Apart from the well-known effect of septal or fimbria-fornix lesions on hippocampal theta rhythm (Green and Arduini, 1954; Winson, 1978; Rawlins et al., 1979; Mitchell et al., 1982), additional evidence in support of the MS-DBB as the theta pacemaker came from observations that MS-DBB neurons fire in theta-band rhythmic bursts, tightly synchronized to field hippocampal theta (Petsche et al., 1962; Gogolak et al., 1968). However, neurons that burst rhythmically in synchrony with hippocampal theta have also been found in some hypothalamic nuclei (Kocsis and Vertes, 1994; Bland et al., 1995), alluding to the possibility that there may be multiple rhythm generators contributing to hippocampal theta rhythm. The large body of evidence available from the lesion studies, however, supports the notion that the integrity of MS-DBB is a necessary prerequisite for the occurrence of normal *in vivo* hippocampal theta rhythm.

Since glutamatergic MS-DBB neurons have only recently been discovered, most studies have focused on the role of cholinergic and GABAergic MS-DBB neurons in hippocampal theta rhythm. Selective lesions of cholinergic neurons of the MS-DBB using 192-IgG-saporin, an immunotoxin specific to cholinergic cells of the basal forebrain, have been shown to cause dose-dependent reductions in the amplitude, but not the frequency, of hippocampal theta *in vivo* (Lee et al., 1994; Bassant et al., 1995; Gerashchenko et al., 2001). In a study by Yoder and Pang (2005), cholinergic and GABAergic neurons of the MS-DBB were specifically lesioned by local injections of 192-IgG-saporin and kainate, respectively, and they found that Type 1 theta was only attenuated but not eliminated by either lesion. These findings indicate that damages to either

cholinergic or GABAergic MS-DBB neurons alone are not sufficient to eliminate hippocampal theta rhythm.

In vivo recordings of MS-DBB neurons reported that GABAergic MS-DBB neurons fire tonically or in bursts that are strongly phase-locked to the ongoing hippocampal theta oscillations, while cholinergic MS-DBB neurons discharge at a very low rate with no apparent temporal relationship with theta (Borhegyi et al., 2004; Simon et al., 2006). Interestingly, there appears to be two distinct populations of GABAergic MS-DBB neurons firing in theta-frequency bursts, tightly coupled to either the trough or the peak of ongoing hippocampal theta rhythm (Borhegyi et al., 2004; Simon et al., 2006). GABAergic MS-DBB neurons have extensive local collaterals as well as axons that project to the hippocampus, targeting interneurons expressing PV, somatostatin, calbindin, calretinin and cholecystokinin (Freund and Antal, 1988; Gulyas et al., 1990; Acsady et al., 1993; Rocamora et al., 1996; Borhegyi et al., 2004). These findings suggest that GABAergic MS-DBB neurons serve to synchronize theta rhythm locally and also provide rhythmic inputs to the hippocampal circuit. As for the cholinergic MS-DBB neurons, they fire sparsely during theta (Simon et al., 2006) and a recent amperometric study reported slow increases in acetylcholine release correlated with the occurrence of theta rhythm in the hippocampus of anaesthetized rats (Zhang et al., 2010). In contrast to the GABAergic neurons, cholinergic septohippocampal neurons terminate on both pyramidal cells and interneurons (Frotscher and Leranth, 1985; Frotscher et al., 1992). Cholinergic MS-DBB neurons may provide hippocampal neurons with slow increases in excitatory tone through muscarinic receptors (Cole and Nicoll, 1983; Widmer et al., 2006) and may also exert fast excitatory effects through nicotinic receptors and facilitate potentiation of hippocampal synapses (Griguoli and Cherubini, 2012). Taken together, evidence to date supports the current model that cholinergic MS-DBB neurons provide hippocampal neurons with slow and/or fast excitation while GABAergic MS-DBB neurons convey phasic, theta-modulated

inhibitory inputs to hippocampal interneurons that can pace their firing during theta (Tóth et al., 1997). Currently, the role of the recently described glutamatergic MS-DBB neurons in hippocampal theta rhythm remains unknown.

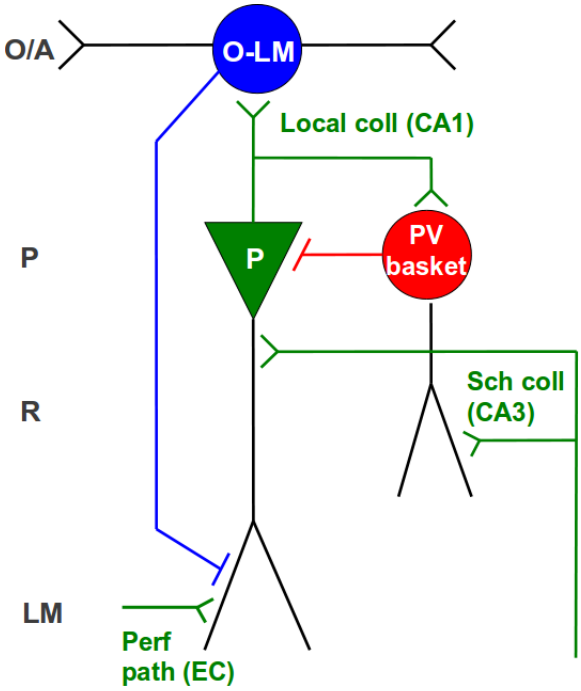

Figure 2. Schematic of axodendritic arborisation patterns of PV basket cells and SOM O-LM cells and their connectivity with CA1 pyramidal cells. Parvalbumin (PV)-positive basket cells innervate pyramidal cells at the soma and proximal dendrites, and they receive excitatory inputs from local collaterals of CA1 pyramidal cells as well as from CA3 pyramidal cells via Schaffer collaterals. In contrast, somatostatin (SOM)-expressing O-LM cells innervate pyramidal cells at the distal dendrites in stratrum lacunosum-moleculare (LM) where they coincide with temporoammonic path inputs from the entorhinal cortex. SOM O-LM cells have horizontally oriented dendrites that receive the majority of excitatory inputs from CA1 pyramidal cells.

2.4. Rhythm generators in the hippocampal formation

The existence of intrinsic rhythm generators in the hippocampal formation has been suggested by studies examining theta-like oscillations in acute hippocampal slices bathed in carbachol, a muscarinic agonist (Konopacki et al., 1987, 1988). However, this form of *in vitro* theta still required cholinergic activation and differed from *in vivo* theta in that it consisted of intermittent bursts of theta cycles and it did not require GABAergic inputs (MacVicar and Tse, 1989; Fellous and Sejnowski, 2000), thus it failed to illustrate a physiological rhythm. Using a complete rat hippocampus preparation *in vitro*, Goutagny and colleagues (2009) demonstrated that the CA1 region can generate its own theta (3 - 10 Hz) oscillations without any pharmacological agents and independently of extra-hippocampal inputs such as those from the MS-DBB. They found that the CA1 theta rhythm depends on both excitatory and inhibitory inputs (abolished by blockers for ionotropic glutamate or GABA receptors) but is resistant to muscarinic blockade or CA3 removal, illustrating that the CA1 rhythm does not rely on muscarinic action or afferent inputs from the CA3. Whole hippocampal isolates have previously been employed to demonstrate network rhythms (Wu et al., 2002) but only oscillations at slower frequencies (0.5 - 4 Hz) were reported previously, mostly likely due to different *in vitro* conditions used.

Using whole-cell recordings, Goutagny et al. (2009) further showed that CA1 pyramidal cells received rhythmic inhibitory postsynaptic potentials (IPSPs) which paced their firing during theta and conversely, interneurons fired rhythmically and displayed robust EPSPs from pyramidal cells and IPSPs from other interneurons. These findings indicated that the CA1 network is able to produce theta-frequency oscillations on its own and that the MS-DBB, long believed to be crucial for hippocampal theta rhythm generation, is not required for the emergence of this intrinsic CA1 theta rhythm. Goutagny et al. (2009) presented the first *in vitro* model to convincingly illustrate that the hippocampal

formation, specifically the CA1 region, possesses its own theta rhythm generators. Given that pyramidal cells receive prominent inhibitory inputs from the interneurons during both *in vitro* (Goutagny et al., 2009) and *in vivo* theta (Fox, 1989; Ylinen et al., 1995), it remains to be determined which CA1 interneuron subtype plays a key role in generating the currents responsible for the field theta oscillation.

The CA1 region contains more than twenty different interneuron subtypes that are categorized by soma location, axodendritic arborisation pattern and molecular expression profile (Freund and Buzsáki, 1996; Somogyi and Klausberger, 2005; Klausberger and Somogyi, 2008). The ever-growing list of interneuron types includes those that target pyramidal cells at the somatic domain (basket cells), axon initial segment (axon-axonic cells), basal and proximal dendrites (bistratified and ivy cells), distal dendrites (O-LM cells) as well as those that primarily innervate other interneurons (interneuron-specific cells). Moreover, there are GABAergic subtypes that project to CA3 and DG (back-projection cells) and double-projection cells sending axons to the subiculum and the medial septum. It is thought that through this rich diversity of GABAergic neurons, pyramidal cells' firing and synaptic inputs can be dynamically regulated with precise temporal control at distinct subcellular domains.

Two of the most intensively studied CA1 interneuron subtypes with relevance to theta rhythm are PV-positive basket cells and somatostatin (SOM)-positive oriens lacunosum-moleculare (O-LM) cells, as depicted in **Figure 2**. CA1 PV basket cells are located primarily in strata pyramidale and oriens and they innervate pyramidal cells at the level of the soma and proximal dendrites. A single basket cell has been estimated to innervate more than 1000 pyramidal cells (Sik et al., 1995; Halasy et al., 1996). PV basket cells are activated by local collaterals of CA1 pyramidal cells and by Schaffer collateral input from CA3 pyramidal cells (Ishizuka et al., 1990; Buhl et al., 1996; Gulyas et al., 2003). They receive GABAergic inputs from the MS-DBB (Freund and Antal, 1988) and other PV

basket cells with whom they are also connected via gap junctions (Cobb et al., 1997; Fukuda and Kosaka, 2000). PV basket cells are often considered together with PV axo-axonic cells that inhibit pyramidal cells at the axon initial segment, and they are collectively referred to as PV perisomatic-targeting interneurons. Together, these neurons are hypothesized to pace and synchronize the firing of a large network of pyramidal cells during hippocampal theta rhythm. In support of this idea, dual intracellular recordings in hippocampal slices have demonstrated that activation of a single perisomatic-targeting interneuron is sufficient to reset the membrane potential oscillations and entrain firing of multiple pyramidal cells (Cobb et al., 1995). Subthreshold membrane potential oscillations in pyramidal cells have previously been suggested to participate in generating hippocampal theta oscillations (Leung and Yim, 1991). A recent study employing optogenetics revealed that silencing PV interneurons indeed affects the timing of pyramidal cell firing during theta rhythm *in vivo* (Royer et al., 2012). Because of their fast-firing properties, PV basket cells are also thought to mediate gamma-frequency (30 - 150 Hz) network oscillations, also prominently observed in the hippocampal formation (Gloveli et al., 2005; Gulyás et al., 2010).

CA1 SOM O-LM cells have their soma and dendrites located in stratum oriens/alveus and they send axonal projections exclusively to pyramidal cells' distal dendrites in stratum lacunosum-moleculare (LM layer). SOM O-LM cells receive a massive excitatory input from collaterals of local CA1 pyramidal cells (Blasco-Ibáñez and Freund, 1995; Maccaferri and McBain, 1995, 1996a) and GABAergic inputs from a type of interneuron-specific interneurons expressing vasoactive intestinal polypeptide (VIP) (IS-III) (Acsady et al., 1996), septohippocampal GABAergic neurons (Gulyas et al., 1990) and from other SOM interneurons (Kogo et al., 2004). SOM O-LM neurons provide inhibitory inputs to pyramidal cells at the same layer where excitatory inputs from the entorhinal cortex arrive via perforant path fibers (Sik et al., 1995). They are sometimes considered together with SOM bistratified cells also located in stratum oriens that

innervate pyramidal cells at the level of apical and basal dendrites, and are collectively termed SOM dendrite-targeting interneurons. These interneurons modulate the strength of afferent excitatory inputs on pyramidal cells (Maccaferri and McBain, 1995; Yanovsky et al., 1997) and limit electrogenesis in pyramidal cell dendrites by suppressing calcium (Miles et al., 1996) and sodium spikes (Lovett-Barron et al., 2012). They have also been demonstrated to control pyramidal cells' burst-firing *in vitro* and *in vivo* (Lovett-Barron et al., 2012; Royer et al., 2012). Through these actions, SOM dendrite-targeting interneurons appear to play an important role in regulating synaptic integration and pyramidal cell output during theta rhythm. In addition, SOM O-LM cells have been reported to display spontaneous theta-frequency firing at rest, suggesting that they may possess intrinsic rhythm-generating properties (Maccaferri and McBain, 1996b). SOM-positive neurons in CA1 stratum oriens also include a large number of GABAergic neurons with projections to the medial septum as well as to other hippocampal subfields (Jinno and Kosaka, 2002; Gulyas et al., 2003; Jinno et al., 2007). These long-range projection SOM neurons may be instrumental in synchronizing theta oscillations across the septohippocampal network.

Unit recordings from identified interneurons in anaesthetized rats have characterized the firing behaviour of the above-mentionned CA1 interneuron subtypes during *in vivo* hippocampal theta rhythm (for review, see Klausberger and Somogyi, 2008). More recently, the firing patterns of CA1 PV and SOM interneurons during theta in freely behaving mice have also been described (Royer et al., 2012). These studies revealed that different CA1 interneuron subtypes display distinct firing characteristics during theta, varying in the degree of phase-locking to theta, the number of spikes fired per theta cycle and the theta phase at which they preferred to fire. Both CA1 PV and SOM interneurons appear to fire strongly phase-locked to the field theta rhythm but with different phase preferences (Klausberger et al., 2003; Royer et al., 2012). As outlined above, PV and SOM interneurons play important yet distinct roles in controlling pyramidal

cell activity during theta rhythm. The question of which interneuron subtype plays a key role in generating the field theta rhythm still remains to be answered.

Identification of potential rhythm generators both within the hippocampal formation and across the septohippocampal network is important for gaining a better understanding of how theta oscillations are generated, modulated and synchronized across neighbouring circuits as well as between distant brain regions. It is our hope that a greater exploration of this issue will help bring new insights into the mechanisms with which theta rhythms contribute to cognitive functions such as learning and memory.

I.3. Rationale and aims

3.1. Role of glutamatergic MS-DBB neurons (Project 1)

As discussed above in Section 1.2.2, much evidence points to the existence of a substantial number of glutamatergic neurons in the MS-DBB and it is likely that they account for a significant proportion of the septohippocampal projection. While there has been many studies investigating the contributions of cholinergic and GABAergic MS-DBB neurons (Section 1.2.3), the role of glutamatergic MS-DBB neurons in the septohippocampal network function and theta rhythm generation remains unknown. Some evidence indicates that glutamatergic MS-DBB neurons may exhibit slow- or cluster-firing patterns (Sotty et al., 2003), but a thorough characterization of their electrophysiological properties remains to be done. Considering that both cholinergic and GABAergic MS-DBB neurons play important roles in the emergence of the *in vivo* hippocampal theta rhythm, it is unknown whether glutamatergic MS-DBB neurons also functionally modulate hippocampal activity and what role they may play during theta oscillations.

To address these issues, the aims for my first project were to (1) investigate the intrinsic properties of glutamatergic MS-DBB neurons and to (2) examine the hypothesis that they provide a functional excitatory input to the hippocampus (**Fig. 3**).

To fulfill these aims, I carried out whole-cell patch-clamp recordings in several different *in vitro* preparations, ranging from autaptic cultures, acute slices to intact septohippocampal preparations. In order to visualize glutamatergic MS-DBB neurons, we employed transgenic mice in which a fluorescent protein was expressed under the control of the VGLUT2 promoter (VGLUT2-eGFP mice). Chapter 2 describes a control experiment performed in order to confirm that the eGFP expression was specific to glutamate-releasing neurons of the MS-DBB. Chapter 3 illustrates electrophysiological characterization of glutamatergic MS-DBB neurons. Finally, experiments in Chapter 4 demonstrate that these neurons indeed provide hippocampal neurons with a functional excitatory input.

3.2. Role of CA1 PV vs. SOM interneurons (Project 2)

As for potential theta rhythm generators in the CA1 region, PV and SOM interneurons are both very good candidates. As reviewed in Section 1.2.4, PV interneurons have the potential to synchronize a large network of pyramidal cells and they have been shown to control the timing of pyramidal cell firing during *in vivo* theta. On the other hand, SOM interneurons can regulate dendritic electrogenesis in pyramidal cells, limit their burst-firing and some of them may provide long-range inputs that can synchronize theta oscillations across the septohippocampal network. During *in vivo* theta rhythm, both PV and SOM interneurons appear to fire strongly phase-locked to theta, but with different phase preferences. It remains unknown what factors determine the interneurons' firing behaviour during theta and whether their activity has a causal role in generating

Figure 3

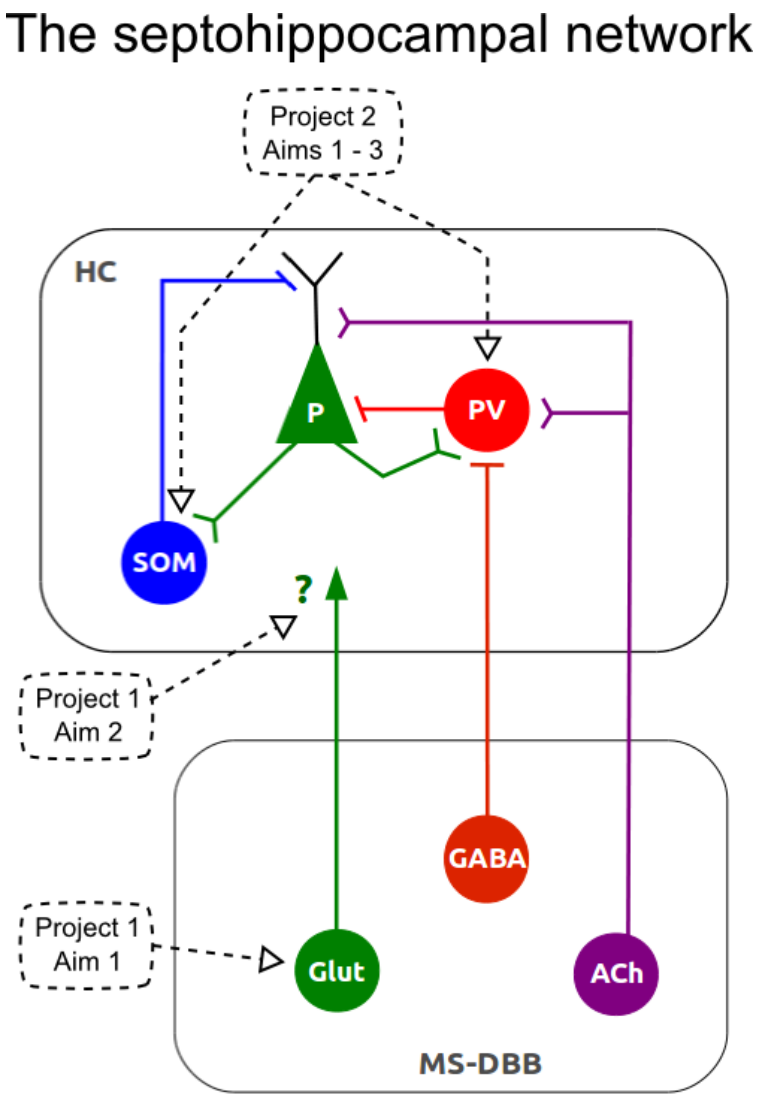
The septohippocampal network
Project 2
Aims 1 - 3
HC
P
PV
SOM
?
Project 1
Aim 2
GABA
Project 1
Aim 1
Glut
ACh
MS-DBB

Figure 3. Schematic of the septohippocampal network, with the key neuronal types examined in this Thesis indicated. The role of recently described glutamatergic MS-DBB neurons in the septohippocampal network function and theta rhythm generation remains unknown. The aims for my first project were to (1) investigate the intrinsic properties of glutamatergic MS-DBB neurons and to (2) examine the hypothesis that they provide a functional excitatory input to the hippocampus. Previous evidence indicates that both parvalbumin (PV)- and somatostatin (SOM)-expressing interneurons may play key roles in generating intrinsic CA1 theta oscillations. The aims for my second project were to (1) describe the intrinsic properties of PV and SOM interneurons, (2) examine their firing behaviour and synaptic activity during *in vitro* CA1 theta rhythm, and to (3) investigate the hypothesis that PV and/or SOM interneurons act as rhythm generators for the CA1 theta oscillation.

the field theta rhythm.

In order to explore these questions, the aims for my second project were to (1) describe the intrinsic properties of PV and SOM interneurons, (2) examine their firing behaviour and synaptic activity during *in vitro* CA1 theta rhythm, and to (3) investigate the hypothesis that PV and/or SOM interneurons act as rhythm generators for the CA1 theta oscillation (**Fig. 3**).

To tackle these goals, I carried out recordings in the intact hippocampal preparation that can self-generate CA1 theta oscillations, when given appropriate *in vitro* conditions as described in Section 1.2.4. Using the intact preparations, I performed simultaneous field and whole-cell recordings of PV and SOM interneurons, visualized with the help of the Cre-lox transgenic technology. We were also able to employ the latest optogenetic methods to test the causal role of these interneuron subtypes in network theta generation. Chapter 5 describes the electrophysiological characteristics of PV and SOM CA1 interneurons. In Chapter 6, I illustrate the two interneuron subtypes' firing behaviour and synaptic inputs during theta rhythm and also identify the cellular behaviour of CA1 pyramidal cells. Finally, experiments in Chapter 7 reveal that silencing PV interneurons' firing, but not that of SOM interneurons, causes a considerable change in the network CA1 theta oscillation.

Chapter II: VGLUT2-expressing MS-DBB neurons functionally release glutamate

II.1. Introduction

Expression of a vesicular glutamate transporter (VGLUT) confers cells the ability to use glutamate as a neurotransmitter and VGLUT expression is considered to be a specific marker for glutamatergic neurons (Takamori et al., 2000; Fremeau et al., 2001). In the MS-DBB, VGLUT2 is the dominant isoform of VGLUT expressed by glutamatergic neurons (Sotty et al., 2003; Danik et al., 2005). Thus, in our investigation of glutamatergic MS-DBB neurons, we used transgenic mice in which the expression of VGLUT2 is linked with that of the enhanced green fluorescent protein (eGFP) to enable visualization of these neurons (VGLUT2-eGFP mice). Using these mice, we can identify VGLUT2-expressing neurons by the presence of the fluorescent protein (eGFP) in the cell body, which is a great advantage because VGLUT2 protein is concentrated in axon terminals. Before using the VGLUT2-eGFP mice as a tool, we performed a control experiment to verify that the eGFP expression in these mice does not compromise the ability of cells to release glutamate and to ensure that the fluorescent protein is expressed solely by glutamatergic neurons.

This is necessary because of existing evidence that single MS-DBB neurons may have the capacity to co-release multiple neurotransmitters. Previous studies from our lab showed that a proportion of MS-DBB neurons co-express mRNAs for multiple neurotransmitter phenotypes (Sotty et al., 2003; Danik et al., 2005). We and another group have also demonstrated that in culture, some cholinergic MS-DBB neurons can functionally co-release acetylcholine, glutamate and/or GABA (Allen et al., 2006; Huh et al., 2008). Thus, in order to use eGFP to visualize specifically glutamatergic neurons, it is important to confirm that the eGFP-expressing MS-DBB neurons in VGLUT2-eGFP mice can functionally release glutamate and no other neurotransmitter. To this end, we established microisland cultures using MS-DBB neurons from VGLUT2-eGFP

transgenic mice, allowed the isolated neurons to form autaptic connections over time and determined the neurotransmitter(s) released by each neuron using whole-cell patch-clamp electrophysiology and pharmacology.

In order to visually identify GABAergic MS-DBB neurons, we also employed another transgenic mouse line where the expression of eGFP is driven under the control of the promoter for GAD65, a marker for GABAergic neurons. In the MS-DBB, GABAergic neurons express GAD65, GAD67 or both (Castañeda et al., 2005). Therefore, a similar characterization of neurotransmitter identification was performed on MS-DBB neurons from GAD65-eGFP mice, in order to verify that GAD65-expressing MS-DBB neurons could functionally release GABA.

II.2. Materials and Methods

Animals

Experiments were performed using VGLUT2-eGFP transgenic mice unless otherwise stated. VGLUT2-eGFP mice (strain name: STOCK Tg(Slc17a6-EGFP)FY115Gsat/Mmcd), developed under the GENSAT project (Gong et al., 2003), were obtained from the Mutant Mouse Regional Resource Center (MMRRC, Davis, CA). In these mice, the genotype was modified to contain multiple copies of a modified bacterial artificial chromosome (BAC) in which the eGFP reporter gene was inserted immediately upstream of the coding sequence of the targeted gene (VGLUT2). In experiments where GABAergic MS-DBB neurons were examined, another transgenic mouse line developed using the BAC technology was used, in which the eGFP was expressed under the control of the glutamic acid decarboxylase 65 gene (GAD65) (strain name: STOCK Tg(Gad2-EGFP)31Gsat/Mmcd). For both transgenic mouse strains, the background was FVB/N-Swiss Webster hybrid and heterozygotes were purchased from the

MMRRC and mated with wild-type Swiss Webster (CFW) mice (Charles River, St. Constant, Quebec, Canada). The transgene expression in the offspring was checked by illuminating the brain of live pups (1 – 2 d old) using a GFP flashlight (NightSea, Bedford, MA). In some experiments noted, wild-type CFW mice were used. Animals were treated according to protocols and guidelines approved by McGill University and the Canadian Council of Animal Care.

Autaptic cultures

Cell cultures were prepared using MS-DBB cells from VGLUT2-eGFP or GAD65-eGFP transgenic mice according to previously described protocols (Huh et al., 2008) adapted from Bourque and Trudeau (2000) with some modifications. All drugs were obtained from Sigma (St. Louis, MO) unless otherwise noted. Astrocytic microislands were first established and then MS-DBB neurons were cultured on the microislands. Briefly, glass coverslips were treated with poly-L-ornithine, agarose and sprayed with liquid collagen (Cohesion Technology, Palo Alto, CA) using a microatomizer to create microislands permissive to cell growth. To obtain astrocytes, we extracted hippocampal tissue from 1-d-old mice and dissociated the tissue using papain (Worthington Biochemical, Lakewood, NJ). Cells were grown in flasks with media containing basal medium eagle, glucose, Mito+ serum extender (Becton Dickinson Labware, Bedford, MA), penicillin/streptomycin (Invitrogen, Burlington, Ontario), GlutaMAX-1 (Invitrogen) and 5% heat-inactivated fetal calf serum (Invitrogen). After 48 hours of incubation (37^{o}C/5%CO^{2}), astrocytes were exposed to cold (4^{o}C) media and vigorous shaking to eliminate any surviving neurons and loosely attached cells. The remaining astrocytes were allowed to further proliferate, harvested and plated at 60,000 living cells/ml on pretreated coverslips. 5-Fluoro-2'deoxyuridine (FDU) was added to inhibit further proliferation. Next, MS-DBB neurons were obtained from 11- to 14-d-old VGLUT2-eGFP or GAD65-eGFP mice, dissociated and plated at 80,000 living cells/ml on preestablished astrocytic microislands. The

neurons were cultured in media containing astrocyte-conditioned media, Neurobasal-A (Invitrogen), penicillin/streptomycin, GlutaMAX-1, B-27 (Invitrogen) and 5% heat-inactivated fetal calf serum. Media was changed after 24 hours, at which point additional FDU was administered, and fresh media was added every seventh day. Recordings were performed on neurons cultured for 17-30 d.

Electrophysiology and eGFP labelling visualization

All electrophysiological recordings were done at room temperature. Prior to recording, neurons were checked for the presence of soma eGFP labelling by illuminating with a 488-nm wavelength light using a fluorescence system (PTI, Monmouth Junction, NJ). The electrophysiology setup was equipped with an upright BX51W1 Olympus microscope, a 20x water-immersion objective, Nomarsky optics, an infrared camera (Cohu, San Diego, CA), a monochrome digital camera for fluorescence imaging (DAGE-MTI, Michigan City, IN) and a custom-made submerged Plexiglas recording bath. Patch pipettes (3 - 5 MΩ) were pulled from borosilicate glass capillaries (Warner Instrument, Hamden, CT) and filled with intrapipette solution containing (mM) 144 K-gluconate, 10 HEPES, 3 $MgCl_2$, 2 Na_2ATP, 0.3 GTP, 0.2 EGTA, adjusted to pH 7.2 with KOH. Neurons were recorded using visually-guided whole-cell patch-clamp technique. An Axopatch-1C amplifier (Axon Instruments, Foster City, CA) and pClamp9 software (Molecular Devices, Sunnyvale, CA) were used. The junction potential estimated at -14 mV was not corrected.

For recording of autaptic neurons, we used an extracellular solution containing (in mM) 140 NaCl, 10 glucose, 6 sucrose, 3 KCl, 2 $CaCl_2$, 2 $MgCl_2$, 10 HEPES, adjusted to pH 7.3 with NaOH, perfused at 1-2 ml/min. Microislands were visually inspected to ensure that recordings were done on astrocytic islands that contained only one neuron. After an isolated fluorescent neuron was found (**Fig. 4*A***), the neuron was recorded in voltage-clamp to detect an autaptic current

(**Fig. 4*B***). The current was considered to be an EPSC if its reversal potential was near 0 mV and an IPSC if it reversed at a potential more negative than -40 mV. We then determined the neurotransmitter released pharmacologically by bath-applying 6,7-dinitroquinoxaline-2,3(1H,4H)-dione (DNQX) (20 μM), tubocurarine (10 μM) and/or bicuculline methiodide/chloride (10 μM).

Data are presented as mean ± standard error of the mean, unless otherwise stated. Electrophysiological data were plotted using Clampfit software (Molecular Devices, Sunnyvale, CA).

II.3. Results

3.1. Experiment 1: VGLUT2-eGFP+ MS-DBB neurons functionally release glutamate

Figure 4*A* shows an example of an isolated MS-DBB neuron expressing VGLUT2-eGFP in the soma. The eGFP fluorescence level in the cell body was sufficient to clearly distinguish VGLUT2-(+) neurons from VGLUT2-(-) neurons. Autaptic currents were recorded by holding the neuron in voltage clamp at -60 mV, depolarizing it to +15 mV for 1 ms to evoke an action potential, then holding the neuron at -80 mV for 150 ms to reveal the postsynaptic autaptic current (**Fig. 4*B***) and this protocol was repeated every 60 s. Once a stable baseline for the current was obtained, drugs were applied to block currents mediated by AMPA/kainate receptors (DNQX), nicotinic receptors (tubocurarine) or $GABA_A$ receptors (bicuculline) in order to determine the neurotransmitter released.

We found that out of 11 VGLUT2-eGFP-(+) MS-DBB neurons characterized, all 11 cells exhibited autaptic EPSCs that were completely blocked by 20 μM DNQX (control: -756.3 ± 293.3 pA; DNQX: -101.2 ± 17.03 pA). **Figure 4*C*** shows a typical example of a VGLUT2-eGFP-(+) neuron that

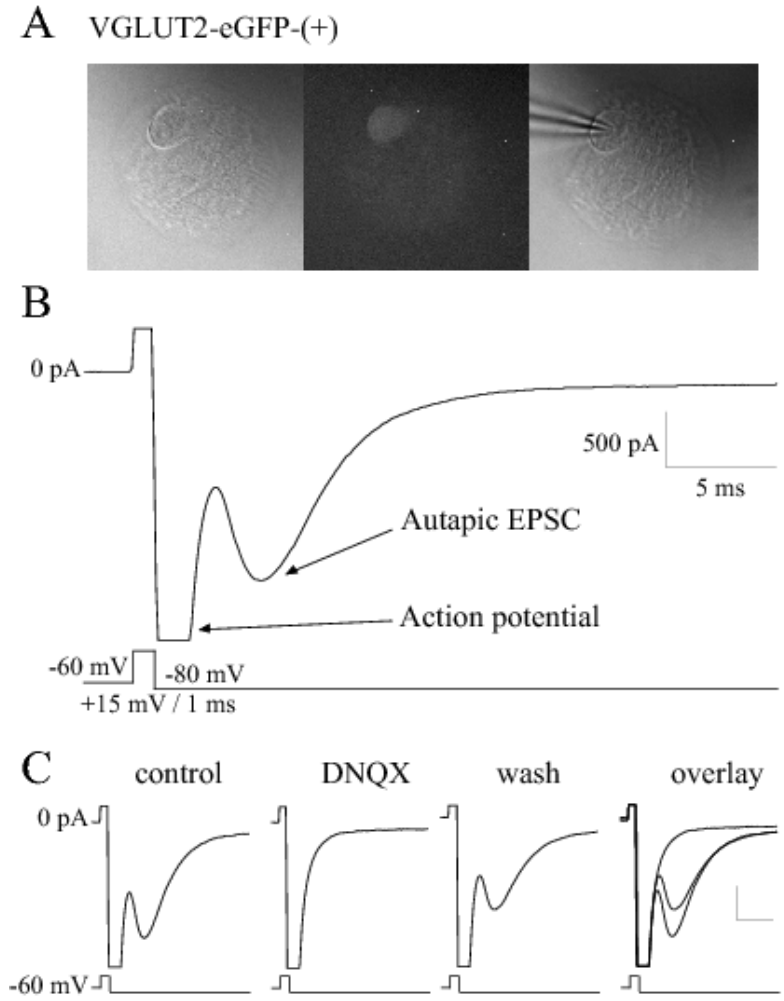

Figure 4. VGLUT2-eGFP-(+) MS-DBB neurons functionally release glutamate. ***A,*** An isolated fluorescent MS-DBB neuron cultured from VGLUT2-eGFP transgenic mice. ***B,*** Autaptic neurons were held in voltage clamp and stimulated to fire an action potential, resulting in neurotransmitter release and postsynaptic autaptic currents. An example of an autaptic EPSC displayed by a VGLUT2-eGFP-(+) MS-DBB neuron is shown. ***C,*** A typical VGLUT2-eGFP-(+) cell exhibited an EPSC that was completely and reversibly blocked by 20 μM DNQX, indicating that the neuron released glutamate. Scale bars, 500 pA, 5 ms.

displayed an autaptic EPSC that was completely and reversibly blocked by DNQX. In some neurons, the autaptic currents were further tested with 10 μM tubocurarine or 10 μM bicuculline and we found that the autaptic currents were not further reduced by these drugs (DNQX and tubocurarine: 5 cells, 96.7 ± 2.3 % normalized to DNQX effect size; DNQX and bicuculline: 4 cells, 99.5 ± 0.4 %; data not shown), confirming that the only neurotransmitter released by these neurons is glutamate. These results demonstrate that VGLUT2-eGFP-(+) MS-DBB neurons can functionally release glutamate.

3.2. Experiment 2: GAD65-eGFP+ MS-DBB neurons functionally release GABA

A similar set of characterizations was performed on MS-DBB neurons from GAD65-eGFP transgenic mice. Similar to VGLUT2-eGFP mice, the eGFP fluorescence level was sufficient in the cell body to clearly identify GAD65-(+) neurons from GAD65-(-) neurons in GAD65-eGFP mice. We found that out of 8 GAD65-eGFP-(+) MS-DBB neurons tested, all 8 neurons displayed autaptic IPSCs that were completely blocked by 10 μM bicuculline (control: -194.0 ± 41.8 pA; bicuculline: -41.3 ± 11.2 pA). **Figure 5** illustrates an example of a GAD65-eGFP-(+) cell that displayed an autaptic IPSC that was completely and reversibly inhibited by bicuculline. These results confirm that GAD65-eGFP-(+) MS-DBB neurons are able to functionally release GABA.

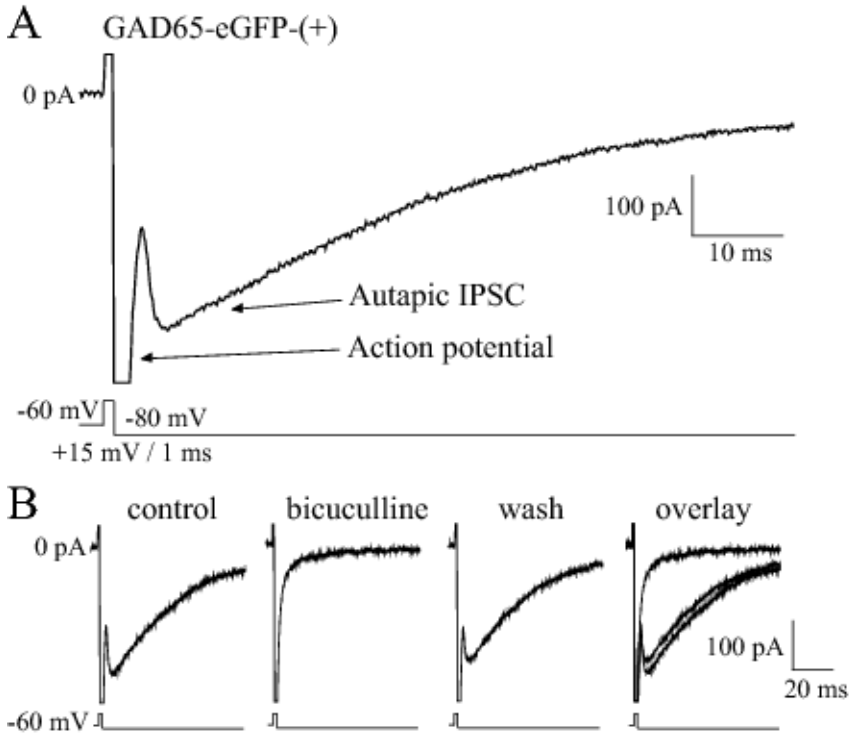

Figure 5. GAD65-eGFP-(+) MS-DBB neurons functionally release GABA. ***A,*** MS-DBB neurons from GAD65-eGFP transgenic mice were cultured to establish autaptic cultures. In voltage clamp, isolated neurons were stimulated to fire an action potential and postsynaptic autaptic currents were characterized. An example of an autaptic IPSC displayed by a GAD65-eGFP-(+) MS- DBB neuron is shown. ***B,*** A typical GAD65-eGFP-(+) neuron exhibited an IPSC that was completely and reversibly blocked by 10 μM bicuculline. Scale bars, 100 pA, 20 ms.

II.4. Discussion

These results show that the eGFP expression is specific to the target neurons in the MS-DBB in both mouse lines, confirming that VGLUT2-eGFP and GAD65-eGFP transgenic mice can be used reliably to visualize glutamatergic and GABAergic MS-DBB neurons, respectively. We further show that the fluorescent protein expression does not compromise crucial neuronal functions such as neurotransmitter release. Specifically, we found that the only neurotransmitter functionally released by eGFP+ MS-DBB neurons in VGLUT2-eGFP mice is glutamate. This is an important finding because several recent studies have also used the VGLUT2-eGFP mice to visualize glutamatergic neurons in the MS-DBB (Dumalska et al., 2008; Henderson et al., 2010). We also confirm that eGFP+ MS-DBB neurons in GAD65-eGFP mice only release GABA.

Our findings provide an important functional verification of the specificity of eGFP expression in these transgenic mouse lines, confirming that the labelled neurons indeed release only the neurotransmitter that they are expected to release. However, these results are in apparent contrast with evidence that single MS-DBB neurons may have the capacity to co-release multiple neurotransmitters. For example, Sotty et al. (2003) reported, using single-cell multiplex RT-PCR, that over half of the randomly sampled rat MS-DBB neurons containing VGLUT2 mRNA also expressed GAD67 and/or ChAT transcript. In that study, it was also shown that a large proportion of GAD67-mRNA+ MS-DBB neurons co-expressed VGLUT2 and/or ChAT transcripts. In addition, we and another group have also demonstrated using autaptic cultures that a significant proportion of cholinergic MS-DBB neurons can functionally co-release acetylcholine, glutamate and/or GABA (Allen et al., 2006; Huh et al., 2008).

Based on these previous findings, we would have expected to find some instances of multiple neurotransmitter co-release by VGLUT2-eGFP+ or GAD65-

eGFP+ MS-DBB neurons in our study. This may be due to a number of possible reasons. One explanation is that some of the neurons sampled in our study may have expressed transcripts for multiple neurotransmitter phenotypes but were only able to functionally release one transmitter. If this is indeed the case, one may conclude that the functional co-release of multiple transmitters as demonstrated by previous studies is a unique feature for only cholinergic neurons in the MS-DBB. This view is supported by our previous data showing the absence of transmitter co-release in non-cholinergic neurons of the MS-DBB (Huh et al., 2008). Alternatively, a small proportion of glutamatergic and GABAergic MS-DBB neurons may co-release multiple transmitters but we may not have been able to detect it due to our relatively small sample size. A quantitative investigation into the incidence of co-expression of multiple transmitter phenotypes at the protein level will help answer this question. Employing the same VGLUT2-eGFP transgenic mouse line used in our study and immunohistochemical methods, Henderson and colleagues (2010) found that a small proportion (6%) of VGLUT2-eGFP+ MS-DBB neurons co-expressed GAD67 but that none overlapped with ChAT expression. Thus, the question remains unanswered as to whether small fractions of glutamatergic and GABAergic MS-DBB neurons are able to functionally co-release multiple transmitters. Nonetheless, our results in these control experiments accomplish the goal of demonstrating that VGLUT2- and GAD65-eGFP transgenic mice can be dependably used as tools to visualize the target neuronal populations in the MS-DBB in subsequent experiments.

Chapter III: Electrophysiological characterization of glutamatergic MS-DBB neurons

III.1. Introduction

Cholinergic and GABAergic neurons have long been known to exist in the MS-DBB and their electrophysiological characteristics are well described in the literature. In acute slices, cholinergic MS-DBB neurons fire slowly, distinguished by broad action potentials and slow afterhyperpolarization (AHP) (Griffith and Matthews, 1986; Markram and Segal, 1990) whereas most GABAergic MS-DBB neurons display fast- or burst-firing properties and a large I_h, a hyperpolarization-activated inward current (Morris et al., 1999; Knapp et al., 2000). *In vivo*, cholinergic neurons discharge infrequently while GABAergic neurons produce rhythmic bursts phase-locked to the ongoing hippocampal theta oscillations (Borhegyi et al., 2004; Simon et al., 2006). Due to these distinct properties and firing behaviour, cholinergic neurons are thought to provide hippocampal neurons with long-lasting tonic depolarizations (Cole and Nicoll, 1983; Widmer et al., 2006) while GABAergic neurons provide rhythmic inhibitory inputs which in turn phasically disinhibit pyramidal cells (Freund and Antal, 1988; Tóth et al., 1997).

On the other hand, little is known about the newly described glutamatergic MS-DBB neurons, their intrinsic properties and their role in hippocampal theta rhythm. Using *in vitro* electrophysiology in slices and single-cell RT-PCR, Sotty et al. (2003) reported that MS-DBB neurons expressing VGLUT2-mRNA are primarily slow-firing cells with some of the neurons (43%) displaying a cluster-firing pattern, firing clusters of multiple spikes interspersed by prominent subthreshold oscillations upon prolonged depolarization. However, in that study it was also found that among the MS-DBB neurons containing transcripts for ChAT or GAD67, some also co-expressed VGLUT2-mRNA and these neurons displayed a wide range of different firing patterns such as slow-, fast- and burst-firing. Therefore, a thorough characterization of the glutamatergic MS-DBB neurons is required to properly define their intrinsic properties. By doing so, we

will be able to find answers to outstanding questions, such as whether glutamatergic neurons can be distinguished from other MS-DBB neurons based on electrophysiological characteristics and whether they possess any rhythmic properties that may be important for rhythm generation.

Here, we recorded from a large number of glutamatergic MS-DBB neurons in acute slice preparations and characterized their electrophysiological properties. We also recorded from GABAergic MS-DBB neurons to determine whether the two populations could be differentiated from one another based on intrinsic properties. In order to visualize glutamatergic and GABAergic MS-DBB neurons in slices, we employed the same VGLUT2-eGFP and GAD65-eGFP transgenic mice used in the previous chapter.

III.2. Materials and Methods

Animals

Same transgenic animals as described in Chapter 2, Section 2.2 were used.

Slice preparation

Brain slices containing the MS-DBB were obtained from 12- to 18-d-old VGLUT2-eGFP or GAD65-eGFP transgenic mice. Mice were sacrificed by decapitation and the brain was rapidly removed and placed in ice-cold high-sucrose solution containing (mM): 252 sucrose, 24 $NaHCO_3$, 10 glucose, 3 KCl, 2 $MgCl_2$, 1.25 NaH_2PO_4 and 1 $CaCl_2$ (pH 7.3, oxygenated with 95% O_2-5% CO_2). Coronal slices of 300 μm were cut using a vibrotome (Campden Instruments, UK) and placed in a petri dish containing artificial cerebrospinal fluid (aCSF) containing (mM) 126 NaCl, 24 $NaHCO_3$,10 glucose, 3 KCl, 2 $MgCl_2$, 1.25 NaH_2PO_4 and 1 $CaCl_2$ (pH 7.3, oxygenated with 95% O_2-5% CO_2) and left to equilibrate for 1 h at room temperature before recording.

Electrophysiology and eGFP labelling visualization

All electrophysiological recordings were done at room temperature. Prior to recording, neurons were checked for the presence of soma eGFP labelling by illuminating with a 488-nm wavelength light using a fluorescence system (PTI, Monmouth Junction, NJ). The same electrophysiology setup, fluorescence system, intrapipette solution and pipette resistance were used as in Chapter 2, Section 2.2.

For electrophysiological characterization of MS-DBB neurons in slices, standard aCSF containing (mM) 126 NaCl, 24 $NaHCO_3$,10 glucose, 3 KCl, 2 $MgCl_2$, 1.25 NaH_2PO_4 and 2 $CaCl_2$ (pH 7.3, oxygenated with 95% O_2-5% CO_2) was perfused at 2-3 ml/min. Properties examined include resting membrane potential (Vrest), spontaneous firing, firing pattern, mean firing rate, action potential and AHP parameters, sag amplitude and kinetics (see **Table 1**). An approximate location of the recorded cell in the slice was also noted. Recordings were kept for analysis only if they met the stable recording criteria; spikes overshot 0 mV, spike amplitude exceeded 60 mV, access resistance was <30 MΩ, Vrest and spontaneous firing rate fluctuated less than ±10% for the duration of the cell's characterization. Intrinsic properties of each cell were examined in current-clamp mode following published protocols (Sotty et al., 2003). The membrane potential of the cell was held at -80 mV and a series of 1-s depolarizing current steps (0 – 200 pA) were applied. The membrane was then held at -60 mV and sets of 1-s and 5-s depolarizing currents were administered. Action potential and AHP parameters were measured from the voltage trace where the cell fired only one action potential from -60 mV. Firing frequencies were determined from the trace where the neuron was depolarized from -60 mV using the same current step required to depolarize the cell to spike threshold from -80 mV; mean firing rate (Hz) was the number of spikes evoked by the 1-s depolarizing step, initial firing rate ($F_{INITIAL}$) was the neuron's firing frequency during the first 200 ms, final firing rate (F_{FINAL}) was that during the last 200 ms and spike accommodation (%) was

calculated as: $(F_{INITIAL} - F_{FINAL}) / F_{INITIAL} \times 100$. When present, properties of the depolarizing sag were measured from -50 mV in response to the 1-s hyperpolarizing current step leading to an initial hyperpolarization to -120 mV.

Firing patterns were examined in current clamp using 1-s depolarizating steps from -60 mV unless otherwise noted. Neurons firing regularly with the mean firing rate of ≤7 Hz were classified as 'slow-firing' cells and those with higher firing rates were considered 'fast-firing' cells. Neurons displaying clusters of action potentials and clear subthreshold oscillations were categorized as 'cluster-firing' cells. 'Burst-firing' neurons fired at least two spikes on top of a conspicuous low-threshold spike (LTS) when depolarized from -80 mV. Several additional properties were measured for burst- and cluster-firing neurons (**Tables 1-2**). Neurons displaying a depolarizing sag of ≥10 mV when initially hyperpolarized to -120 mV were judged as having a 'large sag' and kinetics of the depolarizing sag were measured only for these neurons.

The degree of rhythmicity in spontaneous firing was measured as follows. The cell was recorded at Vrest to check for the presence of spontaneous spiking for 30 s and then a current was injected to hold the cell at -70 mV for 30 s to reveal spontaneous synaptic events before the cell was characterized for basic electrophysiological properties. For neurons that displayed 4 – 12 Hz spontaneous firing, an interspike interval (ISI) histogram and a spike autocorrelogram were constructed using Spike2 software (Cambridge Electronic Design, Cambridge, UK). In order to quantify the rhythmicity of spontaneous firing, a 'theta index' (adapted from Royer et al., 2010) was calculated based on the fitted curve of the autocorrelogram obtained using a moving average function (**Fig. 8**). Here, the theta index is defined as the ratio 'a/b' where 'b' is the total amplitude of the second peak of the autocorrelogram (rhythmic and noise portions) and 'a' is the amplitude of the rhythmic portion of the second peak (total amplitude – amplitude of trough).

Pharmacology

ZD7288 (50 μM; Tocris Cookson, Ellisville, MO) was used to block I_h in some experiments. Some neurons were recorded in the presence of blockers of synaptic inputs: DNQX (10 μM), bicuculline (5 μM), tubocurarine (5 μM), DL-2-Amino-5-phosphonopentanoic acid (DL-AP5; 25 μM), atropine (10 μM).

Statistical analysis

Data are presented as mean ± standard error of the mean, unless otherwise stated. Electrophysiological data were plotted and analyzed using Clampfit (Molecular Devices, Sunnyvale, CA), Spike2 (Cambridge Electronic Design, Cambridge, England) and Prism 4 (GraphPad Software, San Diego, CA). Statistical methods used were Student's t test, ANOVA and post-hoc Newman-Keuls tests. *p* values of <0.05 were considered to be statistically significant.

Table 1. Electrophysiological properties of VGLUT2-eGFP-(+) MS-DBB neurons in coronal mouse brain slices, N = 66 neurons

Firing pattern	Cluster-firing	Fast-firing		Burst-firing	Slow-firing
		Large sag	No sag		
n (% of N)	13 (19.7%)	12 (18.2%)	19 (28.8%)	11 (16.7%)	11 (16.7%)
Vrest (mV)	-53.0 ± 1.6	-50.3 ± 1.0*	-51.5 ± 1.3	-52.0 ± 0.9*	-49.5 ± 1.0
Proport. spont. firing	46.2%	50.0%	58.8%	54.5%	18.2%
Mean frequency (Hz)	2.8 ± 0.7	3.7 ± 1.3	4.6 ± 1.2	2.5 ± 0.6	3.5 ± 0.5
Range (Hz)	1 - 6	1 - 9	1 - 10	1 - 5	3 - 4
Mean firing rate (Hz)	8.8 ± 1.2 [fs,f]	15.8 ± 1.6 [c,b,s]	13.6 ± 1.8 [c,b,s]	9.1 ± 0.9 [fs,f]	5.3 ± 0.3 [fs,f]
$F_{INITIAL}$ (Hz)	12.7 ± 2.2	18.3 ± 2.3 [s]	15.8 ± 1.9 [s]	12.3 ± 1.6	5.9 ± 0.6 [fs,f]
F_{FINAL} (Hz)	6.2 ± 1.3 [fs,f]	15.4 ± 2.1 [c,b,s]	13.4 ± 1.7 [c,b,s]	7.7 ± 1.0 [fs,f]	4.1 ± 0.6 [fs,f]
Spike freq. accom. (%)	51.8 ± 10.4 [fs,f]	15.4 ± 6.2 [c]	13.4 ± 3.8 [c]	37.3 ± 9.1	27.3 ± 12.4
Spike threshold (mV)	-41.2 ± 0.9	-43.1 ± 1.0	-44.1 ± 1.2 [s]	-43.9 ± 1.3 [s]	-38.9 ± 1.1 [f,b]
Spike amplitude (mV)	78.1 ± 2.9	80.7 ± 2.0	79.8 ± 2.2	81.9 ± 3.4	76.6 ± 2.2
Spike half-width (ms)	1.3 ± 0.1	1.3 ± 0.1	1.3 ± 0.1	1.2 ± 0.1 [s]	1.7 ± 0.1 [b]
AHP amplitude (mV)	7.5 ± 1.5	5.9 ± 0.9	8.1 ± 0.6	4.9 ± 0.6	7.4 ± 0.9
AHP duration (ms)	253.2 ± 39.9	262.8 ± 31.4	284.5 ± 34.1	292.6 ± 20.8*	318.9 ± 31.1
Sag amplitude (mV)	6.4 ± 1.3 [fs]	16.1 ± 1.4 [c,f,b,s]	4.6 ± 0.7 [fs]	3.2 ± 1.1 [fs,*]	4.9 ± 1.4 [fs]
Rebound spike delay (ms)	124.5 ± 42.6	221.7 ± 87.1	94.2 ± 18.4	74.7 ± 7.9	74.3 ± 6.1*
Sag activation time (ms)	-	131.1 ± 21.3	-	-	-
Sag decay constant (ms)	-	176.9 ± 19.5	-	-	-
Subthres. oscill. freq. (Hz)	17.8 ± 2.4	-	-	-	-
Intracluster/burst freq. (Hz)	15.8 ± 2.2	-	-	58.6 ± 11.4	-
# spikes per cluster/burst	4.9 ± 0.6	-	-	2.3 ± 0.3	-
LTS amplitude (mV)	-	-	-	15.3 ± 1.2*	-
LTS duration (ms)	-	-	-	162.7 ± 39.5	-

[c, fs, f, b, s, *] Statistically significant differences ($p < 0.05$) are indicated: [c] *versus* cluster-firing cells; [fs] *versus* fast-firing cells with large sag; [f] *versus* fast-firing cells with no sag; [b] *versus* burst-firing cells; [s] *versus* slow-firing cells; * *versus* GAD65-eGFP-(+) cells with a similar firing pattern. Mean value ± S.E.

Figure 6

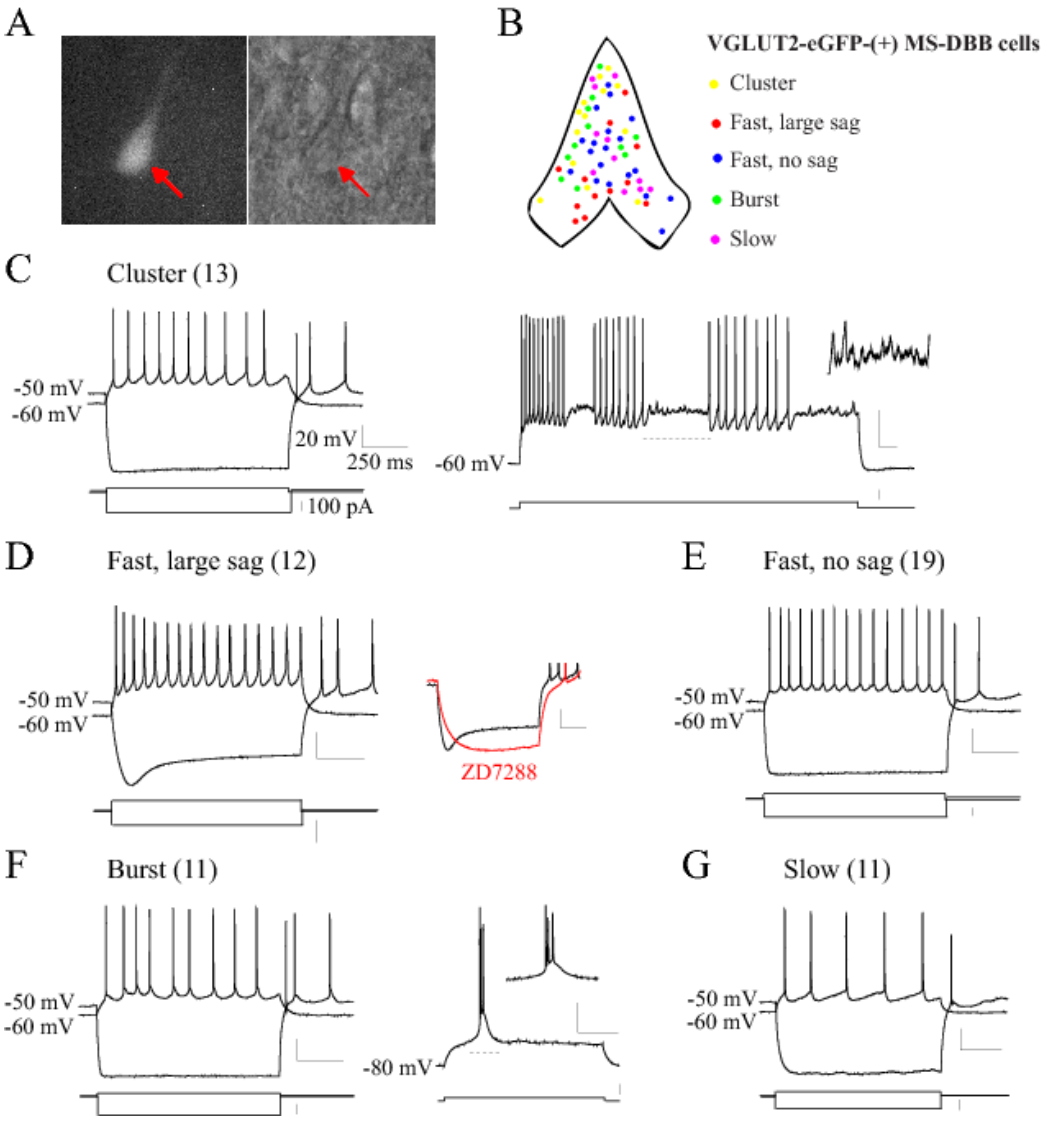
A
B
VGLUT2-eGFP-(+) MS-DBB cells
Cluster
Fast, large sag
Fast, no sag
Burst
Slow
C
Cluster (13)
-50 mV
-60 mV
20 mV
250 ms
100 pA
-60 mV
D
Fast, large sag (12)
-50 mV
-60 mV
ZD7288
E
Fast, no sag (19)
-50 mV
-60 mV
F
Burst (11)
-50 mV
-60 mV
-80 mV
G
Slow (11)
-50 mV
-60 mV

Figure 6. Electrophysiological characteristics of glutamatergic MS-DBB neurons. ***A,*** A VGLUT2-eGFP-(+) MS-DBB neuron (soma indicated by an arrow) in an acute slice. ***B,*** Approximate locations of recorded VGLUT2-eGFP-(+) neurons in the MS-DBB are indicated, colour-coded by firing pattern; cluster- and burst-firing glutamatergic neurons were found in lateral regions of the MS-DBB, fast-firing cells were located more medially, slow-firing neurons were found in all MS-DBB subregions. ***C,*** Cluster-firing glutamatergic neurons displayed clusters of spikes observable during 5-s depolarizing steps (right), interspersed with subthreshold oscillations (right, inset). ***D,*** Upon hyperpolarization, some fast-firing glutamatergic neurons showed a prominent depolarizing sag that was completely blocked by 50μM ZD7288 (inset). ***E,*** Other fast-firing neurons possessed little or no sag. ***F,*** Burst-firing glutamatergic neurons presented bursts of several action potentials when depolarized from -80 mV (right) but fired regularly from -60 mV (left). ***G,*** Slow-firing glutamatergic neurons fired in a tonic manner at a low rate and typically showed little sag. Numbers in brackets indicate number of cells. Scale bars, 20 mV, 250 ms (voltage traces), 100 pA (current steps).

III.3. Results

3.1. Experiment 1: Glutamatergic MS-DBB neurons display a wide range of electrophysiological characteristics

By using VGLUT2-eGFP transgenic mice, we were able to visually select fluorescent glutamatergic MS-DBB neurons (**Fig. 6*A***) and record specifically from these neurons. Electrophysiological characterization was done in current-clamp mode and the properties examined included resting membrane potential (Vrest), spontaneous firing at rest, firing pattern upon depolarization, action potential properties and presence of a depolarizing sag upon hyperpolarization. For comparison, similar characterizations were performed on GABAergic MS-DBB neurons using brain slices from GAD65-eGFP transgenic mice and their electrophysiological properties are summarized in **Table 2** and **Figure 7**.

We found that glutamatergic MS-DBB neurons display a wide range of firing patterns that include cluster-, fast-, burst- and slow-firing (see **Table 1** and **Fig. 6**). Cluster-firing cells (13 out of 66 cells) were unique in their tendency to fire clusters of action potentials when subjected to long 5-s depolarizations (**Fig. 6*C*, right**) and the clusters were interspersed with subthreshold membrane oscillations (**Fig. 6*C*, right inset**). Importantly, cluster-firing was only observed among VGLUT2-eGFP-(+) cells and not GAD65-eGFP-(+) cells (0/35) in response to the 5-s depolarizations. Cluster-firing cells were mostly silent or showed little spontaneous firing at rest and when depolarized they displayed a low mean firing rate (8.8 ± 1.2 Hz) and large frequency accommodation (52 ± 10 %). Upon hyperpolarization, most cluster-firing cells (9/13) showed little or no depolarizing sag (**Fig. 6*C*, left**). Cluster-firing neurons were located in lateral parts of the MS-DBB, avoiding the midline (**Fig. 6*B***).

The largest proportion of glutamatergic MS-DBB neurons was fast-firing

(31/66). More than half of fast-firing cells were spontaneously active with firing frequencies between 1 and 10 Hz. Upon depolarization, fast-firing cells displayed a regular, tonic firing pattern (**Fig. 6*D-E***) and a significantly higher mean firing rate (14.5 ± 1.3 Hz) than cluster-, burst- or slow-firing cells (ps < 0.05). During the 1-s depolarizing step, fast-firing cells showed the least amount of frequency accommodation (14 ± 4 %) and their F_{FINAL} was significantly higher than all other cell types (ps < 0.05). In response to hyperpolarization, some fast-firing cells displayed a prominent depolarizing sag (12/31; **Fig. 6*D***) while other fast-firing cells showed little or no sag (19/31; **Fig. 6*E***). The amplitude of sag displayed by the fast-firing, large-sag group was larger than that displayed by all other cell types. To determine whether the depolarizing sag is due to I_h, a hyperpolarization-activated current that has been associated with GABAergic MS-DBB neurons (Morris et al., 2004), the specific I_h blocker ZD7288 was applied. ZD7288 (50 μM) abolished the depolarizing sag in all the glutamatergic cells tested (4/4; **Fig. 6*D*, inset**), demonstrating that some fast-firing glutamatergic MS-DBB neurons possess significant I_h.

Interestingly, a proportion of GAD65-eGFP-(+) MS-DBB cells also exhibited the two types of fast-firing, with some neurons possessing large sag and others showing little or no sag (**Fig. 7*C-D***). Fast-firing glutamatergic neurons and fast-firing GABAergic neurons were not significantly different in any of the electrophysiological properties tested, except for Vrest; GABAergic cells were more depolarized at rest (**Tables 1-2**). The amplitude and kinetics of the depolarizing sag were not significantly different between glutamatergic *vs.* GABAergic neurons (ps > 0.05). Fast-firing glutamatergic neurons were located in all parts of the MS-DBB with the greatest concentration near the midline (**Fig. 6*B***). The relative locations of fast-firing GABAergic MS-DBB neurons were similar (**Fig. 7*B***).

Figure 7

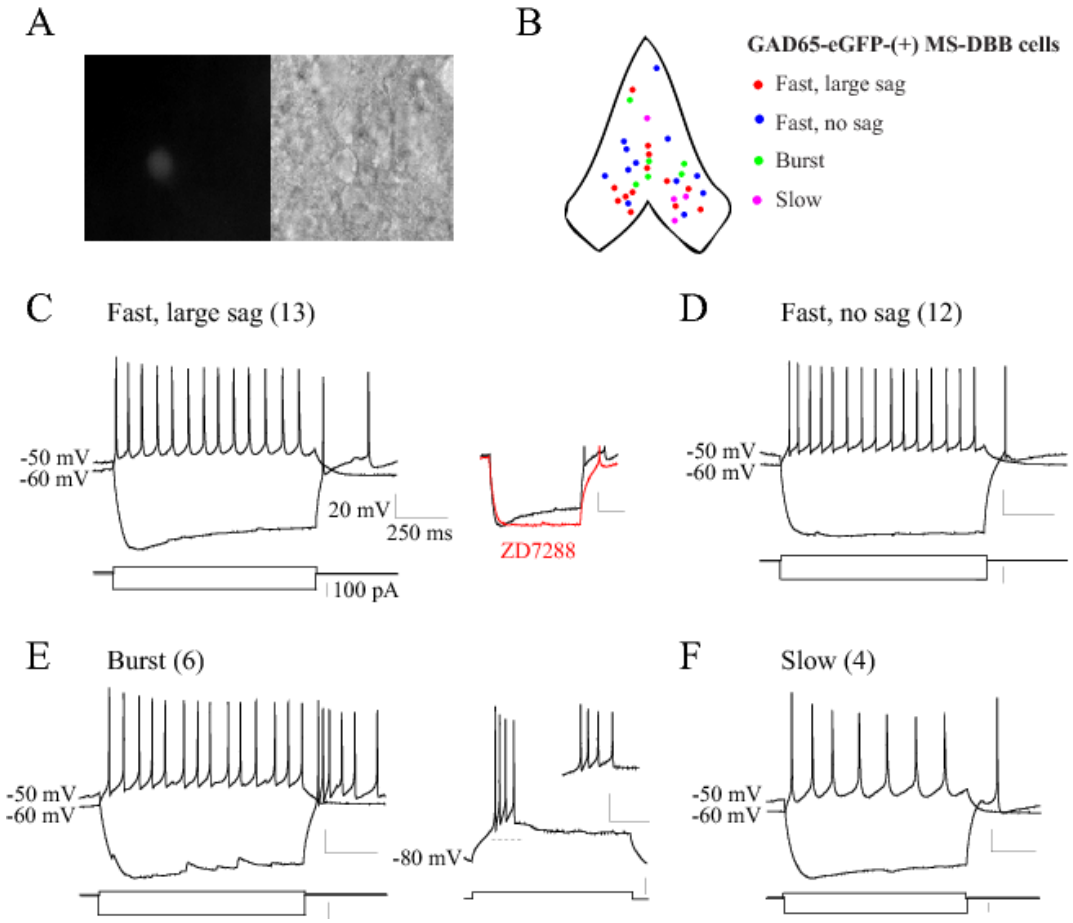
A
B
GAD65-eGFP-(+) MS-DBB cells
Fast, large sag
Fast, no sag
Burst
Slow
C
Fast, large sag (13)
-50 mV
-60 mV
20 mV
250 ms
100 pA
ZD7288
D
Fast, no sag (12)
-50 mV
-60 mV
E
Burst (6)
-50 mV
-60 mV
-80 mV
F
Slow (4)
-50 mV
-60 mV

Figure 7. Electrophysiological characteristics of GABAergic MS-DBB neurons. ***A,*** A GAD65-eGFP-(+) MS-DBB neuron expressing fluorescence in the soma in an acute slice. ***B,*** Approximate locations of recorded GAD65-eGFP-(+) neurons in the MS-DBB are indicated, colour-coded by firing pattern; fast- and burst-firing cells were located close to the midline, slow-firing neurons were found in all MS-DBB subregions. ***C,*** In response to hyperpolarizing currents, some fast-firing GABAergic neurons showed a prominent depolarizing sag that was completely blocked by 50μM ZD7288 (inset). ***D,*** Other fast-firing neurons possessed little or no sag. ***E***, Burst-firing GABAergic neurons presented bursts of several action potentials when depolarized from -80 mV (right) but fired regularly from -60 mV (left) and typically showed a large sag. ***F,*** Slow-firing GABAergic neurons fired in a tonic manner at a low rate. Numbers in brackets indicate number of cells. Scale bars, 20 mV, 250 ms (voltage traces), 100 pA (current steps).

Table 2. Electrophysiological properties of GAD65-eGFP-(+) MS-DBB neurons in coronal mouse brain slices, N = 35 neurons

Firing pattern	Fast-firing		Burst-firing	Slow-firing
	Large sag	No sag		
n (% of N)	13 (37.1%)	12 (34.3%)	6 (17.4%)	4 (11.4%)
Vrest (mV)	-44.7 ± 0.8*	-46.9 ± 1.8	-43.0 ± 0.9*	-45.5 ± 1.8
Proport. spont. firing	100%	90.9%	100%	100%
Mean frequency (Hz)	5.5 ± 0.7	5.2 ± 0.7	6.7 ± 1.9	4.0 ± 0.4
Range (Hz)	1 - 10	2 - 10	3 - 16	3 - 5
Mean firing rate (Hz)	17.4 ± 3.5	10.8 ± 0.8	19.0 ± 4.4	6.0 ± 0.7
$F_{INITIAL}$ (Hz)	21.2 ± 4.2	13.3 ± 1.1	24.2 ± 8.2	6.3 ± 1.3
F_{FINAL} (Hz)	15.4 ± 3.2	10.4 ± 0.9	17.5 ± 2.5	6.3 ± 1.3
Spike freq. accom. (%)	23.9 ± 7.6	20.8 ± 5.8	13.1 ± 9.1	-12.5 ± 31.5
Spike threshold (mV)	-43.5 ± 0.7	-43.3 ± 1.6	-44.4 ± 1.9	-40.7 ± 1.5
Spike amplitude (mV)	79.7 ± 1.8	78.4 ± 2.7	71.9 ± 2.5	78.8 ± 3.4
Spike half-width (ms)	1.4 ± 0.1	1.5 ± 0.2	1.1 ± 0.0	1.8 ± 0.4
AHP amplitude (mV)	6.7 ± 0.7	6.7 ± 1.1	4.0 ± 0.4	8.4 ± 2.2
AHP duration (ms)	305.3 ± 31.4 [b]	277.9 ± 22.9	154.6 ± 76.7 [fs,s,*]	370.4 ± 55.6 [b]
Sag amplitude (mV)	16.1 ± 1.8 [f]	5.4 ± 0.9 [fs]	10.9 ± 2.2*	9.4 ± 3.9
Rebound spike delay (ms)	119.1 ± 34.4 [s]	170.9 ± 46.8 [s]	71.4 ± 13.2 [s]	418.9 ± 217.6 [fs,f,b,*]
Sag activation time (ms)	159.9 ± 19.4	-	165.5 ± 22.5	-
Sag decay constant (ms)	217.2 ± 18.1	-	252.2 ± 20.8	-
Intraburst freq. (Hz)	-	-	42.5 ± 10.7	-
# spikes per burst	-	-	3.3 ± 0.4	-
LTS amplitude (mV)	-	-	8.1 ± 0.8*	-
LTS duration (ms)	-	-	314.6 ± 72.5	-

[fs, f, b, s, *] * Statistically significant differences ($p < 0.05$) are indicated: [fs] *versus* fast-firing cells with large sag; [f] *versus* fast-firing cells with no sag; [b] *versus* burst-firing cells; [c] *versus* slow-firing cells; * *versus* VGLUT2-eGFP-(+) cells with a similar firing pattern. Mean value ± S.E.

The third firing pattern displayed by glutamatergic MS-DBB neurons was burst-firing (11/66). Burst-firing cells were characterized by firing of several action potentials together on top of a noticeable depolarizing hump (low threshold spike or LTS) when released from a hyperpolarized potential of -80 mV (**Fig. 6*F*, right**) but firing regularly when depolarized from -60 mV (**Fig. 6*F*, left**). Burst-firing glutamatergic neurons were mostly quiescent or firing very little at rest. When depolarized, they displayed a relatively low mean firing rate (9.1 ± 0.9 Hz) and moderate frequency accommodation (37 ± 9 %). All burst-firing glutamatergic neurons expressed little or no sag upon hyperpolarization, a characteristic clearly distinct from burst-firing GABAergic neurons that showed significantly larger depolarizing sag ($p < 0.05$; **Fig. 7*E*, left**). Other parameters that differed between burst-firing glutamatergic *vs*. GABAergic neurons were Vrest, AHP duration, LTS amplitude (ps < 0.05) and LTS duration (marginally significant; $p = 0.06$; **Tables 1-2**). Interestingly, burst-firing glutamatergic MS-DBB neurons were located in the lateral regions similar to cluster-firing cells (**Fig. 6*B***) whereas burst-firing GABAergic MS-DBB neurons were predominantly located close to the midline (**Fig. 7*B***).

Lastly, some glutamatergic MS-DBB neurons displayed slow-firing properties (11/66). Almost all slow-firing neurons (9/11) were silent at rest. When depolarized, they fired regularly at a low rate (5.3 ± 0.3 Hz) with some frequency accommodation (27 ± 12 %; **Fig. 6*G***). Slow-firing glutamatergic neurons displayed wider action potentials (greater spike half-width) than other glutamatergic cell types but the difference was found to be statistically significant only with burst-firing glutamatergic neurons ($p < 0.05$). When hyperpolarized, most slow-firing cells (10/11) displayed little or no sag. Slow-firing was also observed in a subset of GABAergic MS-DBB neurons (**Fig. 7*F***) and the two slow-firing groups were electrophysiologically similar. Slow-firing neurons were found in all subregions of the MS-DBB for both glutamatergic and GABAergic neurons (**Fig. 6*B* and Fig. 7*B***).

These results demonstrate that glutamatergic MS-DBB neurons display a highly heterogeneous set of firing patterns. Cluster-firing is unique to glutamatergic neurons but fast-firing glutamatergic neurons are electrophysiologically virtually identical to fast-firing GABAergic neurons. Burst- and slow-firing glutamatergic neurons also share many similarities with their GABAergic counterparts.

3.2. Experiment 2: A proportion of glutamatergic MS-DBB neurons show a highly rhythmic spontaneous firing pattern

Given that some glutamatergic MS-DBB neurons show fast-firing characteristics, a prominent I_h and are spontaneously active, we next examined whether such glutamatergic MS-DBB neurons have the intrinsic capacity to fire rhythmically in theta-range frequencies at rest. Such rhythmic properties are important to investigate since they could contribute to the 'theta rhythm generator' capacity traditionally attributed to the MS-DBB (Buzsaki, 2002). Previous studies using rat slices have reported that neurochemically unidentified fast-firing MS-DBB neurons are often spontaneously active (Morris et al., 1999; Henderson et al., 2001) but the rhythmic nature of the spontaneous firing has not been examined. Our aim was to compare the rhythmic firing properties of spontaneously active fast-firing glutamatergic *vs.* GABAergic neurons. To this end, we examined the spontaneous firing of each cell at its resting membrane potential acquired at the start of recording of each cell. If the cell displayed stable spontaneous firing at 4 – 12 Hz (for criteria of stable recordings, see Methods), the voltage trace containing the spontaneous spikes was further analyzed to construct an ISI histogram and an autocorrelogram. From the autocorrelogram, the 'theta index' was calculated (**Fig. 8*B***) which is a measure of how regularly and rhythmically a cell's spontaneous spikes occurred and gives values between 0

(arrhythmic) and 1 (rhythmic). It was also verified whether these spontaneously active neurons were driven by synaptic inputs by examining synaptic potentials at -70 mV.

We found that 21% of the fast-firing glutamatergic MS-DBB neurons recorded (6/29) fired spontaneously at 4 – 12 Hz. The remaining fast-firing MS-DBB neurons showed little (<4 Hz) or no spontaneous firing. Among the fast-firing glutamatergic cells that fired spontaneously at theta frequencies, the mean spontaneous firing rate was 8.6 ± 0.6 Hz and the theta index varied between 0.56 and 1 (mean: 0.84 ± 0.07). When held at -70 mV, spontaneous synaptic potentials could be detected in some cells but these events were infrequent (0 – 3 Hz) and non-rhythmic, indicating that the rhythmic spontaneous firing is probably an intrinsic property and not a result of rhythmic extrinsic input. **Figure 8*Ai*** shows a fast-firing glutamatergic MS-DBB neuron that displayed highly rhythmic spontaneous firing that was maintained for at least 30 s at Vrest of -50 mV but the cell revealed very little synaptic activity at -70 mV. Notably, the interval between the spikes remained exceptionally uniform throughout the recording, leading to well-defined clear peaks in the autocorrelogram (theta index of 1; **Fig. 8*Aii***). **Figure 9*Ai*** illustrates an example of another fast-firing glutamatergic MS-DBB cell that fired less rhythmically, indicated by broader peaks in the autocorrelogram and theta index of 0.68.

Figure 8

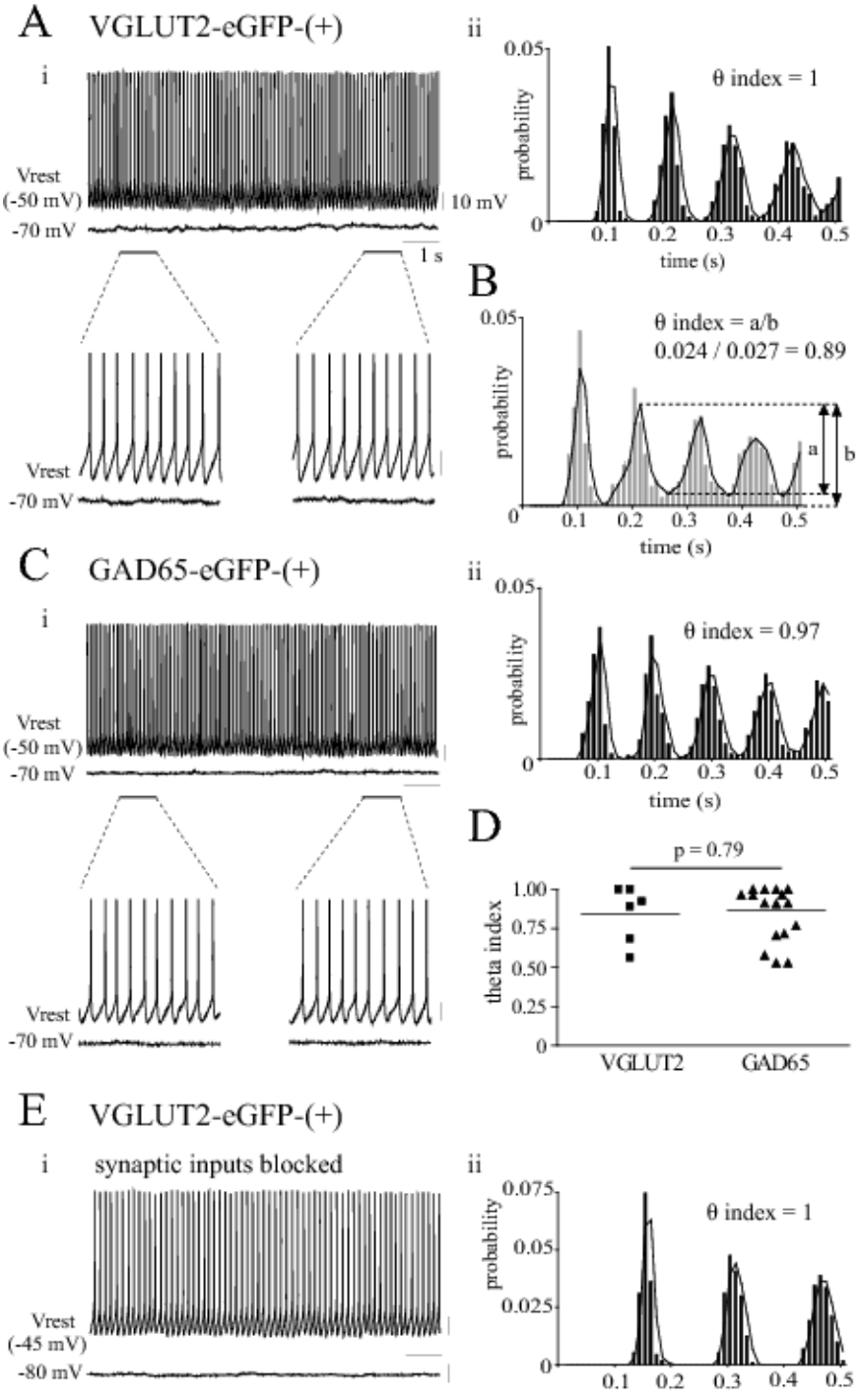
A
VGLUT2-eGFP-(+)
i
ii
Vrest
(-50 mV)
-70 mV
10 mV
1 s
θ index = 1
probability
time (s)
B
θ index = a/b
0.024 / 0.027 = 0.89
a
b
C
GAD65-eGFP-(+)
θ index = 0.97
D
p = 0.79
theta index
VGLUT2
GAD65
E
VGLUT2-eGFP-(+)
synaptic inputs blocked
Vrest
(-45 mV)
-80 mV

Figure 8. Rhythmic spontaneous firing of glutamatergic and GABAergic MS-DBB neurons. ***Ai***, A subset of fast-firing glutamatergic MS-DBB neurons displayed highly rhythmic spontaneous firing in theta frequencies that was not driven by rhythmic extrinsic input (top: raw continuous voltage traces for 10 s at Vrest and at -70 mV, bottom: two 1-s segments enlarged to show the extremely regular spontaneous firing and the lack of rhythmic synaptic input). ***ii***, The autocorrelogram of the spontaneous spikes recorded for 30 s with the theta index value indicated. Notice the clearly defined peaks and the high theta index value, indicating highly rhythmic spontaneous firing. ***B***, The theta index was calculated from the autocorrelogram, defined as the ratio 'a/b' where 'b' is the amplitude of the second peak and 'a' is the amplitude of the rhythmic portion of the second peak. ***Ci-ii,*** Some fast-firing GABAergic MS-DBB neurons also showed highly rhythmic spontaneous firing. ***D,*** A scatter plot of theta index values for glutamatergic and GABAergic MS-DBB neurons shows that the degree of rhythmicity in spontaneous firing was not significantly different between the two groups. ***Ei-ii,*** Glutamatergic MS-DBB neurons showed highly rhythmic spontaneous firing in the presence of blockers for synaptic inputs (10 μM DNQX, 5 μM bicuculline, 5 μM tubocurarine, 25 μM DL-AP5, 10 μM atropine). Scale bars, 10 mV, 1 s.

Figure 9

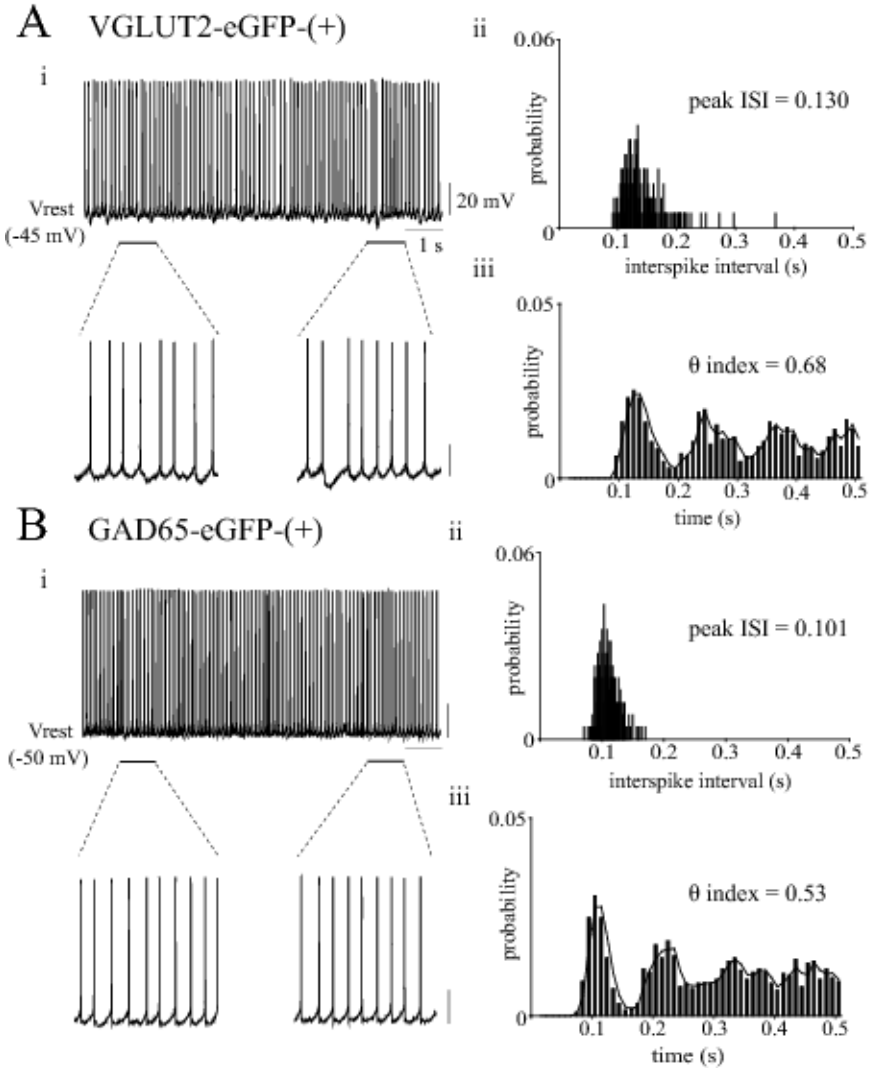
A
VGLUT2-eGFP-(+)
i
ii
iii
Vrest
(-45 mV)
20 mV
1 s
peak ISI = 0.130
probability
interspike interval (s)
θ index = 0.68
time (s)
B
GAD65-eGFP-(+)
Vrest
(-50 mV)
peak ISI = 0.101
θ index = 0.53

Figure 9. Examples of less rhythmic spontaneous firing by glutamatergic and GABAergic MS-DBB neurons. ***Ai,*** Some fast-firing glutamatergic MS-DBB neurons displayed spontaneous firing in theta frequencies but the firing was not very rhythmic (top: raw continuous voltage traces for 10 s at Vrest, bottom: two 1-s segments have been enlarged). ***ii,*** The ISI histogram of the spontaneous spikes recorded for 30 s with the peak ISI value indicated. ***iii,*** The autocorrelogram of the same dataset with the theta index value indicated. A larger spread in the ISI distribution, broader peaks in the autocorrelogram and the low theta index value illustrate the relative irregularity in this cell's spontaneous firing. ***Bi-iii,*** Some fast-firing GABAergic MS-DBB neurons also showed less rhythmic spontaneous firing in theta frequencies. Scale bars, 20 mV, 1 s.

As for the GABAergic MS-DBB neurons, 75% of fast-firing GABAergic neurons recorded (18/24) fired spontaneously in theta-range frequencies. The mean spontaneous firing rate among these cells was 6.3 ± 0.5 Hz and the mean theta index was 0.87 ± 0.04 (for examples of GABAergic cells' spontaneous firing, see **Fig. 8*C* and 9*B***). Theta index values were not significantly different between glutamatergic and GABAergic neurons ($p = 0.79$; **Fig. 8*D***) illustrating that the degree of rhythmicity in spontaneous firing was similar between glutamatergic and GABAergic neurons. These results suggest that both glutamatergic and GABAergic MS-DBB neurons fire rhythmically at rest but more GABAergic neurons exhibit this property. In all cases, spontaneous firing was in the form of repetitive single spikes and rhythmic burst-firing was not observed at rest in glutamatergic or GABAergic cells, consistent with other *in vitro* studies (Griffith, 1988; Henderson et al., 2001).

In order to demonstrate that the rhythmic spontaneous firing is an intrinsic property, we recorded from glutamatergic and GABAergic MS-DBB cells in the presence of blockers for both excitatory and inhibitory synaptic inputs (10 μM DNQX, 5 μM bicuculline, 5 μM tubocurarine, 25 μM DL-AP5, 10 μM atropine). Out of five fast-firing glutamatergic neurons tested, two exhibited spontaneous firing in theta frequencies (6.5 and 5.6 Hz) that was highly rhythmic (theta index of 1 and 0.98, respectively). **Figure 8*E*** shows the rhythmic spontaneous spikes and the lack of synaptic potentials displayed by one of the glutamatergic neurons in the presence of the blockers and the resulting autocorrelogram. As for GABAergic neurons, four out of five fast-firing cells displayed spontaneous firing in the theta range (4.6 – 11.4 Hz) with varying degrees of rhythmicity (theta index of 0.56 – 1) in the presence of the blockers. Two of these GABAergic neurons exhibited highly rhythmic spontaneous spikes (theta index of 1 and 0.94; data not shown).

Altogether, these results demonstrate that a subset of fast-firing glutamatergic MS-DBB neurons exhibit intrinsic spontaneous firing in theta-range

frequencies that is as rhythmic as that displayed by fast-firing GABAergic cells, suggesting that they may be able to provide rhythmic excitatory input locally and potentially contribute to hippocampal oscillations.

III.4. Discussion

It has been generally assumed that in the MS-DBB, slow-firing neurons are cholinergic while other firing patterns such as fast- and burst-firing correspond to GABAergic neurons (Jones et al., 1999; Henderson et al., 2001). Here, we demonstrate that glutamatergic MS-DBB neurons as a population exhibit a highly heterogeneous set of firing patterns with a significant proportion (47%) displaying fast-firing properties that are virtually indistinguishable from fast-firing GABAergic cells. Our finding of fast-firing glutamatergic MS-DBB neurons is supported by recent evidence that some VGLUT2-eGFP-(+) MS-DBB neurons express Kv3.1b (Henderson et al., 2010), a delayed rectifier channel involved in rapid spike repolarization common to fast-spiking CNS neurons (Rudy and McBain, 2001). We also demonstrate that in response to hyperpolarizing currents, an important subset (39%) of fast-firing glutamatergic MS-DBB neurons exhibit prominent depolarizing sag mediated by I_h with amplitude, kinetics and pharmacological profile similar to those of GABAergic MS-DBB neurons. Given previous reports that blocking I_h in the MS-DBB substantially decreases the frequency of hippocampal theta rhythm *in vivo* (Kocsis and Li, 2004), our results suggest that I_h-expressing GABAergic and glutamatergic MS-DBB neurons may both participate in hippocampal theta oscillations.

Importantly, we found that some electrophysiological characteristics could be used to distinguish between glutamatergic and GABAergic MS-DBB neurons. Namely, the only firing pattern unique to glutamatergic neurons was cluster-firing interspersed with subthreshold membrane oscillations, in line with Sotty and

colleagues (2003) that also detected cluster-firing only in MS-DBB neurons solely expressing glutamatergic markers (VGLUT transcripts). Some glutamatergic neurons exhibited burst-firing that is distinct from burst-firing observed in GABAergic cells, similar to the two types of burst-firing reported by Henderson et al. (2001). Subsets of glutamatergic and GABAergic neurons displayed slow-firing pattern with broad action potentials similar to cholinergic MS-DBB neurons (Gorelova and Reiner, 1996; Sotty et al., 2003) but a direct comparison with cholinergic neurons was not done here. Taken together, cluster-firing may be used as an electrophysiological marker for glutamatergic neurons in the MS-DBB, whereas fast- and burst-firing patterns alone may not be used as reliable indicators for glutamatergic or GABAergic MS-DBB neurons.

The MS-DBB has long been thought of as an important rhythm generator for the hippocampus (Buzsaki, 2002) because *in vivo* many MS-DBB cells fire rhythmically phase-locked to hippocampal oscillations (Stewart and Fox, 1989) and lesions of the MS-DBB cause large reductions in the power of hippocampal theta (Green and Arduini, 1954; Lee et al., 1994; Yoder and Pang, 2005). These lines of evidence have been taken to indicate that rhythmic MS-DBB neurons are critically involved in hippocampal theta rhythm. GABAergic MS-DBB neurons have been identified to account for some of the rhythmic cells *in vivo* (Borhegyi et al., 2004; Simon et al., 2006) but it remains unknown whether glutamatergic MS-DBB neurons also fire rhythmically during hippocampal theta. Rhythmic firing by glutamatergic neurons have previously been demonstrated in other areas of the basal forebrain *in vivo* (Manns et al., 2003). It has also been reported that some non-cholinergic, non-GABAergic MS-DBB neurons fire tonically or in clusters during *in vivo* hippocampal theta (Simon et al., 2006). If glutamatergic neurons fire rhythmically during network oscillations, it remains to be demonstrated whether the rhythmic firing is due to intrinsic membrane properties, extrinsic factors or a combination of both. Earlier reports using extracellular and sharp electrodes have noted that some

spontaneously active MS-DBB neurons appear to be rhythmic (Segal, 1986; Morris et al., 1999; Henderson et al., 2001) but the neurochemical identity of these neurons and quantification of their rhythmicity have not been explored. Our results revealed that subsets of both glutamatergic and GABAergic MS-DBB neurons show highly rhythmic spontaneous firing in the theta range that is not driven by extrinsic rhythmic inputs, suggesting that some MS-DBB neurons possess intrinsic rhythmic properties. Our results are the first to demonstrate *in vitro* that some glutamatergic and GABAergic MS-DBB neurons may have the intrinsic capacity to be theta rhythm generators.

Chapter IV: Functional glutamatergic septohippocampal projection

IV.1. Introduction

Anatomical studies have estimated that glutamatergic MS-DBB neurons account for 4 – 23% of the septohippocampal projection (Colom et al., 2005; Henderson et al., 2010). While cholinergic and GABAergic septohippocampal projections have been well described, no study has yet demonstrated the functional significance of the glutamatergic projection. To this aim, we used a septohippocampal preparation where a half-septum, the ipsilateral hippocampus and the interconnecting fornix-fimbria fibers are preserved in an *in vitro* preparation. A previous study used a comparable *in vitro* preparation where a thick slice contained both the septum and the hippocampus (Tóth et al., 1997) but the experiments were carried out in the presence of blockers for glutamatergic receptors, so glutamatergic responses were not observed. The septohippocampal preparation employed here has been used previously to study septohippocampal interactions (Goutagny et al., 2008; Manseau et al., 2008). Here, we demonstrate that activating the MS-DBB can elicit functional glutamatergic responses in CA3 pyramidal cells in two ways: electrical stimulation of the septohippocampal fibers (Experiment 1) and direct chemical activation of MS-DBB neurons via NMDA microinfusions (Experiment 2).

IV.2. Materials and Methods

Animals

Wild-type CFW mice (12- to 18-d-old) were used unless otherwise stated. For a control experiment to test the effect of NMDA microinfusions on glutamatergic MS-DBB neurons, 12- to 18-d-old VGLUT2-eGFP transgenic mice were used (for more details about this mouse line, please see Chapter 2, Section

2.2).

Septohippocampal preparation

The acute preparation containing a hemiseptum, ipsilateral hippocampus and fornix-fimbria fibers were dissected as described previously (Manseau et al., 2008). After decapitation, the brain was quickly removed and placed in ice-cold high-sucrose solution (same composition as in Chapter 3 slice preparation). From a hemisected brain, the septum and hippocampus along with the interconnecting fibers were carefully dissected out using a microspatula and the surface of the hippocampus was cut at an angle to expose the pyramidal layer of CA3. Each septohippocampal preparation was left to rest in aCSF (1 mM $CaCl_2$) at room temperature for 1 – 2 h before recording. The preparation was oriented in the recording chamber as shown in **Figure 10*Ai*** to allow direct access of the recording pipette to the CA3 pyramidal layer and perfused with standard aCSF (2 mM $CaCl_2$) at 2-3 ml/min. Pyramidal cells were identified visually by the location of their soma in the pyramidal layer (**Fig. 10A*iii***) and electrophysiologically by their slow-firing tendencies (**Fig. 10A*ii***).

For electrical stimulation experiments, a monopolar tungsten microelectrode (World Precision Instruments, Sarasota, FL) was placed in the septal end of the fornix and stimulation parameters were controlled by an isolated pulse stimulator (model A360, WPI). One to three current pulses (400 μA, 100 μs duration, separated by 20 ms) were administered at 10-s intervals to detect evoked responses in CA3 pyramidal neurons. In some cases, single stimuli at different intensities (25 – 400 μA) or multiple stimuli at various frequencies (1 – 6 Hz) were given. For analysis, only the recordings from those preparations where septohippocampal connections were demonstrated to be intact (*i.e.*, preparations where at least one CA3 cell showed a response to fornix stimulation) were included.

Figure 10

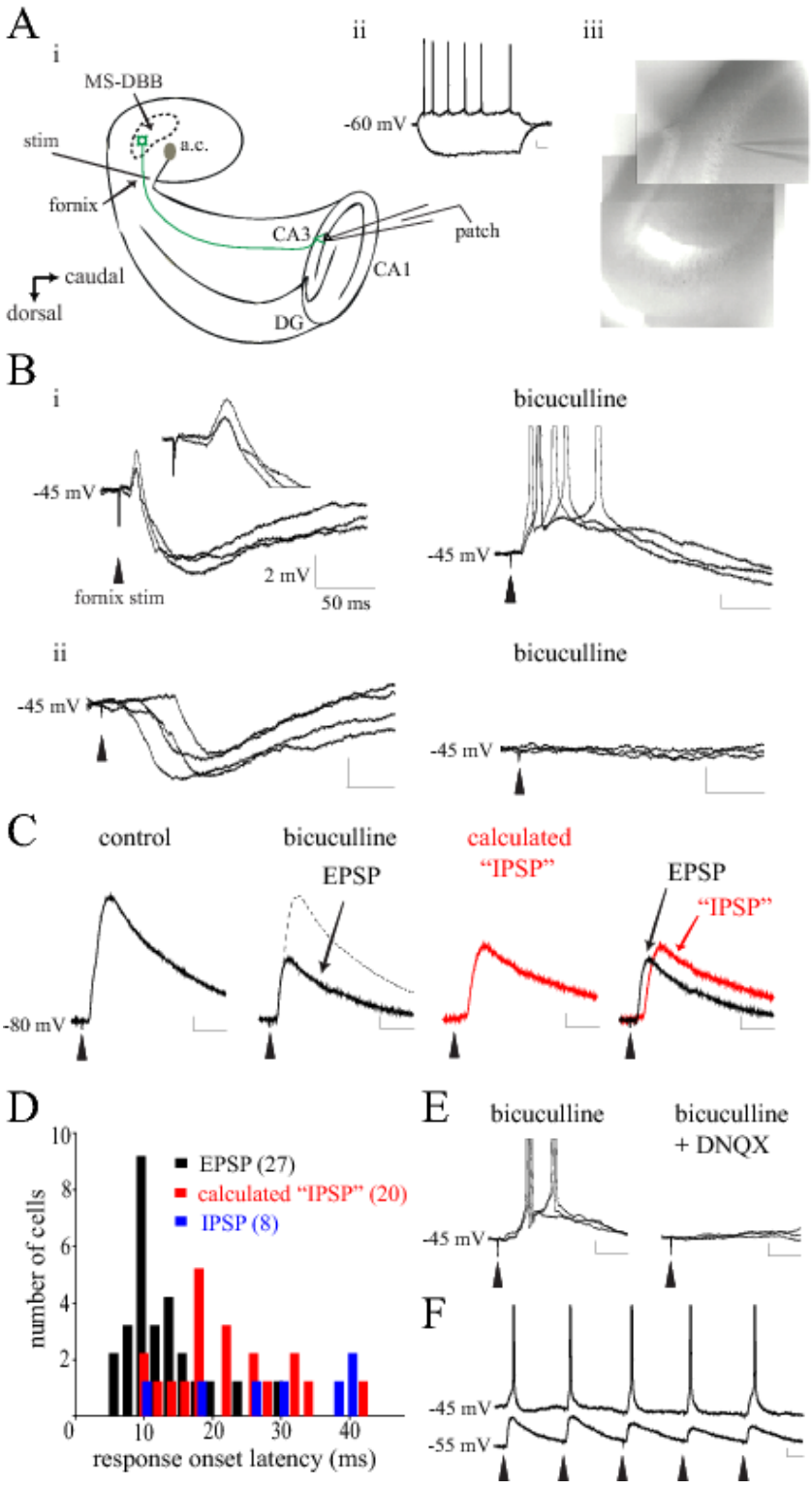
A
i
MS-DBB
stim
a.c.
fornix
CA3
CA1
patch
caudal
dorsal
DG
ii
-60 mV
iii
B
i
-45 mV
2 mV
50 ms
fornix stim
bicuculline
-45 mV
ii
-45 mV
bicuculline
-45 mV
C
control
bicuculline
EPSP
calculated
"IPSP"
EPSP
"IPSP"
-80 mV
D
number of cells
EPSP (27)
calculated "IPSP" (20)
IPSP (8)
response onset latency (ms)
E
bicuculline
bicuculline
+ DNQX
-45 mV
F
-45 mV
-55 mV

Figure 10. Electrical stimulation of septohippocampal fibers induced fast-onset glutamatergic responses in CA3 pyramidal cells. ***Ai***, The septohippocampal preparation containing a hemiseptum, ipsilateral hippocampus and intact fornix-fimbria pathway was cut at an angle to reveal the CA3 pyramidal layer and placed in the recording chamber as shown. A stimulating electrode was positioned on the septal side of the fornix and CA3 pyramidal cells were recorded using a patch pipette. CA3 pyramidal cells were identified by their location (***iii***) and electrophysiological criteria (***ii;*** Scale bars, 20 mV, 250 ms). ***Bi,*** At -45 mV, in most cases fornix stimulation led to both an early-onset EPSP (inset) and a late-onset IPSP. Applying bicuculline (5 μM) revealed a potent EPSP that could depolarize some pyramidal cells to spike threshold (right). ***ii***, Some pyramidal cells responded with only the late-onset IPSP that was blocked by bicuculline. The EPSP was mediated by glutamate as it was completely blocked by 20 μM DNQX (***E***), and repeated stimuli at 5 Hz could evoke rhythmic EPSPs (***F***). ***C,*** In those cells displaying both EPSP and IPSP, bicuculline was applied to isolate the EPSP and this component was subtracted from control to calculate the "IPSP" component. ***D,*** Examination of the onset latencies for EPSPs, calculated IPSPs, *vs.* actual IPSPs indicates that the EPSPs occurred with a significantly faster onset compared to the other responses (*p*s <0.0001). Numbers in brackets indicate number of cells. Scale bars unless otherwise noted, 2 mV, 50 ms.

Experiments with local NMDA microinfusions required the use of a puffer pipette (a patch pipette gently broken at the tip to achieve resistance of ~1 MΩ) positioned with the tip touching the MS-DBB area in the septohippocampal preparation (**Fig. 11*Ai***). The puffer pipette was loaded with 20 – 30 µl of NMDA dissolved in normal aCSF at a final concentration of 200 µM and controlled by a picospritzer system (Medical Systems, Greenvale, NY). Single or sets of three pressure pulses (10 – 30 p.s.i., 100 ms duration, separated by 200 ms) were applied at 20-s intervals to examine responses in nearby MS-DBB neurons or in CA3 pyramidal cells. A maximum of 30 NMDA puffs were applied in each preparation to minimize toxicity and physical damage. For both fornix stimulation and NMDA infusion experiments, a minimum of three responses were averaged to calculate the mean amplitude and latency of the response for each cell. DNQX (20 µM) or bicuculline (5 µM) were applied to identify the neurotransmitter involved.

Statistical analysis

Data are presented as mean ± standard error of the mean, unless otherwise stated. Electrophysiological data were plotted and analyzed using Clampfit (Molecular Devices, Sunnyvale, CA) and Prism 4 (GraphPad Software, San Diego, CA). Statistical tests used were Student's t test, ANOVA, post-hoc Newman-Keuls. p values of <0.05 were considered to be statistically significant.

IV.3. Results

3.1. Experiment 1: Electrical stimulation of fornix fibers lead to glutamatergic responses in hippocampal neurons

We investigated whether glutamatergic MS-DBB neurons send functional

projections to the hippocampus, using the septohippocampal preparation. As shown in **Figure 10*Ai***, a stimulating electrode was placed on the septal side of the fornix bundle to electrically stimulate septohippocampal fibers and postsynaptic responses were examined in CA3 pyramidal cells. In 62 CA3 pyramidal cells, electrical stimulation of the fornix (400 μA, 100 μs duration) led to consistent time-locked postsynaptic responses in 46 cells. No clear response was observed in the remaining 16 cells. Among the 46 cells with a response, at the holding potential of -45 mV, 34 cells displayed a mixture of EPSP and IPSP (**Fig. 10*Bi***), 11 cells showed only IPSP (mediated by GABA release, see **Fig. 10*Bii***) and 1 cell showed EPSP only. **Figure 10*Bi*** illustrates an example of a CA3 pyramidal cell that displayed both EPSP and IPSP. Fornix stimulation led to an early-onset EPSP followed by a late-onset IPSP and the different timing and direction of these two responses were clearly visible at -45 mV (EPSP: early/depolarizing, IPSP: late/hyperpolarizing).

For those cells displaying both EPSP and IPSP, 5 μM bicuculline was applied to block the IPSP and reveal the EPSP more clearly (**Fig. 10*Bi*, right**). In the presence of bicuculline, the EPSP triggered action potentials from -45 mV in 17/34 pyramidal cells tested. When stimulation of various intensities were tested (25 – 400 μA), we found that stronger stimuli led to systematically larger EPSPs in 14/14 cases (25 μA: 0.7 ± 0.3 mV; 400 μA: 6.3 ± 1.2 mV; one-way ANOVA, $p = 0.0008$; data not shown). DNQX (20 μM) completely blocked EPSPs in 6/6 cells tested (**Fig. 10*E***) confirming that they were mediated by glutamate release. Finally, repeated fornix stimulations given at 5 Hz could reliably evoke rhythmic EPSPs in 5/7 cells, leading to spikes that faithfully followed each stimuli in one cell (**Fig. 10*F***). These results demonstrate that electrical stimulation of the septohippocampal pathway can induce glutamatergic postsynaptic responses in a significant proportion (35/62; 56%) of CA3 pyramidal cells.

Figure 11

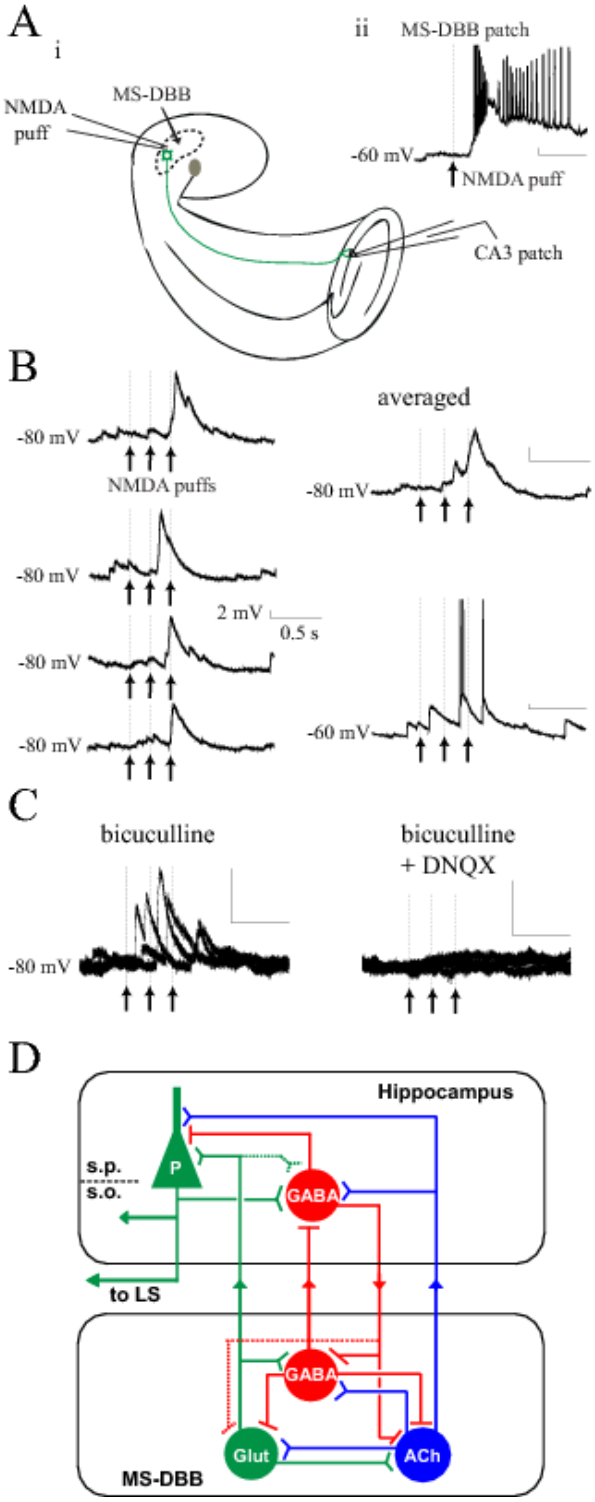
A
i
ii
MS-DBB patch
NMDA puff
MS-DBB
-60 mV
NMDA puff
CA3 patch
B
averaged
-80 mV
NMDA puffs
-80 mV
2 mV
0.5 s
-80 mV
-80 mV
-80 mV
-60 mV
C
bicuculline
bicuculline
+ DNQX
-80 mV
D
Hippocampus
s.p.
s.o.
P
GABA
to LS
GABA
Glut
ACh
MS-DBB

Figure 11. Local NMDA microinfusions to the MS-DBB triggered glutamatergic responses in CA3 pyramidal cells. ***Ai***, In the septohippocampal preparation, MS-DBB neurons were locally activated by infusing small amounts of NMDA directly into the MS-DBB area using a puffer pipette while recording from CA3 pyramidal cells. ***ii,*** A single NMDA application (200 μM, 100 ms) robustly depolarized a nearby VGLUT2-eGFP-(+) MS-DBB neuron. ***B,*** CA3 pyramidal cells responded to NMDA injections in the MS-DBB with EPSPs that were clearly time-locked to the stimuli (left: four consecutive trials at -80 mV, right top: averaged trace at -80 mV, right bottom: a raw trace at -60 mV). ***C,*** The EPSPs were abolished by 20 μM DNQX indicating that the response was mediated by glutamate. ***D,*** A new model of the septohippocampal network: a subset of glutamatergic MS-DBB neurons may serve as intrinsic rhythm generators that can contribute a functional rhythmic excitatory drive to the local septal network as well as to the hippocampus. In the model, solid lines represent physiologically confirmed pathways and dotted lines indicate pathways that remain to be demonstrated.

Importantly, the timing of EPSPs *vs.* IPSPs evoked by the fornix stimulation was different. In order to measure the onset latency of the two types of responses in CA3 pyramidal cells, fornix stimulation was given while the cells were held at -80 mV (a membrane potential where NMDA receptor-mediated currents are null). In those cells that exhibited both EPSP and IPSP, bicuculline was applied to isolate the EPSP, and the EPSP component was subtracted from the control trace to obtain the IPSP mediated by $GABA_A$ receptors (**Fig. 10*C***). When EPSPs, subtracted IPSPs and actual IPSPs (responses recorded from cells that showed only IPSPs upon fornix stimulation) were compared, the mean onset latency of EPSPs was significantly shorter than that of subtracted IPSPs or actual IPSPs (13.3 ± 1.0 ms, 22.2 ± 1.8 ms, 33.1 ± 5.3 ms, respectively; *ps* <0.0001; see **Fig. 10*D***). The peak amplitudes of EPSPs, subtracted IPSPs and actual IPSPs evoked by a 400-μA stimulus were 6.1 ± 1.1 mV, 4.8 ± 0.5 mV, 6.5 ± 0.7 mV, respectively.

3.2. Experiment 2: Local activation of MS-DBB neurons leads to glutamatergic responses in hippocampal neurons

It may be argued that electrical stimulation of the fornix not only activates septohippocampal pathway but also hippocamposeptal fibers. Pyramidal cells of the hippocampus send important projections to the lateral septum (Linke et al., 1995) and the antidromic activation of the axons of CA3 pyramidal cells may partly contribute to the postsynaptic glutamatergic responses reported here (*i.e.*, indirectly through CA3 recurrent collateral synapses). Although we believe that this is unlikely because antidromic activation was never observed in 62 CA3 pyramidal cells recorded, we decided to use local chemical activation of MS-DBB neurons to elicit monosynaptic responses in CA3 pyramidal cells. To do this, we used a puffer pipette to infuse small amounts of NMDA directly in the MS-DBB

in the septohippocampal preparation and concomitantly recorded from CA3 pyramidal cells (**Fig. 11*Ai***). First, we tried the NMDA puffs and recorded from VGLUT2-eGFP-(+) MS-DBB neurons close to the puffer pipette to test whether glutamatergic neurons are stimulated by NMDA. We confirmed that local NMDA applications (200 μM, 100 ms duration) led to prolonged depolarizations and firing of multiple action potentials in 7/12 glutamatergic MS-DBB cells tested (**Fig. 11*Aii***).

Out of 48 CA3 pyramidal cells recorded we found that applying NMDA locally in the MS-DBB (3 puffs given at inter-puff intervals of 200 ms) clearly evoked time-locked EPSPs in 6 cells. The remaining 42 CA3 pyramidal cells showed no apparent response. **Figure 11*B*** demonstrates an example where the EPSPs occurred ~300 ms after the onset of the first NMDA puff during four consecutive trials. When the same cell was held at -60 mV, the EPSPs triggered the cell to fire action potentials, indicating that the response was excitatory. The EPSPs were resistant to bicuculline (5 μM; 4/4 cells tested) but abolished by DNQX (20 μM; 2/2 cases; **Fig. 11*C***) confirming that they were indeed mediated by glutamate release. The mean onset latency of the EPSPs relative to the onset of the first NMDA puff was 265.4 ± 48.9 ms and the mean peak amplitude at -80 mV was 4.4 ± 0.6 mV (6 cells). These results indicate that local activation of MS-DBB cells gives rise to glutamatergic postsynaptic responses in CA3 pyramidal cells and provide the first electrophysiological evidence that the glutamatergic septohippocampal pathway is functional.

IV.4. Discussion

Although previous anatomical studies have estimated that glutamatergic MS-DBB neurons account for 4 – 23% of the septohippocampal projection (Colom et al., 2005; Henderson et al., 2010), no evidence existed until now as to

whether glutamatergic MS-DBB neurons can modulate hippocampal neurons. It may be that the glutamatergic septohippocampal fibers are relatively few in number but they each innervate the target cells heavily, having a large functional impact. In line with this idea, a recent preliminary study showed numerous VGLUT2-positive septohippocampal puncta in close apposition with the soma and proximal dendrites of CA1 and CA3 pyramidal cells and interneurons (Hernandez et al., 2009). Using fornix stimulation and direct activation of MS-DBB neurons, we demonstrate that glutamatergic MS-DBB neurons provide an excitatory synaptic input to CA3 pyramidal cells. Electrical stimulation of septohippocampal fibers evoked glutamate-mediated EPSPs in 56% of the CA3 pyramidal cells tested. Fornix stimulation, however, is subject to non-specific effects because it may also antidromically activate CA3 pyramidal cells or activate other glutamatergic fibers innervating the hippocampus through the fornix originating from the supramammillary area or the nucleus reuniens (Leranth and Kiss, 1996; Nitsch and Leranth, 1996). To circumvent this issue, we used NMDA microinfusions into the MS-DBB to directly stimulate glutamatergic MS-DBB neurons and demonstrated monosynaptic AMPA-receptor-mediated glutamatergic responses in 13% of the CA3 pyramidal cells tested. The lower probability of detecting a response using chemical activation may be because local NMDA puffs affect only a small number of MS-DBB neurons located very close to the puff pipette and/or because NMDA may activate only a proportion of glutamatergic neurons.

It remains to be determined whether hippocampal interneurons receive glutamatergic septal input. We found that fornix stimulation induced late-onset IPSPs in almost all (45/46) CA3 pyramidal cells examined. The IPSPs appeared with relatively long delays and a large variability in the onset suggesting that they probably reflect a multisynaptic response. Considering that GABAergic MS-DBB neurons selectively innervate hippocampal interneurons (Freund and Antal, 1988), it is likely that the IPSPs recorded in pyramidal cells is a result of the activation of

GABAergic interneurons via glutamatergic septal input. Recordings of interneurons during direct stimulation of MS-DBB neurons will be required to resolve this issue.

Finally, our results suggest a unique role of the glutamatergic MS-DBB neurons in septohippocampal network. Cholinergic MS-DBB neurons may provide long-lasting excitation to both pyramidal cells and interneurons while GABAergic MS-DBB neurons transmit short rhythmic inhibition solely to GABAergic interneurons (Tóth et al., 1997). We propose that glutamatergic MS-DBB neurons can induce fast depolarizations that can trigger spiking in hippocampal pyramidal cells. If the fast glutamatergic depolarizations are rhythmic, they could provide a powerful synchronizing input and potentially contribute to hippocampal theta oscillations. Certainly, our results from Chapter 3 support this notion by showing that some glutamatergic MS-DBB neurons may possess the intrinsic capacity to be theta rhythm generators. Previous evidence indicates that glutamatergic MS-DBB neurons can rhythmically excite neighboring neurons within the MS-DBB (Manseau et al., 2005), and blocking glutamatergic transmission in the MS-DBB has been shown to decrease hippocampal theta rhythm power (Leung and Shen, 2004; Bland et al., 2007). Thus, the role of the glutamatergic neurons may be to contribute a rhythmic excitatory drive to the local network as well as to the hippocampus (**Fig. 11*D***). An approach involving selective inhibition or elimination of glutamatergic MS-DBB neurons will be necessary to determine the exact contribution of these neurons to hippocampal theta and related functions.

The MS-DBB has been classically viewed as the hippocampal theta rhythm generator (Stewart and Fox, 1989; Buzsaki, 2002). However, the role of the MS-DBB in hippocampal theta oscillations must be revised in light of the recent discovery that the hippocampus itself can generate a theta-frequency rhythm independent from the MS-DBB (Goutagny et al., 2009). We therefore suggest that the MS-DBB is one of several extrinsic rhythm generators that

amplify and regulate local theta generators within the hippocampus. Hence, the hippocampal theta rhythm recorded *in vivo* may be a product of several interacting intrinsic and extrinsic theta generators working in concert. It remains to be elucidated what role glutamatergic, GABAergic and cholinergic MS-DBB neurons play in these interactions. A greater understanding of these matters will bring new insights into the mechanisms underlying functions such as spatial learning and memory.

Chapter V: Electrophysiological characterization of CA1 PV and SOM interneurons

V.1. Introduction

In light of the recent evidence that the hippocampus can generate its own theta rhythm (Goutagny et al., 2009), the mechanisms of how such oscillations may arise out of the hippocampal network remain to be investigated. Goutagny and colleagues (2009) showed using pharmacological methods that both the excitatory input from pyramidal cells and the inhibitory input from interneurons are crucial for the generation of the CA1 theta rhythm. Given the huge diversity of interneurons in the CA1 area in terms of morphology, axodendritic projection and protein expression (Freund and Buzsáki, 1996), the contribution of each interneuron subtype to the generation of the network rhythm remains to be worked out in detail. *In vivo,* CA1 interneurons display rhythmic firing patterns that are highly phase-locked to network theta (Klausberger and Somogyi, 2008). Thus, rhythmic inhibitory inputs from the interneurons are thought to synchronize and phasically modulate the firing of CA1 pyramidal cells (Cobb et al., 1995). However, many different types of CA1 interneurons display such rhythmic firing patterns and it is unclear which interneuron subtype plays the primary role as the pacemaker.

It has been suggested that some interneurons may possess intrinsic membrane properties that enable them to generate rhythmic activities. In studies using acute hippocampal slices, a particular class of somatostatin (SOM)-positive CA1 interneurons, O-LM cells, have been shown to fire spontaneously in theta-range frequencies at rest (Maccaferri and McBain, 1996b; Griguoli et al., 2010). O-LM cells are a type of horizontally oriented interneurons whose somata and dendrites are restricted to stratrum oriens/alveus and their axons are found to arborize exclusively in stratum lacunosum-moleculare (LM). O-LM cells' spontaneous theta-frequency firing has been shown to be supported by I_h (Maccaferri and McBain, 1996b; Lupica et al., 2001), a hyperpolarization-

activated current that is associated with CA1 theta rhythm generation *in vitro* (Gillies et al., 2002). Other than playing a role as potential intrinsic theta generators, it has also been suggested recently that O-LM cells may act as theta resonators, producing spike outputs that preferentially follow synaptic inputs modulated at theta frequencies, a property dependent on post-spike afterhyperpolarization kinetics (Kispersky et al., 2012). On the other hand, parvalbumin (PV)-expressing CA1 interneurons with axon arborizations largely limited to stratum pyramidale, the so-called basket cells, have been shown to display fast-firing properties and fast membrane kinetics (Pawelzik et al., 2002). Because of these characteristics, PV basket cells are thought to be critically involved in the generation of gamma-frequency (30 - 150 Hz) network oscillations (Gloveli et al., 2005; Gulyás et al., 2010). The fast-firing properties of PV basket cells are partly mediated by the expression of voltage-gated potassium channels of the Kv3.1b subtype which enable rapid repolarization of action potentials (Rudy and McBain, 2001). Specific types of voltage-gated sodium channels, the Nav1.1 and 1.6 subtypes, have also been found to be expressed by PV interneurons of the hippocampus (Verret et al., 2012).

It remains to be fully investigated the rhythmic properties of specific CA1 interneuron subtypes, especially in the context of the intrinsically generated CA1 theta rhythm. Thus, the aim of the experiments described in this Chapter is to examine the electrophysiological characteristics of parvalbumin (PV)- and somatostatin (SOM)-expressing CA1 interneurons in the intact hippocampal preparation. Electrophysiological characterization of these interneuron classes in this *in vitro* preparation has never been done before and it is an important issue to be addressed, because an intact CA1 network circuitry has been shown to be required for the emergence of spontaneous rhythmic activities (Goutagny et al., 2009). The expression of PV and SOM was chosen for the following reasons. PV interneurons include the fast-spiking PV basket cells, axo-axonic cells as well as some bistratified cells located in stratum pyramidale (Katsumaru et al., 1988;

Baude et al., 2007). PV interneurons innervate pyramidal cells primarily at the level of the soma and proximal dendrites (basket and bistratified) or at the axon initial segment (axo-axonic), so they are collectively referred to as perisomatic-targeting interneurons. On the other hand, SOM interneurons include O-LM cells, bistratified cells as well as some other less commonly encountered subtypes (Katona et al., 1999; Oliva Jr et al., 2000; Losonczy et al., 2002). Since most SOM interneurons target pyramidal cells at the level of the distal dendrites (O-LM) or the proximal dendrites (bistratified), they are called dendrite-targeting interneurons. Therefore, by examining the properties of PV and SOM neurons, we will be able to compare the intrinsic characteristics belonging to perisomatic- *vs.* dendrite-targeting CA1 interneurons. However, it should be noted that some interneuron subtypes have been demonstrated to co-express PV and SOM to some degree (Jinno and Kosaka, 2000). For the purpose of our study, we focus on PV- and SOM- expressing interneurons located in CA1 stratum oriens/alveus (OAIs).

Most previous studies have performed electrophysiological characterizations of unidentified interneurons in acute slices and only determined their cell types afterwards through time-consuming cell reconstruction and immunohistochemical procedures. By taking advantage of the newly available PV-tdTomato and SOM-tdTomato transgenic mice, we are able to visually identify PV- or SOM-expressing neurons at the time of recording and characterize the specific neuron's membrane properties. We performed whole-cell recordings in intact hippocampal preparations which better preserve the OAIs' horizontally oriented dendritic trees, commonly damaged in typical transverse slice configurations (Maccaferri, 2005). In addition, the OAIs are located in the most superficial layer of the intact preparation, making these interneurons easily recordable using the visually guided patch-clamp technique (**Fig. 14*A***).

A

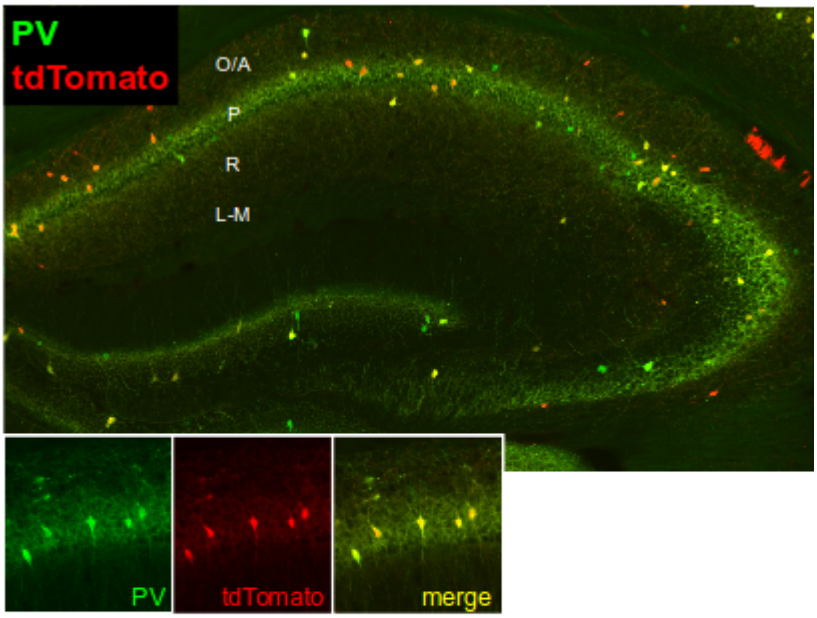

B

PV-tdTomato (n = 4 animals)		
CA1	**% tdTomato+ neurons that are PV+**	**% PV+ neurons that are tdTomato+**
str. oriens	**87.6 ± 5.3 %**	**75.5 ± 2.9 %**
str. pyramidale	**80.1 ± 6.8 %**	**82.6 ± 5.3 %**

Figure 12. The specificity of tdTomato expression in PV-tdTomato mice was examined using PV immunohistochemistry. ***A,*** An image is taken from the middle level of the hippocampus along the septo-temporal axis. The bottom inset shows that the green image is PV immunoreactivity, the red image is tdTomato fluorescence and the yellow colour indicates co-expression. ***B,*** The table shows quantification based on cell counting (n = 4 animals). Images are from Dr. Bénédictee Amilhon.

A

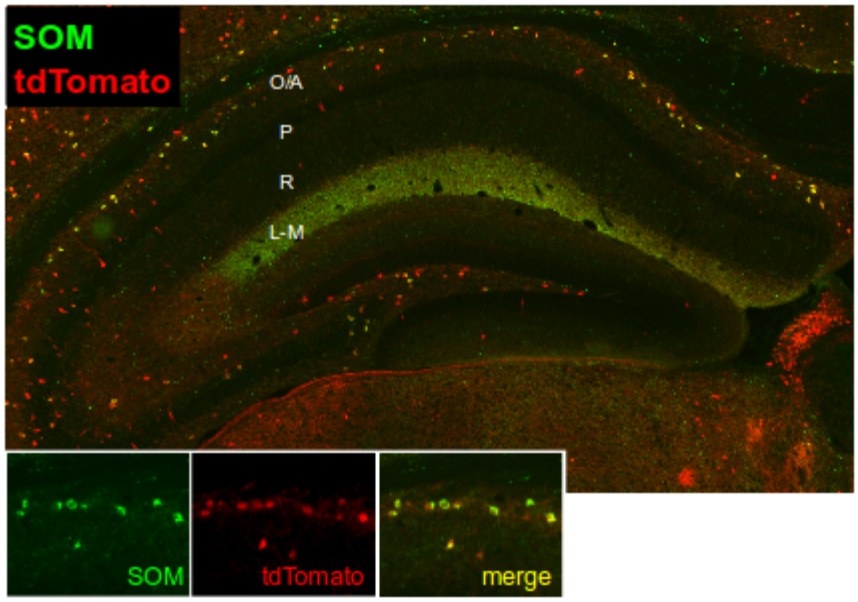

B

SOM-tdTomato (n = 4 animals)		
CA1	**% tdTomato+ neurons that are SOM+**	**% SOM+ neurons that are tdTomato+**
str. oriens	**81.5 ± 1.9 %**	**100.0 ± 0.0 %**

Figure 13. The specificity of tdTomato expression in SOM-tdTomato mice was examined using SOM immunohistochemistry. ***A,*** An image is taken from the middle level of the hippocampus along the septo-temporal axis. The bottom inset shows that the green image is SOM immunoreactivity, the red image is tdTomato fluorescence and the yellow colour indicates co-expression. ***B,*** The table shows quantification based on cell counting (n = 4 animals). Images are from Dr. Bénédicte Amilhon.

V.2. Materials and Methods

Animals

Animals of both sexes (P20-28) were used. In order to visualize the two interneuron subtypes, transgenic mice were used where a fluorescent protein tdTomato was expressed under the control of the PV or SOM promoter. PV-Cre mice (strain name: B6;129P2-Pvalb$^{tm1(cre)Arbr}$/J, stock number: 008069, the Jackson Laboratory) and SOM-Cre mice (strain name: STOCK Sst$^{tm2.1(cre)Zjh}$/J, from Dr. Josh Huang, Cold Spring Harbor Laboratory) were obtained and mated with a reporter mouse line, Ai9 mice expressing tdTomato (strain name: B6;129S6-Gt(ROSA)26Sor$^{tm9(CAG-tdTomato)Hze}$/J, stock number: 007905, the Jackson Laboratory), in order to produce PV-tdTomato and SOM-tdTomato offspring. The three mouse lines (PV-Cre, SOM-Cre and Ai9) are on slightly different genetic backgrounds although they are all mixes between C57BL/6 and a type of 129 mice. PV-Cre mice are C57BL/6;129P2, SOM-Cre mice C57BL/6;129S4Sv/Jae, and Ai9 mice are C57BL/6;129S6. All animals were treated according to protocols and guidelines approved by McGill University and the Canadian Council of Animal Care.

The specificity of the fluorescence expression in PV-tdTomato and SOM-tdTomato mice was confirmed using PV and SOM immunohistochemistry (**Fig. 12-13**). This work was done by Dr. Bénédicte Amilhon, a postdoctoral fellow in the lab with the help of Stephanie Scodras, a research assistant. From their work, it was confirmed that in PV-tdTomato mice, the majority (87.6%: mean of 4 animals) of tdTomato-expressing neurons located in CA1 stratum oriens were positive for PV immunoreactivity, indicating a high degree of specificity. Consistent with previous reports (Mátyás et al., 2004; Jinno and Kosaka, 2006), CA1 PV interneuron somata were found predominantly in stratum pyramidale (47%) or in stratum oriens (52%) and their axonal projections were largely

confined to the perisomatic region, demonstrated by the abundance of PV-positive fibers in stratum pyramidale (**Fig. 12**). The fluorescent labelling in SOM-tdTomato mice was also found to be highly specific, with 81.5% (mean of 4 animals) of tdTomato-positive neurons co-expressing SOM (**Fig. 13**). CA1 SOM interneuron somata were mostly located in stratum oriens (80%) and the SOM-positive fibers were found to be most numerous in stratum lacunosum-moleculare, in line with the morphology of O-LM cells as reported previously (Mátyás et al., 2004; Jinno and Kosaka, 2006).

Intact hippocampal preparation

The acute preparation containing the intact hippocampus was dissected as described previously (Goutagny et al., 2009). Briefly, after decapitation, the brain was quickly removed from the skull and placed in ice-cold high-sucrose solution (same composition as in Chapter 3 slice preparation). From a hemisected brain, the septum and hippocampus along with the interconnecting fibers were carefully and rapidly dissected out using microspatulas. The preparation was trimmed with fine scissors to remove any remaining cortical tissue and the septum was cut off. The intact hippocampal preparation was left to rest with the CA1 side facing up in oxygenated room-temperature high-sucrose solution (1 mM $CaCl_2$) for 30 min - 1 h before recording. The intact preparation from only one hemisphere was used for each animal, and the preparation from either the left or the right hemisphere was chosen randomly for each experiment.

Electrophysiology and tdTomato labelling visualization

All electrophysiological recordings were performed at 30 ± 2ºC, using modified aCSF containing (in mM) 126 NaCl, 24 $NaHCO_3$,10 glucose, 4.5 KCl, 2 $MgSO_4$, 1.25 NaH_2PO_4, 0.4 ascorbic acid and 2 $CaCl_2$ (pH 7.3, oxygenated with 95% O_2-5% CO_2). For Experiment 1, the aCSF was perfused at a relatively low rate of 3 - 5 ml/min, in order to minimize synaptic activity. In some cases, a

cocktail of synaptic blockers was used, containing DNQX (5 μM), bicuculline (5 μM) and DL-AP5 (25 μM), to completely inhibit synaptic events. For Experiment 2, a high aCSF perfusion rate of 20 - 25 ml/min and the same mixture of synaptic blockers were used. The electrophysiology setup, fluorescence system and intrapipette solution were the same as in Chapter 2, Section 2.2. In addition, an automatic temperature controller (model TC-324B, Warner Instruments, Hamden, CT) was used. The junction potential estimated at -15.2 mV was not corrected. Pipette resistance of 2.5 - 4 MΩ was used. The intact hippocampal preparation was oriented in the recording chamber as shown in **Figure 14*A*** to allow visually guided whole-cell recordings of fluorescent neurons located in CA1 stratum oriens/alveus within the middle hippocampus. In this configuration, the stratrum oriens/alveus interneurons (OAIs) could be visually patched with ease, since they reside in the most superficial layers of the preparation. Prior to recording, neurons were checked for the presence of tdTomato labelling in the soma by illuminating with a 554-nm wavelength light.

Properties examined include resting membrane potential (Vrest), membrane resistance, membrane time constant, spontaneous firing, firing pattern, mean firing rate, sag amplitude and rebound firing. An approximate location of the recorded cell in the preparation was also noted. Recordings were kept for analysis only if they met the following criteria; spikes overshot 0 mV and access resistance was < 30 MΩ. Once the whole-cell configuration was achieved, the cell's Vrest was noted and the cell's spontaneous spiking, if any, was recorded for 10 - 30 s. Then, while the membrane potential of the cell was held at -60 mV in current clamp, and a series of small-amplitude 1-s hyperpolarizing steps (10-pA increments) were used to determine the membrane resistance and membrane time constant. This part of the analysis was done with the help of Katie A. Ferguson, a Ph.D. student at the University of Toronto who collaborated on this project. The membrane resistance was calculated by computing the slope of the voltage change over the amplitude of the current injected. The membrane time constant was

derived by fitting the voltage change during a small hyperpolarizing current step with a single exponential function and calculating the mean fit over a few small current steps. The membrane time constant effectively represented the amount of time required for the membrane potential to reach ~63% of the total change.

Intrinsic properties of each cell were examined in current-clamp mode following published protocols (Sotty et al., 2003; Huh et al., 2010). A series of 1-s hyperpolarizing current steps (50-pA increments) were applied from the holding potential of -60 mV, in order to measure the magnitude of depolarizing sag activated upon initial hyperpolarization to -120 mV. The presence of any rebound firing following the release from hyperpolarization was also noted. Next, a series of 1-s depolarizing current steps (50-pA increments) from the holding potential of -80 mV were applied, followed by the same series of depolarizing current steps applied at -60 mV, in order to determine the mean firing rate and firing pattern. The mean firing rate was defined as the number of action potentials fired by the neuron in 1 s, when it was depolarized from -60 mV using the same current step required to reach the cell's spike threshold from -80 mV.

Statistical analysis

Data are presented as mean ± standard error of the mean, unless otherwise stated. Data were plotted and analyzed using Clampfit (Molecular Devices, Sunnyvale, CA), Prism 4 (GraphPad Software, San Diego, CA) and custom software in Matlab (MathWorks, Natick, MA). Statistical methods used were Student's t test, ANOVA and post-hoc Newman-Keuls tests. p values of <0.05 were considered to be statistically significant. Images were cropped and adjusted for contrast using Gimp (www.gimp.org) and figures were constructed using Inkscape (www.inkscape.org).

Table 3. Electrophysiological properties of CA1 PV and SOM interneurons located in stratum oriens/alveus, characterized under two conditions

slow perfusion	**PV**	**SOM**	**p value**
n (number of neurons)	5	9	
% spontaneously firing	1/5 = 20%	8/9 = 88.9%	
% spont. firing >3 Hz spont. firing frequency (Hz)	0/5 = 0% n/a	4/9 = 44.4% 10.33 ± 3.668	
Vrest (mV)	-48.00 ± 3.286	-45.67 ± 1.414	0.460
membrane resistance (MΩ)	74.00 ± 16.84	158.0 ± 13.22	0.002**
membrane time constant (ms)	5.396 ± 1.419	14.16 ± 1.216	<0.001***
membrane capacitance (pF)	74.08 ± 7.186	90.50 ± 4.774	0.072
mean firing rate (Hz)	115.4 ± 11.81	39.11 ± 2.816	<0.0001***
sag amplitude (mV)	6.342 ± 1.248	17.12 ± 1.701	<0.001***

fast perfusion	**PV**	**SOM**	**p value**
n (number of neurons)	4	5	
% spontaneously firing	0/4 = 0%	4/5 = 80%	
% spont. firing >3 Hz spont. firing frequency (Hz)	0/4 = 0% n/a	3/5 = 60% 6.036 ± 1.409	
Vrest (mV)	-42.75 ± 2.287	-47.60 ± 1.631	0.119
membrane resistance (MΩ)	73.93 ± 2.873	178.0 ± 6.275	<0.0001***
membrane time constant (ms)	5.955 ± 0.9436	15.37 ± 1.058	<0.001***
membrane capacitance (pF)	79.86 ± 10.62	86.53 ± 5.676	0.574
mean firing rate (Hz)	164.0 ± 8.803	45.60 ± 5.221	<0.0001***
sag amplitude (mV)	10.03 ± 2.670	21.70 ± 1.554	0.005**

* $p < 0.05$, ** $p < 0.01$, *** $p < 0.001$, $^{n/a}$ not available. Mean value ± S.E.M.

Figure 14

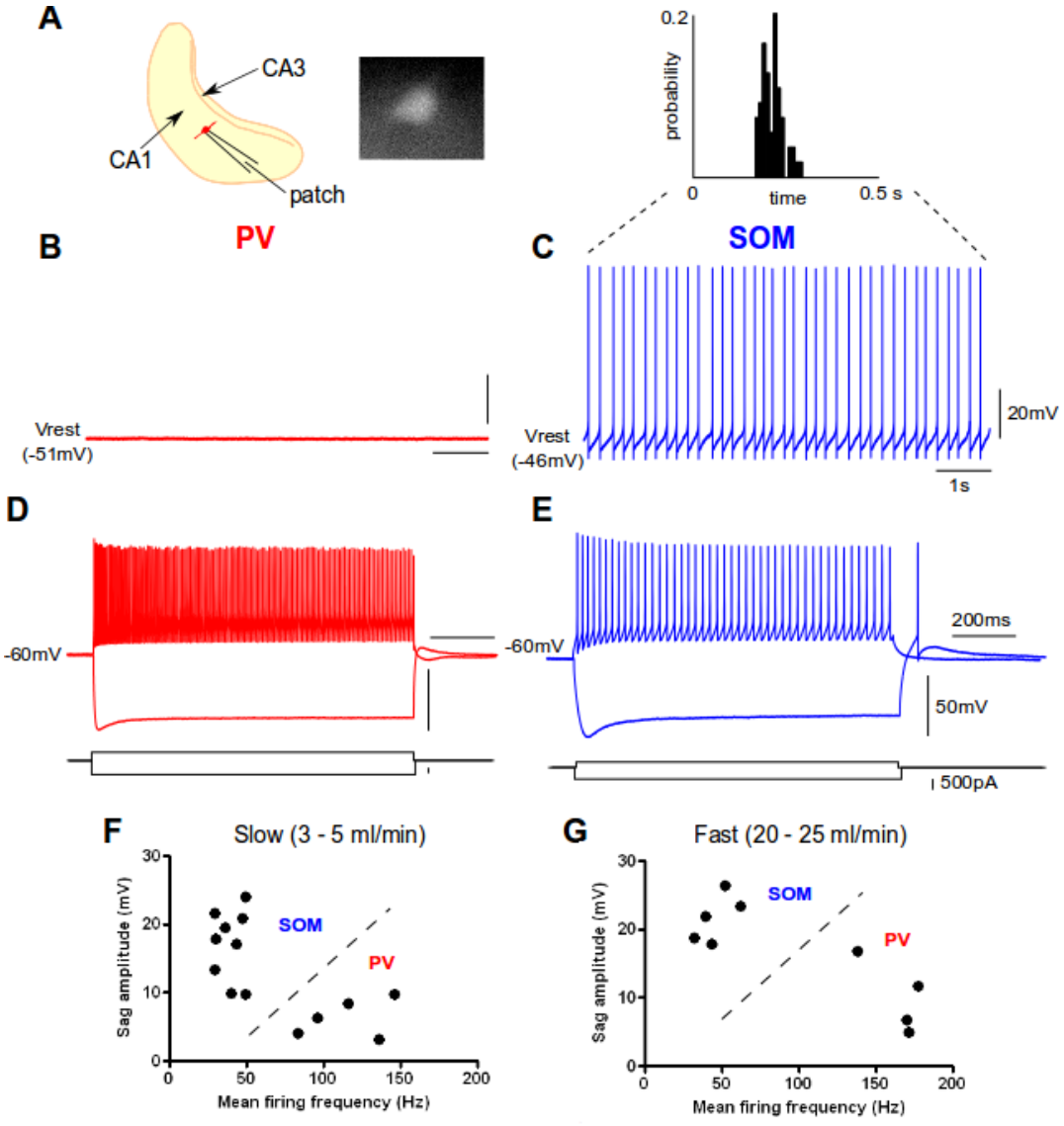
A
CA3
CA1
patch
PV
0.2
probability
0
time
0.5 s
B
C
SOM
Vrest
(-51mV)
Vrest
(-46mV)
20mV
1s
D
E
-60mV
-60mV
200ms
50mV
500pA
F
Slow (3 - 5 ml/min)
Sag amplitude (mV)
SOM
PV
Mean firing frequency (Hz)
G
Fast (20 - 25 ml/min)
Sag amplitude (mV)
SOM
PV
Mean firing frequency (Hz)

Figure 14. Electrophysiological characterization of CA1 PV and SOM interneurons. ***A,*** PV and SOM interneurons located in middle CA1 str. oriens/alveus are identified by the presence of tdTomato fluorescence in the soma (inset) and are selected for whole-cell patch-clamp experiments. ***B,*** A typical PV interneuron shows no spontaneous firing at Vrest. ***C,*** Some SOM interneurons display spontaneous firing in theta-range frequencies. The ISI histogram (above) indicates that the spontaneous firing pattern of the SOM neuron is highly rhythmic with regular intervals between neighbouring spikes. ***D,*** A PV neuron (same neuron as in ***B***) typically fires very fast and exhibits little sag upon hyperpolarization. ***E,*** In contrast, a SOM neuron (same neuron as in ***C***) fires more slowly but displays large sag. Both neurons illustrated here were recorded in the slow perfusion condition and with synaptic blockers. ***F-G,*** Sag amplitude and mean firing rate can be used to clearly distinguish between PV and SOM interneurons in both slow (***F***) and fast (***G***) perfusion conditions.

V.3. Results

3.1. Experiment 1: CA1 PV and SOM interneurons display distinct electrophysiological properties

Using PV- and SOM-tdTomato mice, we were able to visually select and record specifically from PV or SOM stratum oriens/alveus interneurons (OAIs) located in the middle section of the intact hippocampal preparation (**Fig. 14**). In whole-cell mode, we characterized the intrinsic membrane properties of each neuron while aCSF was perfused at a relatively low rate in order to minimize synaptic activities. A total of 5 PV and 9 SOM OAIs were recorded. In approximately half of the recordings performed (2 PV and 5 SOM recordings), synaptic events were inhibited pharmacologically using a mixture of synaptic blockers containing DNQX, bicuculline and DL-AP5.

The results of the electrophysiological characterizations are summarized in **Table 3**. Recordings at the resting membrane potential revealed that PV OAIs were mostly silent with none of the neurons (0/5) displaying spontaneous firing with frequencies greater than 3 Hz, while a significant proportion of SOM OAIs (4/9) exhibited spontaneous firing exceeding 3 Hz (**Fig. 14*B-C***). The spontaneous firing by SOM OAIs occurred in two neurons recorded in control aCSF and two neurons recorded in the presence of the synaptic blockers, thus spontaneous firing was likely not due to synaptic activity. In addition, it did not appear that SOM OAIs were more depolarized at rest compared to PV OAIs, because the two cell types displayed mean resting membrane potentials that were not statistically different from one another ($p = 0.46$). All spontaneous firing was in the form of tonic/regular firing and burst-firing was never observed. When the timing of the spontaneously occurring spikes was analyzed to examine the degree of rhythmicity, all spontaneous firing by SOM OAIs with frequencies > 3Hz led to

sharp peaks in the interspike interval histogram, indicating that the spontaneous firing patterns were highly rhythmic (**Fig. 14*C***). The mean firing rate of these rhythmically active SOM OAIs was ~10 Hz.

Our results further demonstrate that other properties are also markedly different between PV and SOM OAIs. Namely, PV OAIs displayed significantly lower membrane resistance and faster time constant in comparison with SOM OAIs (**Table 3**). We also found that during depolarizing current steps, PV OAIs uniformly exhibited tonic, fast-firing characteristics with the firing rate of every neuron exceeding 80 Hz (**Fig. 14*D***). On the other hand, SOM OAIs displayed tonic firing patterns with firing rates that were consistently lower than 50 Hz (**Fig. 14*E***). Thus, the mean firing rate of PV OAIs was significantly higher compared to SOM OAIs ($p < 0.0001$). In addition, SOM OAIs consistently exhibited large-amplitude depolarizing sag upon hyperpolarization while PV OAIs displayed little sag ($p < 0.001$; **Fig. 14*D-E***). Rebound firing following the release from hyperpolarization was observed in a proportion of SOM OAIs (3/9) but in none of the PV OAIs (0/5). These results indicate that PV and SOM OAIs can be clearly distinguished based on two electrophysiological characteristics; PV neurons possess extremely fast-firing properties with little depolarizing sag while SOM neurons present tonic-firing with large-amplitude sag. When values of these two properties were plotted for each neuron (**Fig. 14*F***), PV and SOM OAIs formed clearly distinct clusters.

3.2. Experiment 2: Characterization of electrophysiological properties with a higher perfusion rate and in the presence of synaptic blockers

Since the intact hippocampal preparation is several times thicker than a typical slice, it may be argued that the low perfusion rate (3 - 5 ml/min) used in Experiment 1 can lead to an insufficient level of oxygenation for all neurons

throughout the tissue. While this may be a potential issue for neurons located deep in the tissue, we believe that the OAIs receive sufficient levels of oxygenation because they are located in the most superficial layer of the preparation. Thus, we predict that the intrinsic properties of neurons are probably affected very little by the perfusion rate, if at all. Nonetheless, we decided to test this directly by repeating the characterization using a much faster aCSF perfusion rate of 20 - 25 ml/min. This perfusion rate is the same as the one used in subsequent experiments to generate the network theta rhythm, so the presence of frequent synaptic currents were too disruptive for characterization of intrinsic properties. Therefore, synaptic activity was completely inhibited using the synaptic blockers. A total of 4 PV and 5 SOM OAIs were recorded in this configuration.

The results are very similar to Experiment 1 and are summarized in **Table 3**. Consistent with Experiment 1, we found that a significant proportion of SOM OAIs (3/5) displayed spontaneous firing that was greater than 3 Hz (mean firing rate: ~6Hz) whereas none of the PV OAIs (0/4) were spontaneously active, despite similar Vrest values between the two groups ($p = 0.12$). Once again, ISI histograms of the SOM OAIs' spontaneous firing patterns revealed that they were highly rhythmic (not shown). The differences between the cell types in membrane resistance and membrane time constant observed in Experiment 1 were replicated (ps < 0.0001). As expected, PV OAIs fired significantly faster than SOM OAIs ($p < 0.0001$) and SOM OAIs expressed a larger-amplitude depolarizing sag compared to PV OAIs ($p < 0.005$). As in Experiment 1, rebound firing following hyperpolarization was exhibited only by a proportion of SOM OAIs (2/5) and no PV OAI (0/4). We found that the mean firing rate and sag amplitude of the neuron could be used to clearly dissociate between the two cell types (**Fig. 14*G***), mirroring the results of Experiment 1.

When we performed a series of 2-way ANOVAs on results from both experiments to examine the effects of the perfusion rate and the cell type simultaneously, we found that the perfusion rate had significant effects on two

measures: sag amplitude and mean firing rate. Namely, the faster perfusion rate increased the amplitude of sag in both cell types compared to the slower perfusion rate ($p = 0.046$). For the mean firing rate, a significant interaction existed ($p < 0.01$) where the faster perfusion led to significantly higher firing rates for PV neurons compared to the slower perfusion rate (Bonferroni posttest: $p < 0.001$), but the perfusion rate did not affect firing rates of SOM neurons ($p > 0.05$). All the other parameters measured (Vrest, membrane resistance, membrane time constant and membrane capacitance) failed to show a significant effect of the perfusion rate (ps > 0.05). These results indicate that the faster perfusion rate affects some electrophysiological properties of OAIs such as the firing frequency and the magnitude of depolarizing sag but does not influence the passive properties of these neurons.

V.4. Discussion

In this chapter, we describe the electrophysiological characteristics of PV and SOM OAIs in the CA1 region of the hippocampus. Importantly, we characterized these interneurons using the intact hippocampal preparation, which likely preserves the entire dendritic tree of these interneurons better than conventional slice preparations and which has been shown to give rise to spontaneous rhythmic network activities (Goutagny et al., 2009). We found that PV OAIs, which most likely include PV basket and axo-axonic cells, displayed fast-firing properties with little depolarizing sag during hyperpolarization, in agreement with previously reported PV interneuron characteristics (Meyer et al., 2002; Pawelzik et al., 2002). On the other hand, SOM OAIs fired in a tonic manner but were slower compared to PV OAIs and exhibited a large depolarizing sag, consistent with the presence of I_h in O-LM cells (Oliva Jr et al., 2000; Zemankovics et al., 2010). In addition, intrinsic burst-firing pattern was never

observed in any of the PV or SOM OAIs recorded, similar to previous findings (Lacaille and Williams, 1990; Morin et al., 1996).

There were also significant differences between the two groups in terms of membrane resistance, membrane time constant and probability of spontaneous firing. Notably, PV OAIs displayed mean firing rates and membrane time constants that were on average ~3-fold faster compared to SOM OAIs. These findings fit with previous suggestions that PV interneurons can support gamma-frequency oscillations (Gloveli et al., 2005; Gulyás et al., 2010). On the other hand, we found that even with all the synaptic inputs blocked, a significant proportion (44 - 60%) of SOM OAIs displayed highly rhythmic spontaneous spiking patterns in theta-range frequencies, in support of the notion that some SOM interneurons may act as intrinsic theta generators due to their spontaneous activity and possession of significant I_h (Maccaferri and McBain, 1996b). Although not investigated here, our data does not rule out the possibility that SOM OAIs may also act as theta resonators that preferentially respond to inputs modulated at theta frequencies due to the interaction between their intrinsic properties and synaptic input kinetics (Goldin et al., 2007; Kispersky et al., 2012).

It is interesting that while the passive properties of neurons were not affected by the perfusion rate, certain active properties (*i.e.*, firing rate and sag amplitude) showed significant changes, indicating that oxygenation levels can change some features of intrinsic cellular behaviour. Although unexpected, these changes are not entirely surprising, considering that the faster perfusion rate is required to generate spontaneous theta-frequency network rhythm from the intact hippocampal preparation (Goutagny et al., 2009). It may be that the changes in active properties demonstrated here at the cellular level are necessary to achieve a more active state of the network.

The most important finding that should be highlighted here is that PV and SOM OAIs can be clearly differentiated based on two electrophysiological characteristics: mean firing rate and depolarizing sag amplitude. In fact, PV and

SOM interneurons formed distinct clusters along these two parameters in both slow- and fast-perfusion conditions (**Fig. 14*F-G***). It is remarkable that each biomarker-defined group exhibits such uniform characteristics, considering that they probably include multiple subtypes with different anatomical distributions (basket and axo-axonic cells for PV neurons, and O-LM and bistratified cells for SOM neurons). This is in stark contrast to the electrophysiological heterogeneity observed for glutamatergic and GABAergic neurons of the MS-DBB, described in Chapter 3. It is currently unknown exactly which anatomically defined interneuron subtypes were sampled here and this is a question that should be explored in the future by doing morphological reconstructions of recorded cells. Nonetheless, these results confirm that CA1 PV and SOM interneurons possess the rhythmic intrinsic properties that were previously reported in the literature; PV OAIs display ultra-fast firing properties appropriate for participation in gamma-frequency oscillations and SOM OAIs exhibit an important I_h and spontaneous firing in the theta-frequency range. Our data provides an important characterization that could be useful for identifying PV *vs.* SOM interneurons when recording from unidentified CA1 interneurons both *in vitro* and *in vivo*. Furthermore, the characteristics described here could be used to fine-tune parameters for computer models of CA1 interneurons and hippocampal networks.

Chapter VI: CA1 PV and SOM interneurons behave distinctly during *in vitro* theta rhythm

VI.1. Introduction

There is a wealth of literature describing the spiking behaviour of CA1 PV and SOM interneurons during *in vivo* hippocampal theta rhythm. Using the juxtacellular recording method in anaesthetized rats, Klausberger and his group have shown that PV interneurons, namely basket and axo-axonic cells, present closely-spaced bursts of multiple action potentials that are phase-locked to the descending phase of field theta and the peak of theta, respectively (Klausberger et al., 2003). It is important to note that in these studies, the reference field theta rhythm was recorded in CA1 stratum pyramidale. SOM-positive O-LM cells, on the other hand, have been shown to fire 1 - 2 spikes predominantly near the trough of theta, which is the same firing phase as the pyramidal cells (Klausberger et al., 2003). Interestingly, bistratified cells located in stratum pyramidale that co-express PV and SOM fire near the trough of theta, which is similar to the O-LM cells' firing phase (Klausberger et al., 2004). SOM-expressing stratum oriens GABAergic neurons with long-range projections to both the medial septum and retrohippocampal areas (double-projection cells) have also been shown to fire near the trough of theta, but at a low firing rate overall (0.7Hz) (Jinno et al., 2007). Although these studies provide a rich description of firing patterns of many anatomically identified CA1 interneuron subtypes during theta, the use of anaesthetics can affect theta rhythm properties (Ylinen et al., 1995) and also influence the firing behaviour of neurons during theta (Fox et al., 1986). In addition, due to the difficult and labour-intensive nature of the technique used in these studies, the observations were generally made based on low sample sizes, ranging from two for axo-axonic cells to seven for bistratified cells.

Other groups have carried out unit recordings of CA1 interneurons during theta rhythm in non-anaesthetized animals, with the reference theta rhythm recorded from CA1 stratum pyramidale in most cases. Csicsvari and colleagues (1999) demonstrated that interneurons in CA1 stratum pyramidale fire at the descending phase, while those located in stratum oriens/alveus fire at the trough of theta. Interestingly, they reported that

oriens/alveus interneurons (OAIs) as a group showed relatively weaker modulation of firing by theta phase, compared to stratum pyramidale interneurons. In register with this, a recent study reported in freely moving rats that a higher percentage of stratum pyramidale interneurons displayed firing that is significantly theta-modulated, compared to OAIs (Czurko et al., 2011). Recently, the firing behaviour of CA1 PV and SOM interneurons during theta has been dissected in awake, behaving mice using optogenetic inhibition to identify the recorded neuron's cell type (Royer et al., 2012). They found that PV neurons fire near the descending phase and trough of theta (theta rhythm recorded in stratum pyramidale) while SOM neurons are phase-locked to the ascending phase of theta. These studies provide a good account of the firing behaviour of different interneuron subtypes during *in vivo* theta. However, there are some discrepancies between different *in vivo* studies in terms of the exact phase preference of PV and SOM interneuron spiking during CA1 theta, and it remains to be determined whether some of the differences arise due to the use of anaesthetics in some studies. It is also largely unknown how the distinct firing patterns by different interneuron classes are achieved during network theta rhythm.

Potential mechanisms underlying the cell-type specific firing during theta include synaptic and intrinsic factors. Excitatory and inhibitory inputs from distinct sources may drive the neurons to fire at different times or modulate their firing in different ways. Certain interneuron types may be particularly affected by activities of other interneurons via gap-junction mediated electrical coupling. Furthermore, the expression of different neurotransmitter and neuromodulator receptors as well as distinct voltage-gated conductances can influence firing behaviour. Thus, it remains to be determined which of these factors give rise to the firing behaviour of a given interneuron subtype observed during theta rhythm. Investigation of this issue is important for understanding how the network rhythm is generated and modulated during *in vivo* and *in vitro* CA1 theta oscillations.

In order to identify some of the potential mechanisms, we employed here the

intact hippocampal preparation that has been demonstrated to intrinsically generate network theta rhythm *in vitro* (Goutagny et al., 2009). Goutagny and colleagues (2009) reported that during this form of *in vitro* theta, CA1 interneurons mostly fire phase-locked to the peak of ongoing CA1 theta rhythm (theta recorded at the level of CA1 stratum radiatum), but the firing behaviour of specific interneuron subtypes has not been investigated. The intact hippocampal preparation excludes inputs from structures such as the medial septum and the entorhinal cortex, limiting the sources of synaptic inputs to those contained within the intrahippocampal circuitry. Thus, the intact preparation provides a unique opportunity to study the mechanisms of interneuron firing behaviour in a simplified version of hippocampal theta rhythm while preserving the local hippocampal network. Moreover, the intact preparation more closely mimics the *in vivo* intrahippocampal circuitry compared to typical acute slice preparations, because neuronal processes that run along the septotemporal axis of the hippocampus and network interactions occurring along that axis are better preserved in this preparation. Since it is an *in vitro* preparation, it is also much easier to perform whole-cell recordings and pharmacological manipulations compared to *in vivo*.

Here, our objective is to investigate CA1 PV- and SOM-expressing interneurons' firing patterns during naturally occurring CA1 theta rhythm *in vitro* and to determine which synaptic and/or intrinsic factors govern their firing behaviour during theta. Combining the intact hippocampal preparation (Goutagny et al., 2009) with the use of transgenic mice to enable visualization of particular cell types (Taniguchi et al., 2011), we hereby performed whole-cell patch-clamp recordings from PV or SOM interneurons during CA1 theta oscillations. By recording in the whole-cell mode, we are able to examine both active and inactive cells, important for understanding the full range of firing patterns during theta, and more importantly we can investigate the dynamics of subthreshold changes in the cell's membrane potential due to events such as synaptic currents. We focused on PV and SOM interneurons because they are two of the best understood classes of CA1 interneurons in terms of intrinsic electrophysiological

characteristics and firing behaviour during *in vivo* theta. As in Chapter 5, PV-tdTomato and SOM-tdTomato mice were used in order to visualize PV and SOM interneurons, respectively.

First, control experiments were carried out to confirm that the *in vitro* theta oscillations recorded from the two mouse lines are qualitatively and quantitatively similar (Experiment 1) and to determine the reversal potentials for EPSCs and IPSCs (Experiment 2). In Experiments 3 and 4, we characterized the interneurons' firing behaviour during theta rhythm as well as the synaptic currents received by these neurons. In Experiment 5, the firing pattern of CA1 pyramidal cells during theta was assessed. Finally in Experiment 6, we show that the rhythmic synaptic inputs received by CA1 PV and SOM interneurons during theta rhythm originate from the local CA1 network.

VI.2. Materials and Methods

Animals

Animals of both sexes (age: P20-28) were used, unless otherwise noted. PV-Cre and SOM-Cre mice were each mated with the reporter line, Ai9 mice, in order to generate PV-tdTomato and SOM-tdTomato mice, respectively. For more details on PV-Cre, SOM-Cre and Ai9 mice, see Chapter 5, Section 5.2. In addition to these mice, another transgenic line, VGLUT2-tdTomato, was used to visualize CA1 pyramidal cells (for Experiment 5 only). VGLUT2-Cre mice (BAC-Vglut2::Cre, from Dr. Ole Kiehn, Karolinska Institute, Sweden) were obtained and mated with the reporter Ai9 mice to generate VGLUT2-tdTomato mice, in which tdTomato is expressed under the control of the VGLUT2 promoter. VGLUT2-Cre mice are on a C57BL/6 background. The specificity of the fluorescence expression in the VGLUT2-tdTomato line is currently being confirmed by a PhD student in the lab, Jennifer Robinson, using the fluorescence in situ hybridization method. In agreement with previous reports (Danik et al., 2005; Herzog et al., 2006), we found that VGLUT2 is expressed by a proportion of CA1 neurons

situated in stratum pyramidale that appear to be pyramidal cells based on their location, shape and electrophysiological criteria. All animals were treated according to protocols and guidelines approved by McGill University and the Canadian Council of Animal Care.

Intact hippocampal preparation and cut preparations

For Experiments 1 - 4, the same intact hippocampal preparation as described in Chapter 5, Section 5.2 was used. For CA1 pyramidal cell recordings in Experiments 2 and 5, the intact hippocampal preparation was dissected as described in Chapter 5, except that the surface of the hippocampus was cut at a ~45º angle using a blade to expose the pyramidal layer of CA1 ("angle-cut" preparation; see **Fig. 20**). The cut was necessary because of the pyramidal cells' depth and optical limitations of the setup. The visual approach allowed identification of pyramidal cells either by their location and morphology or by VGLUT2 expression and it yielded a much better success rate for whole-cell recordings than the blind-patch technique used in the lab previously (Goutagny et al., 2009). Thus, the angle cut was introduced to expose neurons located in the pyramidal layer. In Experiment 6, a curved blade was used to cut off the CA3 region from the intact hippocampal preparation ("CA3-cut" preparation; see **Fig. 22**), in order to confirm that synaptic currents observed in CA1 interneurons originate from CA1 and not from CA3.

Electrophysiology and tdTomato labelling visualization

All electrophysiological recordings were performed at 30 ± 2ºC, using modified aCSF (same composition as in Chapter 5, Section 5.2). For all experiments except for Experiment 2, the aCSF was perfused at a rate of 20 - 25 ml/min which has been tested to be ideal for generation of network theta oscillations in the intact hippocampal preparation (Goutagny et al., 2009). The detailed setup for Experiment 2 is described in the following section, titled 'Electrical Stimulation'. The electrophysiology setup, fluorescence system and intrapipette solution were the same as in Chapter 2, Section 2.2. In addition, a

microelectrode AC amplifier (model 1800, A-M Systems, Sequim, WA), a Humbug 60Hz noise eliminator (Quest Scientific, Vancouver, Canada), an audio monitor (model 3300, A-M Systems) and an automatic temperature controller (model TC-324B, Warner Instruments) were used.

For local field potential (LFP) recordings, a borosilicate-glass field electrode (1 - 5 MΩ) was placed on the surface of CA1 of the middle hippocampus as shown in **Figure 15** and carefully lowered in small steps using a micromanipulator until it reached stratum radiatum (approx. 1000 - 1200 μm from the surface of the preparation) where the theta oscillation magnitude is maximal in this *in vitro* preparation. The electrode location was determined by paying close attention to the LFP trace and the audiomonitor which revealed the presence of multi-unit activity as the electrode passed through stratum pyramidale. The Humbug noise eliminator was used to perform an on-line cancellation of the electrical noise from the LFP signal. The theta-frequency oscillations (3 - 8 Hz) typically began after the preparation had been placed in the recording chamber and perfused with aCSF at 20 - 25 ml/min for ~30 min and slowed down below the cut-off frequency of 2.5 Hz after additional ~2.5 h, at which point the recordings were terminated.

For simultaneous LFP and whole-cell recordings, the hippocampal preparation was oriented in the recording chamber as shown in **Figure 18**. The field electrode was first positioned in middle CA1 and once a stable network theta rhythm was detected, whole-cell recordings were performed on PV or SOM interneurons located in CA1 stratum oriens and alveus, as close to the field electrode as possible (maximum distance of 1 mm) in order to ensure that the field and patch electrodes are sampling the same local CA1 circuit. PV or SOM interneurons were identified by the presence of tdTomato in the soma, using 554 nm excitation-wavelength light. Exceptionally in Experiment 5, the field electrode was positioned in CA1 close to the cut and VGLUT2-tdTomato+ neurons located in CA1 stratum pyramidale under the cut surface were chosen for pyramidal cell recordings, as shown in **Figure 21**.

For Experiment 3-6, the electrophysiological procedures were as follows. For whole-cell recordings, pipette resistance of 2.5 - 4 MΩ was used. The junction potential estimated at -15.2 mV was not corrected. Once a stable whole-cell mode was achieved, access resistance and the neuron's resting membrane potential (Vrest) were noted. Then, the cell was recorded at Vrest and together with the LFP signal (containing network theta oscillations) for 60 s, to observe the neurons' spontaneous firing behaviour. This was followed by additional 60-s recordings at more hyperpolarized potentials (*e.g.*, -70, -75, -80 mV) in current clamp to reveal synaptic potentials. If the neuron presented very few or no spontaneous spikes, it was depolarized slightly to initiate regular firing and such depolarized spiking was also recorded for 60 s. Next, the neuron's basic properties were quickly checked for, including firing pattern, mean firing rate, action potential properties, sag amplitude and rebound firing, as described in Chapter 5, Section 5.2. Lastly, the neuron was held at various membrane potentials (*e.g.*, -80, -70, Vrest, 0 and +15 mV) in voltage clamp in order to record the incoming excitatory and inhibitory synaptic inputs during theta. All throughout the recording of the cell, access resistance and resting membrane potential were checked every 5 - 10 min. An approximate location of the recorded cell in the preparation was noted. Recordings were kept for analysis only if the LFP signal contained oscillations with frequencies exceeding 2.5 Hz and if the cell recordings met the following criteria; spikes overshot 0 mV and access resistance was <30 MΩ.

Electrical stimulation

In Experiment 2, the reversal potentials for EPSCs and IPSCs were determined for CA1 PV and SOM stratum oriens/alveus interneurons (OAIs) and for CA1 pyramidal cells, using electrical stimulation. For these experiments, a slower aCSF perfusion rate of 7 - 8 ml/min was used. In order to stimulate the axons of local CA1 pyramidal cells and interneurons, a monopolar tungsten microelectrode (WPI, Sarasota, FL) was placed on the surface of CA1 (stratrum oriens/alveus) in the middle hippocampus. The stimulation

parameters were controlled using an isolated pulse stimulator (model A360, WPI). One pulse (25 - 300 μA intensity, 0.1 ms duration) was administered every 10 s. CA1 PV or SOM OAIs located in the middle hippocampus and close to the stimulating electrode were recorded in whole-cell mode. For pyramidal cell recordings, the intact preparation was cut at an angle to reveal the CA1 stratum pyramidale ("angle-cut" preparations) and pyramidal cells were identified by their location and morphology. Neurons were first checked for Vrest, spontaneous activity, depolarized to fire action potentials if not spontaneously firing and were held at various potentials in voltage clamp (the exact range of potentials tested varied for each cell: -100 to +30 mV) during electrical stimulation to record evoked synaptic currents. In order to isolate EPSCs, 20 μM bicuculline and 2 μM CGP 52432 were used to block $GABA_A$- and $GABA_B$-receptor mediated responses, respectively (in two pyramidal cell recordings, 5 μM gabazine was used instead of bicuculline). To isolate $GABA_A$-receptor mediated IPSCs, 10 μM DNQX, 25 μM DL-AP5 and 2 μM CGP 52432 were used to block glutamatergic and $GABA_B$-receptor mediated responses. Cells were excluded from analysis if the spikes failed to overshoot 0 mV or access resistance exceeded 30 MΩ at any point during the experiment.

Analysis of LFP theta oscillations

In order to compare the *in vitro* hippocampal theta oscillations recorded from PV-, SOM- and VGLUT2-tdTomato mice, we analyzed the LFP signal recorded for 60 s from the middle CA1 stratum radiatum (**Fig. 15*A-Bi***), approx. 2 hours after the preparation was placed in the recording chamber and perfusion was started. Typically by this time, the oscillation has largely stabilized, producing rhythmic peaks that occur at regular intervals. Using custom software in Matlab (MathWorks, Natick, MA), the LFP signal was first filtered using a bandpass filter (1 - 50 Hz) to eliminate slow drifts and electrical noise from the recording. We next performed a multi-taper Fourier transform on the filtered signal using the Matlab Chronux toolbox (http://chronux.org; Mitra and Bokil, 2008) and generated a power spectrum over the frequency range of 0 - 20 Hz and a

power spectrogram to display the frequency-power relationship over time (**Fig. 15*A-Biii, D***). From the power spectrum, values were extracted such as the peak frequency ("theta peak frequency" in Hz), power of the signal at the peak frequency ("theta peak power" in μV^2) and total power over 2 - 10 Hz ("theta summed power" in μV^2). We also generated an autocorrelogram of the LFP signal (**Fig. 15*A-Bii***) and derived a value reflecting the degree of rhythmicity in the signal ("rhythmicity index"). Since the autocorrelogram peaks become more prominent (more "peaky") with more rhythmic LFP signals, the relative probability value of the second peak was taken as the rhythmicity index. With the first, centre peak always being 1, the rhythmicity index could therefore vary between 0 and 1 with higher values indicating more rhythmic signals.

Analysis of simultaneous LFP and whole-cell recordings

The 60-s trace containing a neuron's spontaneous firing activity in relation to the LFP theta rhythm was analyzed using custom software in Matlab. First, spikes were detected from the intracellular trace using a threshold method and an interspike interval (ISI) histogram was produced, based on the time interval between two neighbouring spikes (**Fig. 18*C,G***). When the neuron presented bursts of action potentials that were synchronized with the theta oscillation, two distinct peaks were visible from the ISI histogram, with the shorter ISI peak representing the frequency of the neuron's firing within the bursts ("intraburst frequency") and the longer ISI peak indicating the theta rhythm frequency ("interburst frequency"). In contrast, when the neuron displayed a tonic firing pattern without bursts, the ISI histogram contained a single peak which reflected the neuron's firing frequency.

Next, for each spontaneously firing neuron, we determined its preferred firing phase in relation to the ongoing theta rhythm using custom Matlab software. A part of this analysis was done by Katie A. Ferguson, a Ph.D. student at the University of Toronto. We first detected the peaks of the theta oscillation in the LFP signal using a threshold method and designated each theta peak the phase value of 0º. Then, the

neuron's action potentials were detected and the timing of each spike peak was expressed in terms of phase relative to the nearest theta peak (-180º to +180º with 0º being the peaks of the oscillation) or in terms of time (ms from theta peak). From these values, phase and time histograms of the neuron's spikes were constructed with bin sizes of 2.5º and 2.5 ms, respectively (**Fig. 18*N-O***). In addition, using the CircStats Matlab toolbox (Berens, 2009), a phase vector plot was produced for each neuron's spontaneous firing during theta rhythm. Because phase is circular by nature (*i.e.,* 0º and 360º representing the same value), the circular statistics tools were necessary to correctly represent the mean spiking phase of the cell (mean vector direction, in º) and a value which indicates the circular spread of the sample around the mean (mean vector length, ranging from 0 to 1). The larger the mean vector length value, the more concentrated the sample is around the mean direction. A "phase-locked" neuron was defined as one whose spiking gives rise to a mean vector length of ≥0.5, while those whose firing led to mean vector lengths of <0.5 were treated as non-phase-locked. The mean vector length has been used previously as a measure of phase-locking (Lasztoczi et al., 2011). Since many neurons produced phase and time firing distributions that are significantly skewed according to the circular symmetry test (CircStats), the median vector direction was used to represent the phase and time distributions, instead of the mean. Since PV neurons fire more spikes per burst compared to SOM neurons, we also constructed phase and time distributions based on the timing of each burst's first spike only, in an attempt to balance the number of spikes analyzed for each cell.

For analyzing the synaptic inputs received during theta rhythm, 60-s traces containing synaptic currents displayed by each neuron at various potentials in voltage clamp were analyzed using Matlab custom software, with the help of Katie A. Ferguson. Using a threshold method, the peaks of EPSCs were detected while the neuron was held at -70 mV (the reversal potential for IPSCs) and IPSCs were recorded at 0 mV (the EPSCs are close to null at this potential). The peak amplitude of the EPSC or IPSC was measured relative to the baseline current and the EPSC/IPSC ratio was calculated for

each cell. The mean EPSC frequency was also calculated for each cell. The timing of EPSCs was computed using a similar method as described above for the timing of spikes; the LFP theta peaks were assigned the value of 0 and the timing of each EPSC peak relative to the nearest theta peak was expressed in relative phase (º) and time (ms).

Statistical analysis

Data are presented as mean ± standard error of the mean, unless otherwise stated. Data were plotted and analyzed using Clampfit (Molecular Devices, Sunnyvale, CA), Prism 4 (GraphPad Software, San Diego, CA) and custom software in Matlab (MathWorks, Natick, MA). Statistical methods used were Student's t test, ANOVA, post-hoc Newman-Keuls tests and a circular symmetry test (CircStats). p values of <0.05 were considered to be statistically significant. Images were processed using Gimp (www.gimp.org) and figures were constructed using Inkscape (www.inkscape.org).

VI.3. Results

3.1. Experiment 1: CA1 in vitro theta oscillations are similar between PV- and SOM-tdTomato transgenic mouse lines

Prior to embarking on a series of experiments to compare the cellular behaviour of CA1 PV and SOM interneurons during hippocampal theta, we carried out a control experiment to ensure that the two transgenic mouse lines used do not differ significantly in their ability to generate *in vitro* theta rhythms. The two Cre lines are on slightly different backgrounds; PV-Cre mice are a mix between C57BL/6 and 129P2, and SOM-Cre mice are a mix between C57BL/6 and 129S4Sv/Jae. This is not a trivial concern, considering that variations in hippocampal oscillations have been noted for different mouse strains *in vivo* and *in vitro* (Franken et al., 1998; Jansen et al., 2009). A total of 10 PV-tdTomato and 9 SOM-tdTomato recordings were used for this comparison (one

recording per animal).

We found that CA1 theta oscillations recorded from PV- and SOM-tdTomato mice are not significantly different along any of the parameters measured (**Fig. 15**). Namely, the peak frequency of the oscillation, peak theta power and summed theta power all failed to show statistical significant differences (ps > 0.05). The rhythmicity index values were also similar between the two mouse lines ($p = 0.72$). These results demonstrate that PV- and SOM-tdTomato mice generate *in vitro* CA1 theta oscillations that are qualitatively and quantitatively very similar.

3.2. Experiment 2: Characterization of EPSC and IPSC reversal potentials

Since we will examine the synaptic currents in PV and SOM stratum oriens/alveus interneurons (OAIs) and CA1 pyramidal cells during theta in subsequent experiments, the aim of this control experiment was to determine the reversal potentials for EPSCs and IPSCs in these cell types. Although these values have previously been reported using acute slices (e.g., Morin et al., 1996), we wished to determine these values under our *in vitro* conditions using the intact preparation and for the specific cell types of interest here. Electrical stimulation was used to activate the local CA1 network and the evoked synaptic currents were recorded in voltage clamp in PV and SOM OAIs, identified by tdTomato fluorescence in the soma, and in CA1 pyramidal cells. Pharmacological blockers used to isolate the EPSCs were bicuculline and CGP 52432, inhibitors for $GABA_A$- and $GABA_B$-receptor mediated responses, respectively (in two pyramidal cell recordings, gabazine was used instead of bicuculline). To observe the $GABA_A$-receptor mediated IPSCs, DNQX, DL-AP5 and CGP 52432 were used to block glutamatergic and $GABA_B$-receptor mediated responses. Initially, we used only the glutamatergic blockers (DNQX and DL-AP5) for isolating the IPSCs, but we found that a large $GABA_B$ component prevented an accurate measurement of the reversal potential for the $GABA_A$-receptor mediated IPSCs. The significant $GABA_B$ component in the

Figure 15

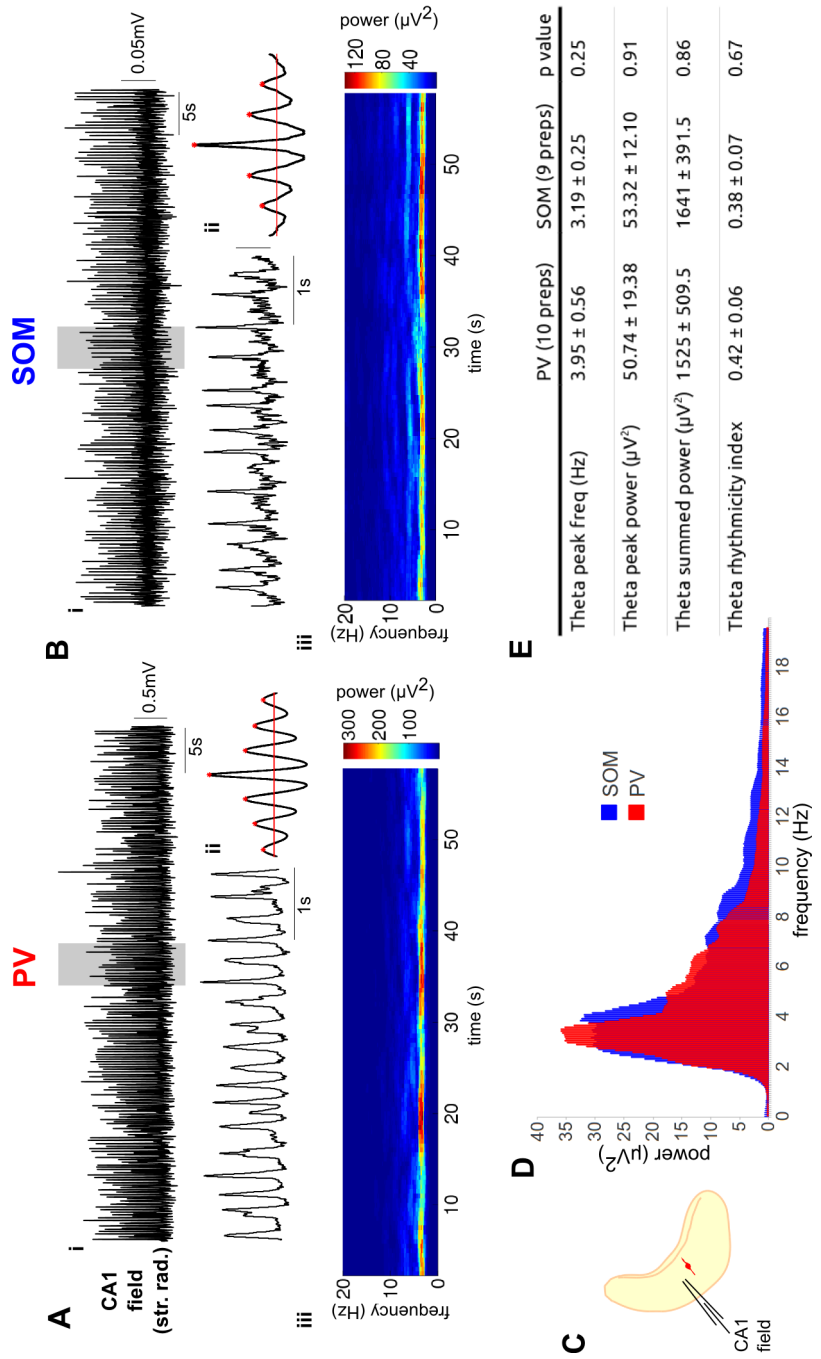
A
PV
i
CA1 field (str. rad.)
0.5mV
5s
ii
1s
iii
frequency (Hz)
time (s)
power (μV2)
B
SOM
0.05mV
C
CA1 field
D
SOM
PV
power (μV2)
frequency (Hz)
E
PV (10 preps) SOM (9 preps) p value
Theta peak freq (Hz) 3.95 ± 0.56 3.19 ± 0.25 0.25
Theta peak power (μV2) 50.74 ± 19.38 53.32 ± 12.10 0.91
Theta summed power (μV2) 1525 ± 509.5 1641 ± 391.5 0.86
Theta rhythmicity index 0.42 ± 0.06 0.38 ± 0.07 0.67

Figure 15. *In vitro* CA1 theta oscillations are similar between PV- and SOM-tdTomato transgenic mice. ***A-B,*** CA1 theta rhythm was recorded with a field electrode placed in stratum radiatum. ***i,*** The raw LFP signal shows that the oscillation is stable with rhythmic peaks occurring at regular intervals. The 5-s long highlighted (grey) segment is expended below. ***ii,*** The autocorrelogram of the LFP signal is used to derive the rhythmicity index, defined as the relative probability of the second peak. For the PV oscillation, the rhythmicity index is 0.45 (***Aii***), and for the SOM oscillation it is 0.33 (***Bii***). ***iii,*** The power spectrogram of the LFP signal illustrates the stability of the oscillation (3.4 Hz for PV and 3.1 Hz for SOM) over 60 s. ***C,*** A schematic of the intact hippocampal preparation, with the field electrode placed in the middle CA1. ***D,*** Averaged power spectra of CA1 theta oscillations recorded from PV- and SOM-tdTomato preparations indicate that the two transgenic mice produce similar *in vitro* theta oscillations. ***E,*** The table lists the parameters measured from the power spectrum of CA1 theta rhythm from PV and SOM preparations. None of the parameters revealed statistically significant differences between the two mouse lines.

Figure 16

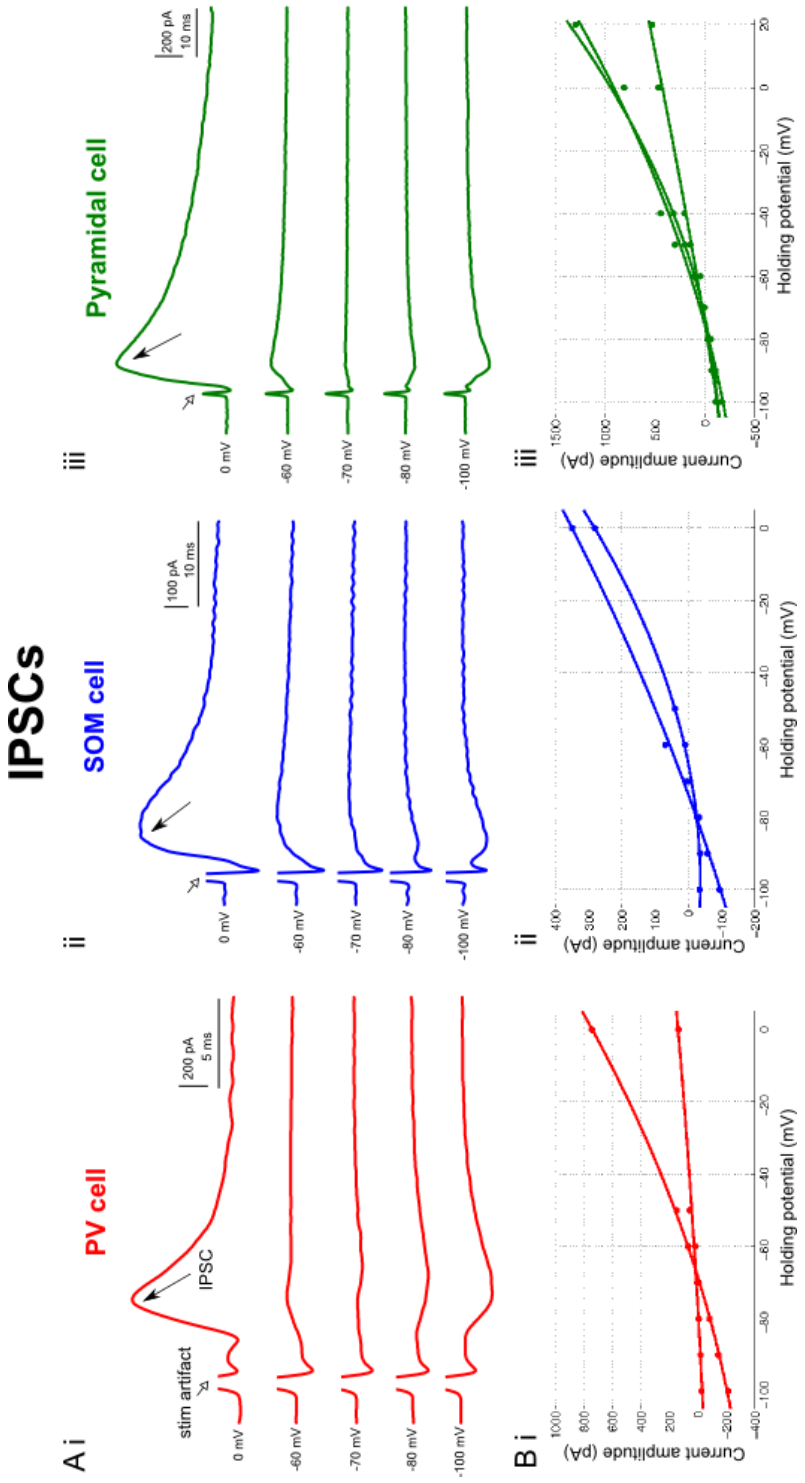
IPSCs
A i
PV cell
stim artifact
IPSC
200 pA
5 ms
0 mV
-60 mV
-70 mV
-80 mV
-100 mV
ii
SOM cell
100 pA
10 ms
iii
Pyramidal cell
200 pA
10 ms
B i
ii
iii
Current amplitude (pA)
Holding potential (mV)

Figure 16. Characterization of the IPSC reversal potential for CA1 PV and SOM stratum oriens/alveus interneurons (OAIs) and pyramidal cells. In the intact preparation, a monopolar tungsten electrode was placed in CA1 stratum oriens/alveus to electrically evoke synaptic currents in neurons recorded in whole-cell mode. Each neuron was held at various potentials in voltage clamp (-100 to 0 mV) while electrical stimulation (25 - 300 μA intensity, 0.1 ms duration) was administered. To isolate $GABA_A$-receptor mediated IPSCs, 10 μM DNQX, 25 μM DL-AP5 and 2 μM CGP 52432 were used. ***A,*** Examples of IPSCs recorded at various holding potentials (indicated on the left, in mV) in a CA1 PV OAI (***i***), a SOM OAI (***ii***) and a CA1 pyramidal cell (***iii***) are shown. Each trace represents an average of three traces and was low-pass filtered at 500 Hz. ***B,*** The IPSC amplitude at each holding potential tested is displayed for two CA1 PV OAIs (***i***), two SOM OAIs (***ii***) and three CA1 pyramidal cells (***iii***). Data points for each cell were fitted using a quadratic polynomial curve fit in Matlab. For all cell types, the IPSCs reversed near -70 mV.

Figure 17

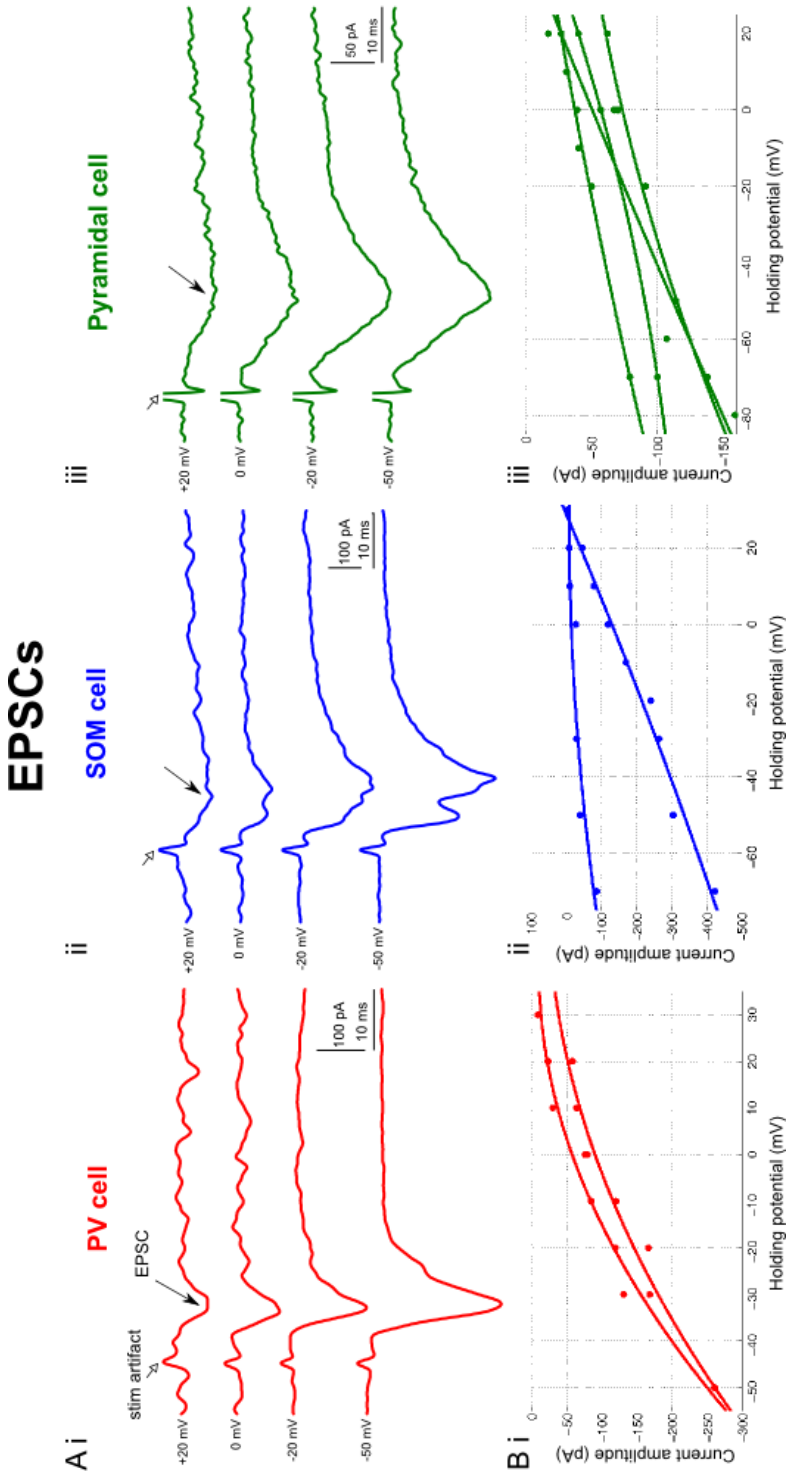
EPSCs
A i
PV cell
stim artifact
EPSC
+20 mV
0 mV
-20 mV
-50 mV
100 pA
10 ms
ii
SOM cell
+20 mV
0 mV
-20 mV
-50 mV
100 pA
10 ms
iii
Pyramidal cell
+20 mV
0 mV
-20 mV
-50 mV
50 pA
10 ms
B i
Current amplitude (pA)
Holding potential (mV)
ii
Current amplitude (pA)
Holding potential (mV)
iii
Current amplitude (pA)
Holding potential (mV)

Figure 17. Characterization of the EPSC reversal potential for CA1 PV and SOM OAIs and pyramidal cells. In the intact preparation, CA1 stratum oriens/alveus was electrically stimulated to evoke synaptic currents in neurons recorded in whole-cell mode. Each neuron was held at various potentials in voltage clamp (-70 to +30 mV) while electrical stimulation (25 - 300 μA intensity, 0.1 ms duration) was administered. In order to isolate EPSCs, 20 μM bicuculline and 2 μM CGP 52432 were used; in two pyramidal cell recordings, 5 μM gabazine was used instead of bicuculline. ***A,*** Examples of EPSCs recorded at various holding potentials (indicated on the left, in mV) in a CA1 PV OAI (***i***), a SOM OAI (***ii***) and a CA1 pyramidal cell (***iii***) are shown. Each trace represents an average of three traces and was low-pass filtered at 300 Hz. ***B,*** The EPSC amplitude at each holding potential tested is displayed for two CA1 PV OAIs (***i***), two SOM OAIs (***ii***) and four CA1 pyramidal cells (***iii***). Data points for each cell were fitted using a quadratic polynomial curve fit in Matlab. For all cell types, the EPSCs failed to reverse, even at the most positive membrane potential tested (+30 mV). However, the EPSC amplitudes at 0 mV were quite small; the average current amplitudes at 0 mV were -77pA for the two PV OAIs, -74 pA for the two SOM OAIs, and -58 pA for the four pyramidal cells.

stimulation-evoked responses among the interneurons is consistent with the expression of the $GABA_B$ receptor subunit $GABA_{B1a/b}$ in various classes of CA1 interneurons (Kulik et al., 2003). Therefore, the $GABA_B$-receptor blocker, CGP 52432, was used in all of the experiments described here.

We found that the electrical stimulation reliably evoked both excitatory and inhibitory synaptic currents in the CA1 PV and SOM OAIs and pyramidal cells. In all cell types tested, the $GABA_A$-receptor mediated IPSCs reversed near -70mV (**Fig. 16**). On the other hand, for all three cell types, the reversal of EPSCs was not observed even at highly depolarized membrane potentials tested (*e.g.*, +30 mV) (**Fig. 17**). This may partly be due to inadequate space-clamping of distal dendrites of the cells recorded here, as these experiments were done in intact preparations which better preserve entire dendritic trees of neurons compared to acute slices. However, it is also likely that the evoked EPSCs are strongly inward rectifying in these neurons, leading to little or no clear reversal of the responses at highly depolarized potentials, as reported previously for PV and SOM CA1 interneurons (Nissen et al., 2010; Szabo et al., 2012). Our results indicate that for all three cell types, the EPSCs are not null at 0 mV but are quite small; the average current amplitudes at 0 mV were -77pA for PV OAIs, -74 pA for SOM OAIs, and -58 pA for pyramidal cells. In order to improve space clamp while examining synaptic currents, CsCl-based intrapipette solution could be used in future experiments instead of the K-gluconate solution to block K^+ channels and increase space constant.

3.3. Experiment 3: CA1 PV and SOM interneurons display distinct spontaneous firing patterns during CA1 theta rhythm

Having established that the two transgenic mice produce very similar *in vitro* hippocampal theta oscillations (Experiment 1), we investigated the firing behaviour of PV and SOM OAIs during CA1 theta rhythm. To do so, we recorded the LFP signal in the middle CA1 stratum radiatum while simultaneously monitoring the spontaneous

activity of a CA1 PV or SOM OAI at Vrest in whole-cell mode (**Fig. 18A**). A total of 6 PV and 11 SOM OAIs were recorded.

We found that almost all PV OAIs (5/6; 83%) displayed spontaneous firing and all of the spontaneously active PV neurons fired single spikes or bursts of action potentials that were robustly synchronized to the ongoing CA1 theta (**Fig. 18*D***). Many SOM OAIs (9/11; 82%) were spontaneously active but only six of these displayed the strongly synchronized pattern of firing (**Fig. 18*J***). The remaining three spontaneously active SOM neurons fired tonically at 2 - 5 Hz with no clear phase-locking to theta (**Fig. 18*L***). This was despite the two groups having similar resting membrane potentials (**Table 4**). "Phase-locked" neurons were defined here as those whose spiking produced a mean vector length of greater than 0.5 on the phase vector plot. Using this criteria, all of the spontaneously firing PV OAIs (5/5; 100%) were found to be significantly phase-locked, but only a proportion of spontaneously active SOM OAIs (6/9; 67%) showed significant phase-locking. In addition, phase-locked PV neurons presented on average 5.4 spikes per burst, which was significantly more than the average of 1.9 spikes fired by phase-locked SOM neurons in each theta cycle ($p = 0.041$). Analysis of the ISI histograms revealed that as a group, phase-locked PV neurons fired at 237 Hz during the bursts, a much higher intraburst frequency compared to that of phase-locked SOM neurons (98 Hz; $p = 0.001$). Meanwhile, the interburst firing frequency did not differ between the cell types ($p = 0.992$) and merely reflected the theta rhythm frequency.

In order to examine the theta phase at which the neurons preferred to fire, we looked at each phase-locked neuron's phase vector plot and time histograms. We found that 3/6 SOM neurons and 1/5 PV neurons produced significantly skewed distributions, as assessed by the circular symmetry test. Therefore, median values were used to represent the phase and time values instead of the mean. We found that relative to CA1 theta oscillations, both PV and SOM phase-locked OAIs showed a tendency to fire slightly before the peaks of theta (**Fig. 18*E,K,N***). With theta peaks as reference (0º and 0 ms), PV neurons fired at -11.3º and -9.6 ms while SOM neurons fired at -5.9º and -4.7

Figure 18

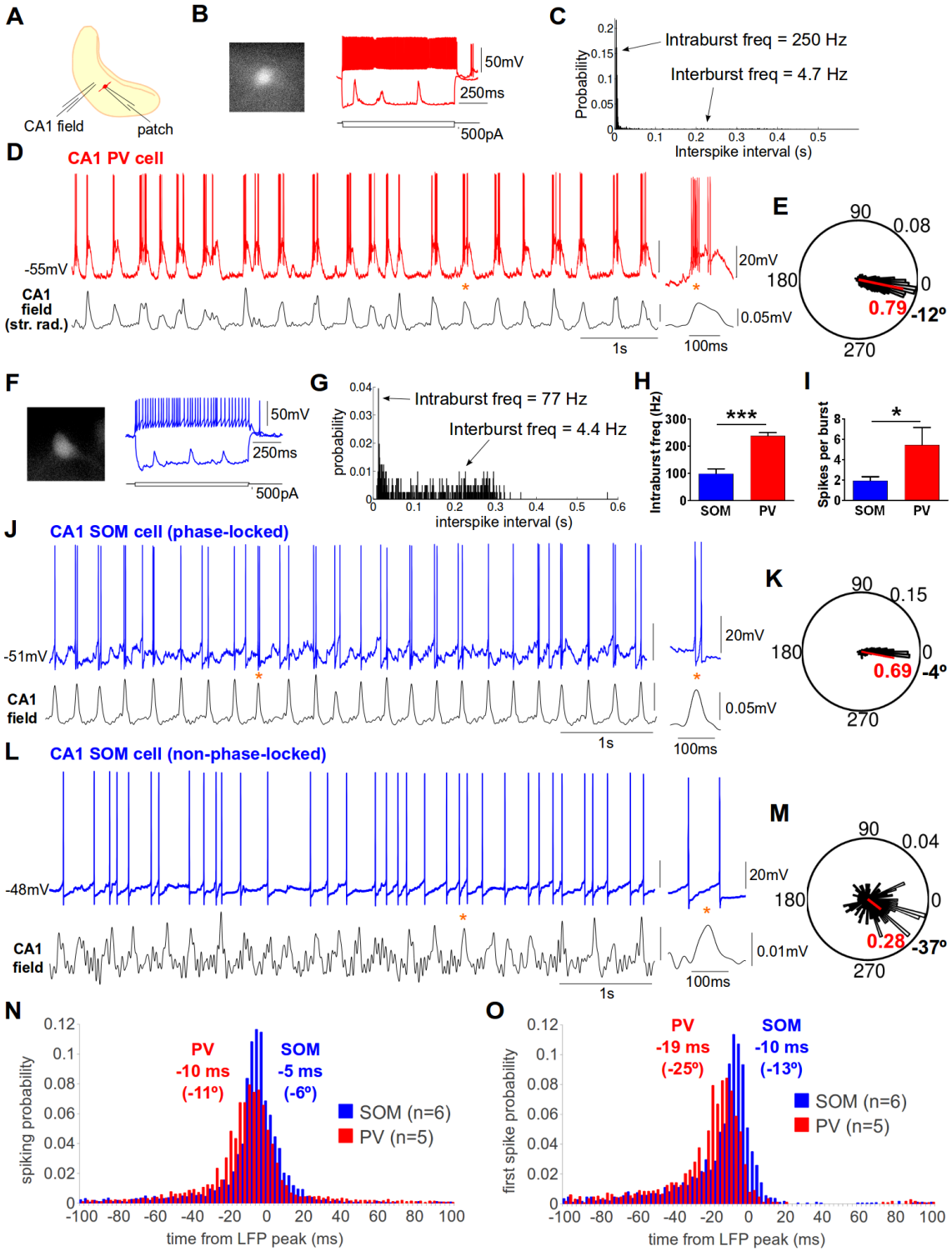
A
CA1 field
patch
B
50mV
250ms
500pA
C
Intraburst freq = 250 Hz
Interburst freq = 4.7 Hz
Probability
Interspike interval (s)
D
CA1 PV cell
-55mV
CA1 field (str. rad.)
20mV
0.05mV
1s
100ms
E
0.79
-12°
F
50mV
250ms
500pA
G
Intraburst freq = 77 Hz
Interburst freq = 4.4 Hz
probability
interspike interval (s)
H
Intraburst freq (Hz)
***
SOM
PV
I
Spikes per burst
*
J
CA1 SOM cell (phase-locked)
-51mV
CA1 field
20mV
0.05mV
K
0.69
-4°
L
CA1 SOM cell (non-phase-locked)
-48mV
CA1 field
20mV
0.01mV
M
0.28
-37°
N
PV -10 ms (-11°)
SOM -5 ms (-6°)
SOM (n=6)
PV (n=5)
spiking probability
time from LFP peak (ms)
O
PV -19 ms (-25°)
SOM -10 ms (-13°)
SOM (n=6)
PV (n=5)
first spike probability
time from LFP peak (ms)

Figure 18. CA1 PV and SOM interneurons display distinct spontaneous firing patterns during CA1 theta rhythm. ***A,*** A schematic of the intact hippocampal preparation with the field electrode placed in the middle CA1 and a nearby OAI being recorded in whole-cell mode. ***B,*** An example of a PV OAI, expressing tdTomato in the soma and displaying the fast-firing pattern and small depolarizing sag, typical of PV interneurons. ***C,*** The ISI histogram of the spontaneous firing of a CA1 PV interneuron. The shorter-interval peak indicates the neuron's intraburst frequency while the longer-interval distribution reflects the cell's spontaneous firing following the theta rhythm. ***D,*** The PV neuron exhibited spontaneous firing in the form of rhythmic bursts of spikes that were strongly phase-locked to the field theta rhythm. On average, the neuron fired 6.8 spikes per burst. ***E,*** The phase vector plot of the neuron's spontaneous firing shows that the timing of the spikes was highly concentrated around the phase of -12º (median value) relative to theta peaks as 0º. The mean phase vector length of 0.79 indicates a high level of phase-locking. Phase-locked neurons accounted for 100% of spontaneously active PV neurons recorded. ***F,*** An example of a SOM OAI, expressing tdTomato in the soma and showing a typical firing pattern that is slower in frequency compared to PV OAIs and a larger-amplitude depolarizing sag. ***G,*** The ISI histogram of the SOM interneuron's spontaneous firing. ***H,*** As a group, PV OAIs exhibited significantly faster within-burst firing frequencies compared to SOM OAIs. ***I,*** PV neurons also fired significantly more spikes per theta cycle than SOM neurons. ***J,*** The SOM OAI presented spontaneous firing that was synchronized to the ongoing theta rhythm, firing on average 1.6 spikes per theta cycle. ***K,*** The phase vector plot of this SOM neuron indicates that this neuron's spontaneous firing was clearly phase-locked (mean phase vector length of 0.69) to -4º. 67% of spontaneously firing SOM interneurons showed significant phase-locking. ***L,*** An example of another SOM OAI whose spontaneous firing was not clearly phase-locked to theta rhythm. ***M,*** The phase vector plot of this neuron confirms that this neuron's spontaneous spikes occurred without specific phase preference, indicated by the widely dispersed phase histogram distribution and the low mean phase vector length (0.28). ***N,***

Averaged time histograms of spontaneous spiking of phase-locked PV *vs.* SOM OAIs, with group means of the spiking time and phase indicated. ***O,*** Averaged time histograms constructed based on only the first spike of each theta cycle, illustrating a trend towards PV OAIs slightly leading SOM OAIs. * $p < 0.05$, *** $p < 0.001$.

Table 4. Characterization of firing behaviour of CA1 PV and SOM OAIs during CA1 theta rhythm in intact hippocampal preparation

Intact preparation	**PV**	**SOM**	**p value**
n (number of neurons)	6	11	
Vrest (mV)	-53.33 ± 2.348	-50.91 ± 0.8470	0.255
% spontaneously firing (% phase-locked neurons)	5/6 = 83.3% (5/5 = 100%)	9/11 = 81.8% (6/9 = 66.7%)	
intraburst frequency (Hz)	237.5 ± 12.50	98.35 ± 18.00	<0.001***
Interburst frequency (Hz)	3.998 ± 0.5424	3.991 ± 0.4558	0.992
number of spikes per burst	5.425 ± 1.716	1.917 ± 0.3995	0.041*
spiking phase vector length	0.8280 ± 0.06538	0.6767 ± 0.1007	0.319
spiking median phase (°)	-11.34 ± 1.946	-5.935 ± 2.310	0.115
spiking median time (ms)	-9.604 ± 1.734	-4.672 ± 1.734	0.078
first spike median phase (°)	-25.39 ± 7.226	-13.08 ± 4.825	0.178
first spike median time (ms)	-19.08 ± 3.428	-10.18 ± 3.790	0.122
EPSC amplitude (pA) (phase-locked only)	1126 ± 183.2 (1259 ± 162.6)	245.7 ± 64.45 (350.5 ± 93.38)	<0.001*** (0.001**)
IPSC amplitude (pA)	219.1 ± 68.54	176.9 ± 30.24	0.524
EPSC/IPSC ratio	7.475 ± 2.274	1.728 ± 0.383	0.006**
EPSC frequency (Hz)	3.603 ± 0.5626	3.602 ± 0.6139	1.000
EPSC median phase (°)	-13.10 ± 2.865	-0.3627 ± 1.599	0.005**
EPSC median time (ms)	-12.96 ± 3.498	-0.5540 ± 1.576	0.010*

* $p < 0.05$, ** $p < 0.01$, *** $p < 0.001$. Mean value ± S.E.M.

ms. Hence, the firing of PV OAIs preceded that of SOM OAIs by 5º in theta phase or 5 ms in time but these differences failed to reach statistical significance ($p = 0.115$ for phase, $p = 0.078$ for time). When only the first spike of each burst was taken into account (**Fig. 18*O***), the timing difference between the two cell types became numerically greater, with PV neurons leading SOM neurons by 12º and 9 ms (ps = 0.178 and 0.122 for phase and time, respectively). In summary, we found that a higher proportion of PV OAIs display spontaneous firing that is strongly phase-locked to the network theta rhythm and that they contribute significantly more spikes per theta cycle compared to SOM OAIs. As for the timing of their firing, phase-locked PV and SOM interneurons both prefer to fire just before the peaks of theta with a trend towards PV neurons leading SOM neurons slightly.

3.4. Experiment 4: CA1 PV interneurons receive a much stronger excitatory input from the network compared to SOM interneurons during theta rhythm

One of the potential factors that could lead to the distinct firing behaviour of CA1 PV and SOM OAIs during theta rhythm is differences in synaptic input. It is possible that PV neurons receive a greater excitatory input from the network, causing a higher percentage of them to become entrained by the rhythm compared to SOM neurons. Alternatively, PV neurons may receive less inhibition from other interneurons so they may be more disinhibited, leading to more spontaneous firing. In order to examine these possibilities, we recorded intracellular synaptic currents in voltage clamp during CA1 theta oscillations. The interneurons were held at -70 mV to observe the EPSCs, as the reversal potential for IPSCs was confirmed to be -70 mV (Experiment 2). The same cells were held at 0 mV to record the IPSCs, because the EPSCs were determined to be very small at this potential (Experment 2). Synaptic currents were recorded in a total of 5 PV and 9 SOM OAIs and all of the cells included here were also analyzed for their spontaneous firing patterns in Experiment 3.

We found that PV OAIs received EPSCs that were 4.5-fold greater in amplitude compared to SOM OAIs (mean: 1126pA for PV neurons *vs.* 245pA for SOM neurons, $p = 0.0001$; **Fig. 19*A-C*, Table 4**). Since only about half of the SOM neurons recorded showed significant phase-locking to theta, we analyzed EPSCs for only the phase-locked neurons (4 PV and 5 SOM neurons). Phase-locked PV interneurons displayed >3-fold larger EPSCs compared to phase-locked SOM interneurons ($p = 0.001$; **Table 4**). Interestingly, among SOM OAIs, there was a trend towards phase-locked neurons exhibiting greater-amplitude EPSCs compared to non-phase-locked neurons ($p = 0.058$; **Fig. 19*D***). In contrast to EPSCs, the IPSC amplitude did not differ significantly between PV and SOM OAIs ($p = 0.524$, **Fig. 19*A-C***). For both PV and SOM interneurons, the IPSCs were smaller in absolute amplitude compared to the EPSCs, leading to EPSC/IPSC ratios that are greater than 1. Not surprisingly, the EPSC/IPSC ratios for PV neurons were significantly larger compared to those for SOM neurons ($p = 0.006$, **Fig. 19*C***), indicating that PV neurons receive much greater excitation from the network compared to SOM neurons despite similar levels of inhibition for the two groups.

To examine the timing of the synaptic currents, only the phase-locked neurons were included in the analysis. Broadly speaking, the IPSCs and EPSCs occurred near theta peaks for both PV and SOM interneurons. Upon closer inspection, however, we found that PV OAIs displayed EPSCs with peaks occurring at -13º and -13 ms relative to theta peaks, while EPSC peaks for SOM OAIs occurred at the same time as the theta peaks (-0.4º and -0.6 ms). The finding that EPSCs occur significantly earlier for PV neurons compared to SOM neurons, by 13º or 12 ms ($p = 0.005$ for phase and $p = 0.010$ for time) is in agreement with the trend observed in Experiment 3 that PV neurons' first spikes precede those of SOM neurons by 12º or 9 ms. Taken together, these results suggest that the excitatory synaptic input which is greater in amplitude and peaks earlier for PV interneurons may drive these cells to fire in a more phase-locked manner and at a slightly earlier phase of theta compared to SOM interneurons, indicating a key role of excitatory inputs in controlling the firing behaviour of interneurons during theta rhythm.

Figure 19

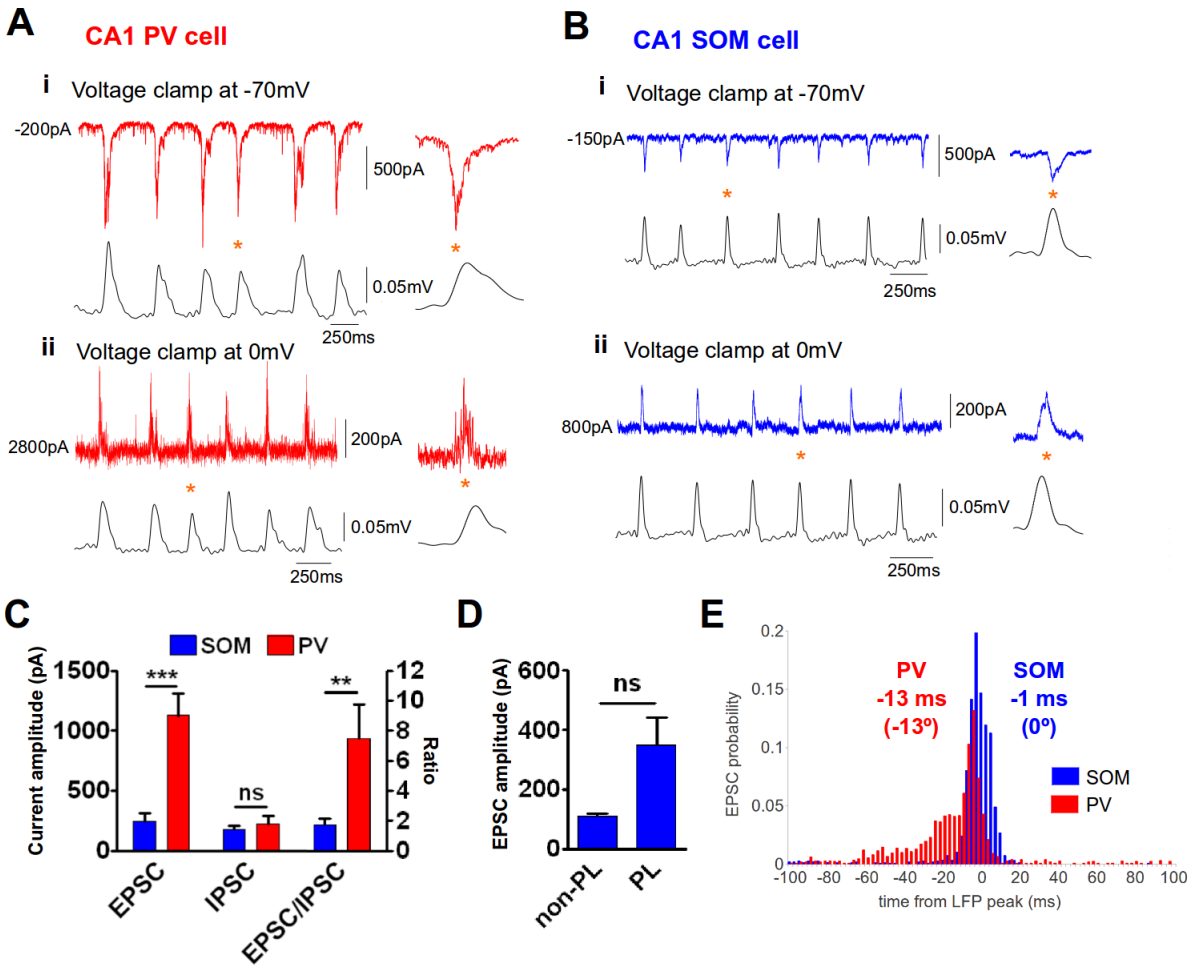
A
CA1 PV cell
i Voltage clamp at -70mV
-200pA
500pA
0.05mV
250ms
ii Voltage clamp at 0mV
2800pA
200pA
0.05mV
250ms
B
CA1 SOM cell
i Voltage clamp at -70mV
-150pA
500pA
0.05mV
250ms
ii Voltage clamp at 0mV
800pA
200pA
0.05mV
250ms
C
SOM
PV
Current amplitude (pA)
Ratio
***
ns
**
EPSC
IPSC
EPSC/IPSC
D
EPSC amplitude (pA)
ns
non-PL
PL
E
EPSC probability
PV
-13 ms
(-13°)
SOM
-1 ms
(0°)
SOM
PV
time from LFP peak (ms)

Figure 19. CA1 PV interneurons receive a much stronger excitatory input compared to SOM interneurons during theta rhythm. ***A-B,*** The presence of EPSCs (***i***) and IPSCs (***ii***) during theta rhythm was investigated in voltage clamp at -70 and 0 mV, respectively. PV interneurons displayed EPSCs that were >4-fold greater in amplitude compared to SOM interneurons, whereas the amplitudes of IPSCs were similar between the cell types. ***C,*** A graph illustrates the mean amplitude of EPSCs and IPSCs as well as the EPSC/IPSC ratio for PV and SOM interneurons, indicating that the PV cells received EPSCs that were much greater than SOM cells. ***D,*** There was a trend towards phase-locked SOM neurons displaying larger-amplitude EPSCs compared to non-phase-locked SOM neurons ($p = 0.058$). ***E,*** Averaged time histograms for the timing of EPSC peaks for PV *vs.* SOM interneurons, indicating that EPSCs for PV neurons occurred earlier than those for SOM neurons. ** $p < 0.01$, *** $p < 0.001$, ^{ns} $p > 0.05$.

Figure 20

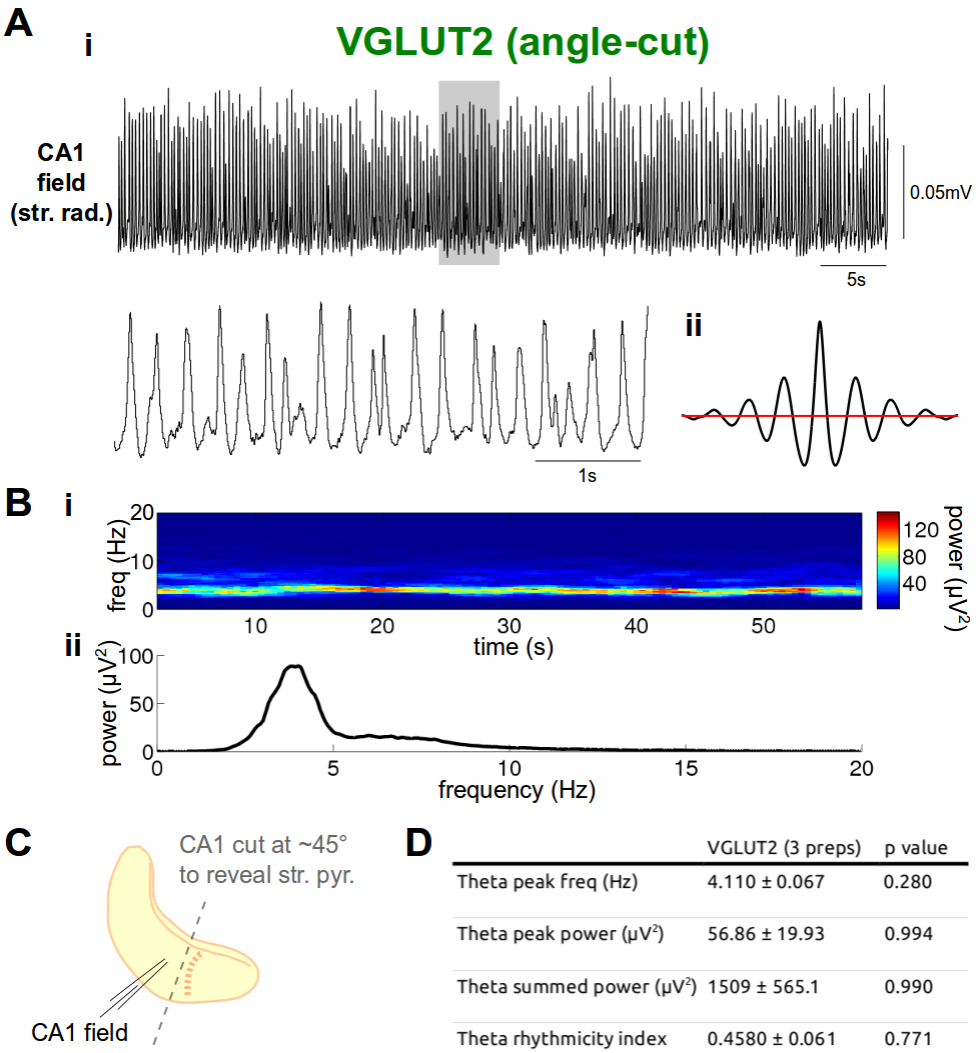

	VGLUT2 (3 preps)	p value
Theta peak freq (Hz)	4.110 ± 0.067	0.280
Theta peak power (μV²)	56.86 ± 19.93	0.994
Theta summed power (μV²)	1509 ± 565.1	0.990
Theta rhythmicity index	0.4580 ± 0.061	0.771

Figure 20. *In vitro* CA1 theta oscillation in angle-cut preparations from VGLUT2-tdTomato mice. ***A,*** CA1 theta rhythm was recorded with a field electrode placed in stratum radiatum. ***i,*** The raw LFP signal shows that the oscillation is stable with rhythmic peaks occurring at regular intervals. The 5-s long highlighted (grey) segment is expanded below for clarity. ***ii,*** The autocorrelogram of the LFP signal. The rhythmicity index (the relative probability of the second peak) for this oscillation is 0.41. ***Bi-ii,*** The power spectrogram (***i***) of the LFP signal in ***A*** illustrates the stability of the oscillation (4.0 Hz) over 60 s. The power spectrum (***ii***) is used to derive the properties listed in ***D***. ***C,*** A schematic of the hippocampal preparation shows how the prep was cut at an angle to reveal the pyramidal cells located in stratum pyramidale and the field electrode was placed in the middle CA1 close to the cut surface. ***D,*** The table lists the parameters measured from the power spectrum of CA1 theta rhythm recorded from VGLUT2 angle-cut preparations. None of the parameters revealed a statistically significant difference from those obtained in intact (PV and SOM) preparations. The *p* values are from 1-way ANOVA tests, comparing values from VGLUT2 angle-cut preps, PV intact preps *vs.* SOM intact preps.

Figure 21

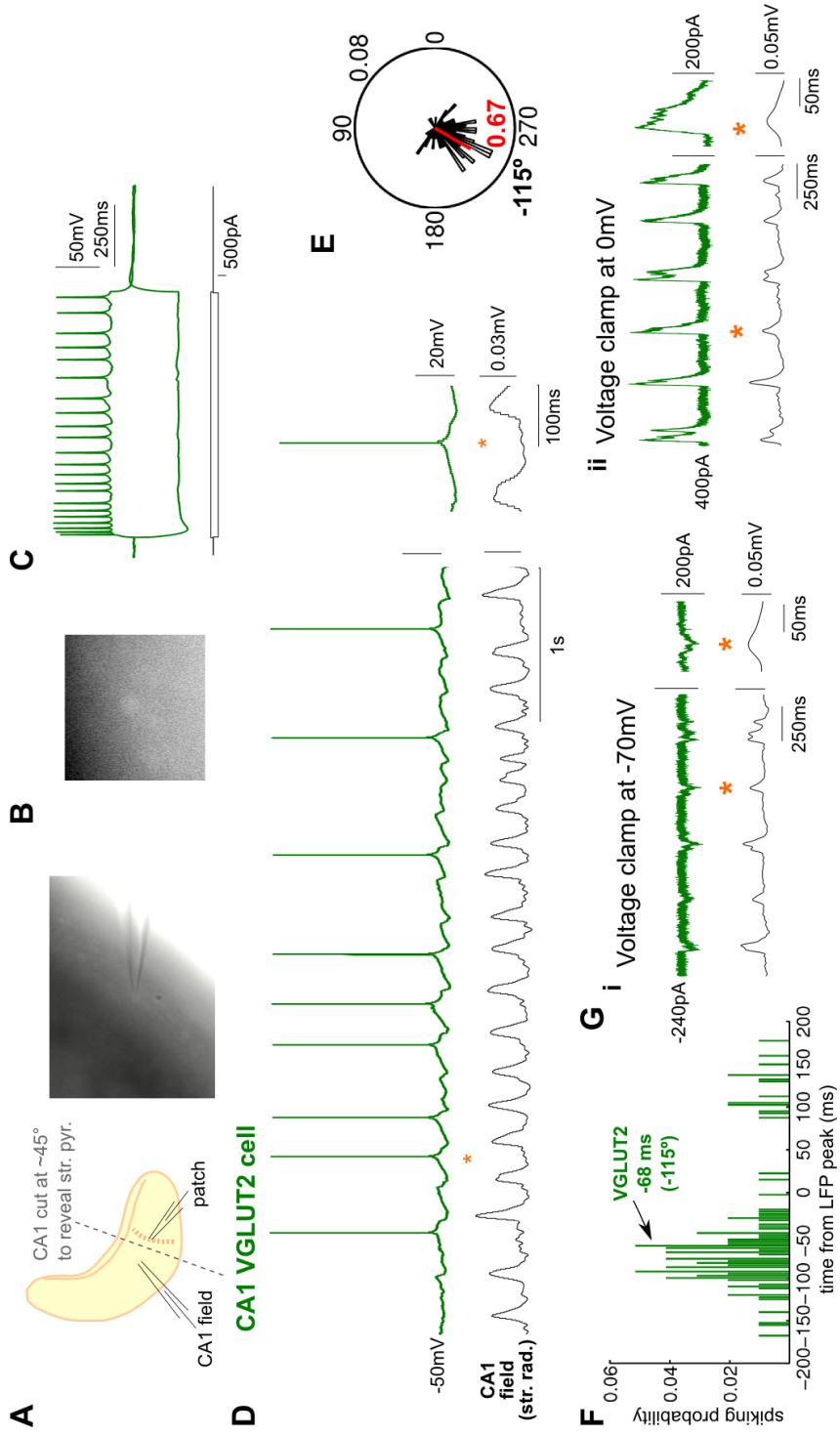
A
CA1 cut at ~45° to reveal str. pyr.
patch
CA1 field
B
C
50mV
250ms
500pA
D
CA1 VGLUT2 cell
-50mV
CA1 field (str. rad.)
1s
20mV
0.03mV
100ms
E
90
0.08
0
180
0.67
270
-115°
F
spiking probability
0.06
0.04
0.02
VGLUT2
-68 ms
(-115°)
−200 −150 −100 −50 0 50 100 150 200
time from LFP peak (ms)
G
i Voltage clamp at -70mV
-240pA
200pA
250ms
0.05mV
50ms
ii Voltage clamp at 0mV
400pA
200pA
250ms
0.05mV
50ms

Figure 21. CA1 pyramidal cells fire sparsely during theta rhythm. ***A,*** A schematic of the intact preparation cut at an angle to reveal pyramidal cells. The field electrode is placed in the middle CA1 close to the cut surface and CA1 pyramidal cells are recorded in whole-cell mode. ***B,*** VGLUT2-tdTomato mice were used to visualize pyramidal cells. An example of a VGLUT2-expressing pyramidal cell, identified by tdTomato fluorescence. ***C,*** The pyramidal cell exhibited a slow-firing pattern. ***D,*** The pyramidal cell fired spontaneously in the form of irregular tonic firing that was phase-locked to the trough of CA1 theta rhythm. From the voltage trace, it is clear that the cell avoided firing at the peaks of theta where prominent IPSPs occurred. ***E,*** The phase vector plot of this pyramidal cell's spontaneous firing shows that it preferred to fire near the phase of -115º (median value) relative to theta peaks as 0º. The mean phase vector length of 0.67 indicates significant phase-locking. ***F,*** The time histogram of the pyramidal cell's spontaneous firing is shown with the median time and phase of firing indicated. ***G,*** The presence of synaptic currents were explored in voltage clamp. ***i,*** EPSCs visible at -70 mV were small in comparison to those exhibited by the interneurons. ***ii,*** IPSCs observed at 0 mV were larger than the EPSCs in absolute amplitude, leading to the EPSC/IPSC ratio of <1. Both EPSCs and IPSCs occurred near the peaks of theta.

3.5. Experiment 5: CA1 pyramidal cells fire sparsely during theta rhythm

An important question remains unanswered as to how CA1 pyramidal cells fire during theta rhythm recorded from the intact hippocampal preparation. An earlier characterization performed in the rat hippocampal preparation using the blind-patch technique revealed that most CA1 pyramidal cells are silent during theta and that a few pyramidal cells that are spontaneously active display sparse firing that occurs near the trough of theta (Goutagny et al., 2009). In that study, the identity of the patched cell was inferred from the cell's electrophysiological characteristics. Namely, slow-firing neurons with wide spike widths were assumed to be pyramidal cells and fast-firing cells were assumed to be interneurons. While this is a popular way to identify pyramidal cells, it is becoming increasing clear that some interneuron subtypes may also exhibit similar electrophysiological properties (*e.g.*, Ivy cells) (Fuentealba et al., 2008). Therefore, we set out to characterize the firing behaviour of visually identified CA1 pyramidal cells in the mouse intact hippocampal preparation.

To do so, we employed transgenic mice in which the fluorescent protein, tdTomato, is expressed under the control of the VGLUT2 promoter. VGLUT2 was used as a marker for pyramidal cells because previous studies have demonstrated that a significant proportion of CA1 pyramidal cells retains VGLUT2 expression into adulthood (Danik et al., 2005; Herzog et al., 2006). In order to visually patch CA1 pyramidal cells, the surface of the intact hippocampal preparation was cut at an angle as illustrated in **Figure 20*C*** to expose the CA1 pyramidal layer. One may argue that such a cut may compromise the network circuitry and perturb theta oscillations. Our analysis of the LFP signal revealed that the angle-cut preparations obtained from VGLUT2-tdTomato mice gave rise to CA1 theta oscillations that are virtually identical to those recorded from intact PV- and SOM-tdTomato preparations, in terms of frequency, power and rhythmicity (1-way ANOVA: ps > 0.05; **Fig. 20**). Thus, we carried out whole-cell recordings from VGLUT2-expressing CA1 pyramidal cells during theta.

We found that out of five CA1 pyramidal cells recorded, only one showed tonic

spontaneous firing and the remaining cells were not spontaneously active at all or displayed too few spikes to be included in the analysis (only 1 - 3 spikes in 60 s). The only spontaneously active cell analyzed showed spiking at a mean rate of 1.57 Hz (**Fig. 21*D***). Considering that the field oscillation was ~4 Hz in this case, the neuron fired once every 2.5 theta cycles, on average. The spontaneous firing was in the form of irregular tonic-firing with single spikes occurring near the rising phase/trough of network theta rhythm. This neuron's phase vector plot (**Fig. 21*E***) shows that its firing was significantly phase-locked with tuning near -115º (relative to theta peaks as 0º). As indicated by the time histogram (**Fig. 21*F***), the pyramidal cell clearly avoided firing near theta peaks (0 ms). This was most likely because prominent IPSPs occurring at the peaks prevented the cell from firing at this phase. The pyramidal cell appeared to fire during the rebound depolarization following the IPSPs. The other four pyramidal cells could be depolarized to initiate firing. When such 'depolarized' firing patterns were analyzed, most spikes also occurred near the rising phase or the trough of theta and clearly avoided theta peaks (not shown). It is remarkable that the absence of firing and the presence of IPSPs at theta peaks observed here in the pyramidal cells compliment our finding from Experiment 3 that both PV and SOM interneurons prefer to fire near the peaks of theta**.**

Synaptic events were examined in voltage clamp in two CA1 pyramidal cells, one of which was the spontaneously active cell. In contrast to PV and SOM OAIs, pyramidal cells displayed EPSCs that were smaller in absolute amplitude compared to the IPSCs (**Fig. 21*G***), giving rise to EPSC/IPSC ratios of less than 1. In fact, 1-way ANOVA and post-hoc tests revealed that EPSC amplitudes and EPSC/IPSC ratios were significantly smaller for pyramidal cells compared to PV OAIs (ps < 0.05). These results indicate that unlike the interneurons, most CA1 pyramidal cells are silent during theta rhythm and only a minority of cells are spontaneously active in the form of sparse tonic firing. Whereas synaptic events in interneurons are dominated by excitatory inputs, pyramidal cells' synaptic inputs appear to be primarily inhibitory.

Figure 22

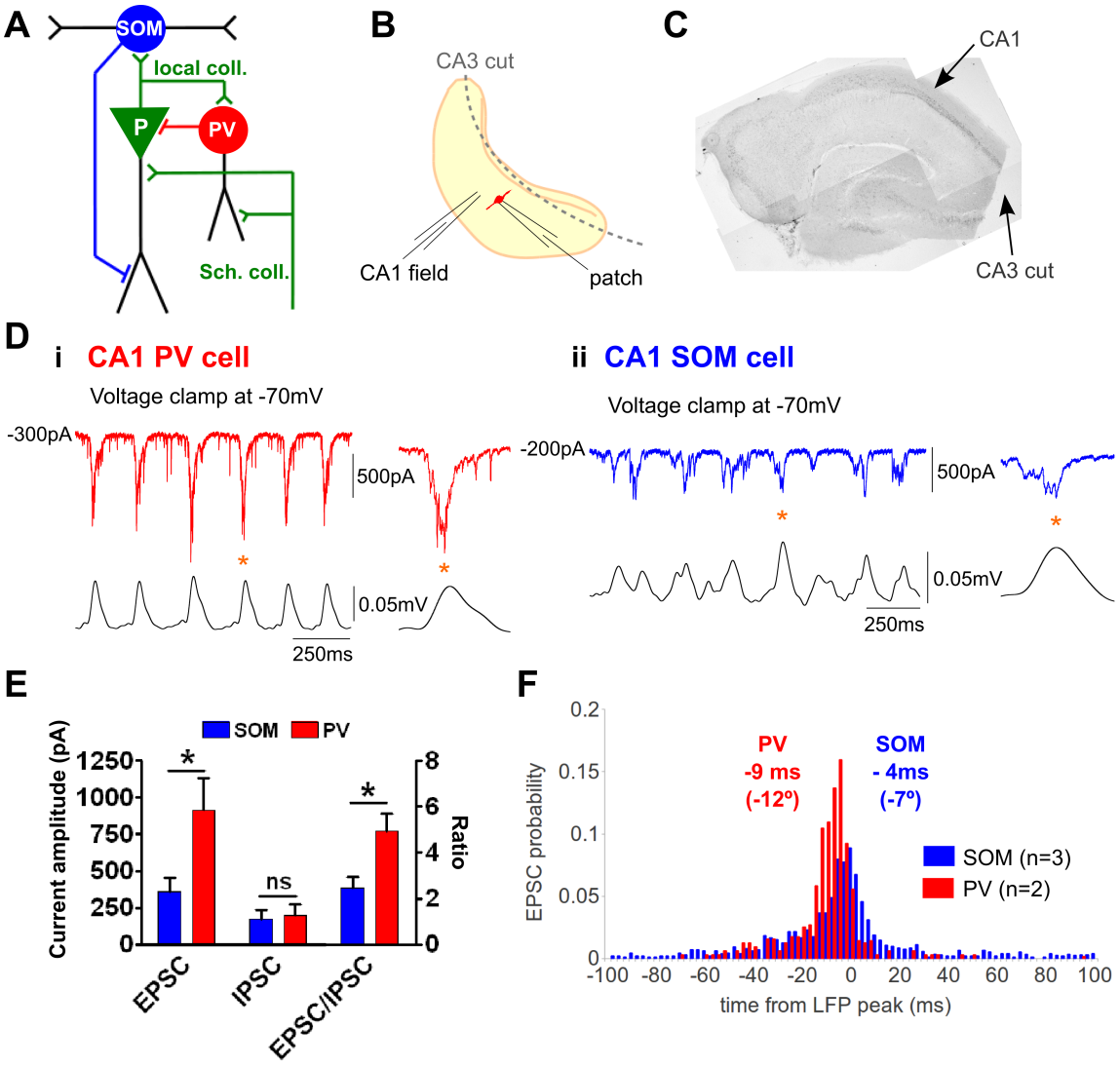
A
SOM
local coll.
P
PV
Sch. coll.
B
CA3 cut
CA1 field
patch
C
CA1
CA3 cut
D
i CA1 PV cell
Voltage clamp at -70mV
-300pA
500pA
0.05mV
250ms
ii CA1 SOM cell
Voltage clamp at -70mV
-200pA
500pA
0.05mV
250ms
E
SOM
PV
Current amplitude (pA)
Ratio
ns
EPSC
IPSC
EPSC/IPSC
F
EPSC probability
PV
-9 ms
(-12°)
SOM
- 4ms
(-7°)
SOM (n=3)
PV (n=2)
time from LFP peak (ms)

Figure 22. Rhythmic excitatory inputs to interneurons are intrinsic to CA1 and do not originate from CA3. ***A,*** A schematic illustrating the possible intrahippocampal sources of glutamatergic inputs (denoted in green) to CA1 PV and SOM interneurons. CA1 PV interneurons receive excitatory inputs from local CA1 pyramidal cells as well as from the CA3 via Schaffer collaterals. In contrast, CA1 SOM interneurons receive the vast majority of their excitatory inputs from the local CA1 collaterals. ***B,*** In order to exclude the CA3 as a source of the rhythmic excitatory inputs, we cut the CA3 off from the intact hippocampal preparation during dissection. ***C,*** The cut is confirmed by a light microscopic image, showing a cross section of the preparation. ***Di-ii,*** The presence of EPSCs during theta rhythm was investigated in voltage clamp at -70 mV in PV and SOM interneurons. These example traces demonstrate that both interneuron types display rhythmic EPSCs that are synchronized to ongoing CA1 theta oscillation. They also illustrate that larger-amplitude EPSCs are exhibited by PV neurons compared to SOM neurons. ***E,*** A graph illustrates the mean amplitude of EPSCs and IPSCs as well as the EPSC/IPSC ratio for PV and SOM interneurons, indicating that the PV neurons receive larger EPSCs compared to SOM interneurons in the CA3-cut preparations. ***F,*** Averaged time histograms for the timing of EPSC peaks for PV *vs.* SOM interneurons, indicating that EPSCs for PV neurons tended to peak earlier than those for SOM neurons. * $p < 0.05$, ^{ns} $p > 0.05$.

Table 5. Characterization of firing behaviour of CA1 PV and SOM OAIs during CA1 theta rhythm in CA3-cut hippocampal preparations

CA3-cut preparation	PV	SOM	p value
CA1 theta rhythm analysis			
n (number of preps)	3	3	
theta peak freq (Hz)	3.673 ± 0.6912	4.804 ± 0.4037	0.231
theta peak power (μV^2)	60.16 ± 18.25	42.25 ± 21.54	0.560
theta summed power (μV^2)	1781 ± 363.1	1102 ± 405.7	0.281
theta rhythmicity index	0.3104 ± 0.1422	0.4188 ± 0.1094	0.579
Cellular behaviour analysis			
n (number of neurons)	3	4	
Vrest (mV)	-48.67 ± 4.485	-49.75 ± 1.109	0.796
% spontaneously firing (% phase-locked neurons)	3/3 = 100% (3/3 = 100%)	4/4 = 100% (3/4 = 75%)	
intraburst frequency (Hz)	200.0 ± 0.00	92.27 ± 37.80	n/a
Interburst frequency (Hz)	4.433 ± 0.7964	5.854 ± 0.5058	0.207
number of spikes per burst	4.900 ± 1.464	1.400 ± 0.1000	0.076
spiking phase vector length	0.7745 ± 0.1093	0.6919 ± 0.1801	0.736
spiking median phase (°)	-14.87 ± 5.913	-11.77 ± 7.362	0.759
spiking median time (ms)	-11.15 ± 5.447	-5.907 ± 3.930	0.478
first spike median phase (°)	-38.87 ± 7.703	-19.34 ± 6.892	0.132
first spike median time (ms)	-28.34 ± 9.868	-10.21 ± 3.358	0.157
EPSC amplitude (pA) (phase-locked only)	915.1 ± 216.2 (915.1 ± 216.2)	359.2 ± 93.91 (383.6 ± 128.2)	0.045* (0.105)
IPSC amplitude (pA)	197.0 ± 74.00	171.5 ± 63.03	0.820
EPSC/IPSC ratio	4.928 ± 0.7536	2.459 ± 0.5008	0.049*
EPSC frequency (Hz)	4.085 ± 1.265	4.700 ± 0.4900	0.626
EPSC median phase (°)	-11.66 ± 0.6390	-6.994 ± 7.454	0.661
EPSC median time (ms)	-9.157 ± 2.871	-4.232 ± 4.622	0.494

* $p < 0.05$, $^{n/a}$ not available. Mean value ± S.E.M.

3.6. Experiment 6: Rhythmic excitatory inputs to interneurons are intrinsic to CA1 and do not originate from CA3

Results from Experiment 4 illustrated that CA1 PV and SOM OAIs display rhythmic excitatory inputs that are correlated with strongly phase-locked spontaneous firing. The source of the rhythmic EPSCs during theta rhythm, however, remains unclear. Considering only the intrahippocampal connections contained within the intact preparation, previous anatomical and electrophysiological studies indicate that SOM OAIs receive the vast majority of their excitatory inputs from the local collaterals of CA1 pyramidal cells, whereas PV OAIs receive glutamatergic inputs from both CA1 local collaterals and CA3 pyramidal cells via Schaffer collaterals (Blasco-Ibáñez and Freund, 1995; Maccaferri and McBain, 1995, 1996a; Takács et al., 2012). Do the rhythmic EPSCs observed in CA1 PV and SOM OAIs come from local CA1 pyramidal cells only or do they partially reflect CA3 input (**Fig. 22*A***)? Given the previous demonstration that CA1 theta rhythm can arise independently of CA3 in the intact preparation (Goutagny et al., 2009), we suspect that most of the rhythmic EPSCs probably originate from local CA1 pyramidal cells during intrinsic CA1 theta oscillations. Alternatively, some of the rhythmic EPSCs may come from the CA3 input, particularly for PV neurons.

We aimed to test this question by cutting the CA3 off from the intact hippocampal preparation at the time of the dissection as illustrated in **Figure 22*B-C***. Our analysis of the LFP signal showed that the CA1 theta oscillations recorded from CA3-cut preparations are not significantly different between PV- and SOM-tdTomato mice (**Table 5**) and from those recorded from intact preparations on all parameters measured, including frequency, power and rhythmicity (2-way ANOVA; ps > 0.05). Thus, CA1 theta oscillations were not significantly altered by severing the CA3, consistent with the previous finding that CA1 oscillations are independent from CA3 rhythms (Goutagny et al., 2009). Using the CA3-cut preparations, we carried out simultaneous LFP and whole-cell recordings from a total of 3 PV and 4 SOM OAIs.

Consistent with results from Experiment 3, we found that CA1 PV and SOM

OAIs displayed distinct firing behaviour during CA1 theta rhythm in the CA3-cut preparations. Due to the low sample size, the results here should be treated as preliminary (for a summary of results, see **Table 5**). All of the PV and SOM interneurons recorded were spontaneously active. Every PV neuron (3/3) and most of the SOM neurons (3/4) displayed significant phase-locking to theta. Similar to the intact preparation recordings, PV neurons fired more spikes per burst (4.9 spikes) and exhibited a higher intraburst firing frequency (200 Hz) compared to SOM neurons (1.4 spikes, 92 Hz). The phase-locked PV OAIs showed preference to fire at -14.9º and -11.1 ms relative to theta peaks, while phase-locked SOM OAIs preferred to fire at -11.7º and -5.9 ms, thus PV neurons led SOM neurons by 3º or 5 ms. When the timing of only the first spike in each theta cycle was taken into account, the numerical difference became more pronounced with PV neurons leading SOM neurons by 19º and 18 ms. However, all of the differences described above failed to reach statistical significance.

Next, synaptic currents in PV and SOM OAIs during CA1 theta rhythm were examined. Importantly, PV interneurons displayed EPSCs that were significantly larger than those observed in SOM interneurons (~2.5-fold difference; $p = 0.045$), while the IPSC amplitude did not differ between the cell types ($p = 0.820$; **Fig. 22*D-E***), replicating the results from the intact preparations. The mean EPSC/IPSC ratio was also significantly higher for PV interneurons compared to SOM interneurons ($p = 0.049$). When the timing of synaptic currents were examined in relation to the theta rhythm, we found that both EPSCs and IPSCs occurred near the peaks of theta. Numerically, EPSC peaks in PV neurons occurred ~ 5º and 5 ms earlier than those observed in SOM neurons (**Fig. 22*F***) although these differences were not statistically significant.

These preliminary results are in agreement with those found in the intact preparations, indicating that CA1 PV and SOM OAIs display their unique firing behaviour and synaptic activities, regardless of the presence of CA3. Importantly, this suggests that the rhythmic excitatory inputs impinging on PV and SOM interneurons during theta rhythm do not originate from CA3 but most likely arise from local CA1

pyramidal cells.

VI.4. Discussion

Here, we show for the first time that two specific CA1 interneuron classes, PV- and SOM-expressing interneurons, display distinct firing behaviour during intrinsically generated *in vitro* hippocampal theta rhythm. We found that PV interneurons are quite uniform in their firing pattern, displaying bursts of multiple action potentials that are highly phase-locked to the ongoing theta rhythm. In contrast, SOM interneurons were found to be more heterogeneous with only about half (6/11) of the neurons showing significant phase-locking, while the other half were either silent or firing tonically without clear phase-locking. We further demonstrated that these differences in firing behaviour may be due to disparity in synaptic inputs. Our voltage-clamp experiments revealed that during theta rhythm, PV interneurons receive rhythmic EPSCs that are >4-fold greater in amplitude compared to those observed in SOM interneurons. Interestingly, the IPSC size was found to be similar between the cell types. Among the SOM population, there was a trend towards phase-locked neurons displaying larger-amplitude EPSCs compared to non-phase-locked neurons. Variations in the degree of phase-locking among CA1 interneurons have been observed previously *in vivo* (Csicsvari et al., 1999; Czurko et al., 2011), but little is known about the factors determining the degree of phase-locking in neurons. Our results provide the first piece of evidence demonstrating that the extent to which interneurons are phase-locked to network theta rhythm may be directly linked to the excitatory inputs received from the local network. It is possible that the heterogeneity in phase-locking and EPSC amplitudes among SOM interneurons may be due to sampling of different interneuron subtypes (*e.g.*, O-LM and bistratified cells). A morphological analysis of recorded neurons will be needed to answer this question.

We found that phase-locked PV neurons fire significantly more spikes per theta cycle and with a much faster within-burst firing rate compared to phase-locked SOM

neurons. Although these differences in firing pattern may be partially attributable to synaptic factors, it seems more likely that they reflect differences in intrinsic properties of PV and SOM interneurons. In Chapter 5, we showed that PV interneurons possess firing rates and membrane time constants that are on average ~3-fold faster than SOM interneurons. This fits with our data presented here that within each burst, PV neurons fire ~2.5 times faster and pack in >2 times more spikes per theta cycle than SOM neurons. Taken together, these results indicate that as a group, PV interneurons are more likely to phase-lock their firing to theta rhythm and each phase-locked PV neuron fires in the form of highly concentrated bursts of multiple spikes. By providing such a highly synchronized and powerful inhibitory output, it is likely that PV interneuron firing has a substantial impact on local networks during theta rhythm. This is the topic of investigation for experiments described in Chapter 7.

In terms of theta phase, we found that both phase-locked PV and SOM neurons preferred to fire just before the peaks of CA1 theta with a trend towards PV neurons to lead SOM neurons slightly. The timing differences between PV and SOM neurons were 5º (theta phase) or 5 ms (actual time) with all spikes considered, and 12º or 9 ms when only the first spike of each burst/theta cycle was included in the analysis. However, these differences were relatively small and failed to reach statistical significance. The timing differences may simply be due to differences in membrane kinetics, as PV neurons were shown to have faster membrane time constants compared to SOM interneurons in Chapter 5. Alternatively, excitatory inputs may arrive earlier for PV neurons and drive these cells to fire sooner than SOM cells. Consistent with this, we found that EPSC peaks occurred significantly earlier for PV neurons compared to SOM neurons (by 13º or 12 ms). Ali and colleagues found that unitary excitatory potentials between CA1 pyramidal cells and interneurons showed faster kinetics for basket cells (a type of PV neuron) in comparison to O-LM cells (a type of SOM neuron) (Ali and Thomson, 1998; Ali et al., 1998). A closer examination of the EPSCs will be required to reveal whether the timing differences are in the onset of the responses or in their kinetics. Nonetheless, it is

interesting to note that the timing differences between PV and SOM interneuron firing mirror the timing differences in the EPSC peaks observed in the two cell types, suggesting that among strongly phase-locked cells, excitatory inputs play a key role in controlling the timing of the cells' spiking during theta rhythm.

Even though rhythmic EPSCs with tight synchrony to the network rhythm were observed in interneurons, paradoxically we found that only a small proportion of the CA1 pyramidal cells recorded (1/5) fired spontaneously during theta. The only active pyramidal cell displayed sparse firing that occurred close to the rising phase/trough of theta (-115º). The cell's spiking clearly avoided theta peaks, probably due to the occurrence of prominent IPSPs preventing the cell from firing at that phase. This is consistent with our finding that both PV and SOM phase-locked interneurons show a strong preference to fire just before the peak of theta. The pyramidal cell appeared to fire during the rebound depolarization following the IPSPs, which was likely mediated by I_h as reported previously (Ascoli et al., 2010) but this remains to be tested directly. In addition, when the quiescent pyramidal cells were depolarized slightly, they also showed a tendency to fire near the rising phase or the trough of theta, avoiding the peaks. This is in agreement with the previous observation made using the blind-patch technique in the intact rat hippocampal preparations that most CA1 pyramidal cells are silent during theta and with depolarizing current injections, they tend to fire at the rising phase of theta (Goutagny et al., 2009).

The relative scarcity of firing by CA1 pyramidal cells demonstrated here indicates that perhaps only a small proportion of pyramidal cells needs to be active in order to provide the excitatory drive necessary to support phase-locked firing of many interneurons. This is probably due to the large (~9:1) pyramidal cell to interneuron ratio (Woodson et al., 1989; Aika et al., 1994) and the highly efficient excitatory synapses that exist between them (Gulyás et al., 1993). In addition, PV interneurons have been shown to possess a very extensive dendritic tree with the vast majority of afferents being excitatory inputs (Gulyás et al., 1999). In turn, the phase-locked interneurons provide

prominent inhibitory inputs that can synchronize subthreshold membrane oscillations and firing of many pyramidal cells (Cobb et al., 1995). Indeed, it has been estimated that a single basket cell (a type of PV interneuron) can contact >1000 CA1 pyramidal cells (Sik et al., 1995; Halasy et al., 1996).

The firing behaviour of CA1 PV and SOM interneurons during *in vitro* theta as reported here has both similarities and differences with *in vivo* theta rhythm. **Figure 23** illustrates the comparison between our data and the available *in vivo* data from Royer et al. (2012) with phase expressed relative to CA1 stratum radiatum theta peaks as 0º, as done in our study. It is important to note that *in vivo*, the reference theta rhythm was recorded in CA1 stratum pyramidale (Royer et al., 2012). Thus in **Figure 23**, *in vivo* spikes occurring near the trough of stratum pyramidale theta were depicted as occurring near the peak of stratum radiatum theta, taking into account the ~180° theta phase reversal observed between the two layers both *in vivo* and *in vitro* (Buzsaki, 2002; Goutagny et al., 2009). Our data indicates that in the intact hippocampal preparation, phase-locked PV and SOM interneurons both fire close to the peak of theta with only subtle phase differences. However, the *in vivo* data place the two cell types at more distinct theta phases. The similarity is that in both cases, PV neurons fire before SOM neurons. The differences probably arise due to the presence of distinct synaptic inputs at play during *in vitro vs. in vivo* theta rhythm. For instance, during the *in vitro* theta the interneurons' firing pattern is driven by a single source of excitatory input from the local CA1 pyramidal cells, causing them to fire very close together. We demonstrated in Experiment 6 that the CA3 input does not play an important role in generation of the *in vitro* CA1 theta rhythm or the cellular behaviour of PV and SOM OAIs during this type of theta. *In vivo,* however, these interneurons are subject to multiple synaptic influences including CA3 inputs and inhibitory inputs from the MS-DBB (Ylinen et al., 1995) that can affect their firing phase significantly. A similar line of reasoning may apply to pyramidal cells. Pyramidal cell firing during *in vitro* theta is relatively concentrated around the rising phase/trough of theta, determined primarily by the inhibitory inputs

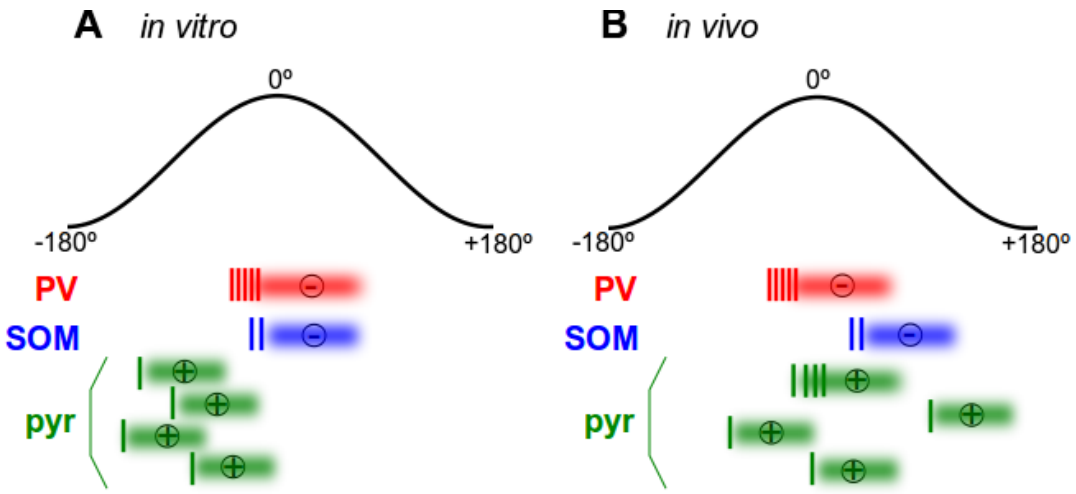

Figure 23. Comparison of firing behaviour of CA1 PV and SOM interneurons and pyramidal cells during *in vitro* theta (our data) and *in vivo* theta (adapted from Royer et al., 2012). The phase of theta rhythm is referenced to CA1 stratum radiatum theta (peaks as 0º), as done in our study. ***A,*** In the intact hippocampal preparation, PV and SOM interneurons both fire near the peak of theta, with PV neurons leading SOM neurons slightly. Pyramidal cells are phase-locked to the rising phase/trough of theta. Even though we found only one spontaneously active pyramidal cell during theta rhythm, multiple pyramidal cells are depicted here to reflect the high pyramidal-cell-to-interneuron ratio in cell density. ***B,*** *In vivo,* PV interneurons prefer to fire in the rising phase/peak of theta while SOM neurons fire mostly in the falling phase. Pyramidal cells are weakly phase-modulated with preference near the rising phase/peak of theta. Vertical lines of different colours represent spikes belonging to different cell types (red: PV, blue: SOM, green: pyramidal cell). Fuzzy bars trailing behind the spikes with + or - symbols represent the postsynaptic effect (+ excitation, - inhibition).

from interneurons and subsequent rebound-firing. CA1 pyramidal cells appear to fire with more variable phase relationships with the ongoing theta rhythm *in vivo* (Royer et al., 2012). This is probably because *in vivo*, CA1 pyramidal cell firing reflects a result of both the inhibitory inputs from interneurons and excitatory inputs from various afferent sources (e.g, CA3, entorhinal cortex and the MS-DBB). The relatively large variability in phase modulation of pyramidal cell firing during *in vivo* theta is also consistent with the well-known observation that only the most strongly activated pyramidal cells fire *in vivo* (i.e., place cells), and place cell firing advances in theta phase as the animal crosses the place field (O'Keefe and Recce, 1993; Skaggs et al., 1996).

In summary, our results presented here reveal new insights into the potential mechanisms for phase-locking. We demonstrate here that as a group, PV interneurons fire in a more phase-locked manner compared to SOM interneurons and the degree of phase-locking appears to depend on the amount of the excitatory drive received from the local network. Once an interneuron is phase-locked to the rhythm, the preferred firing phase closely follows the timing of the excitatory inputs. The interneuron's intrinsic membrane properties may play a key role in determining its output during each theta cycle (*i.e.*, the number of action potentials and the within-cycle firing frequency). Therefore, our results indicate that an interneuron's firing behaviour during theta rhythm is a result of an interaction between intrinsic and extrinsic (synaptic) factors. Our description of the cellular behaviour of distinct CA1 interneuron subtypes and pyramidal cells during *in vitro* theta rhythm will be useful for future studies employing the intact hippocampal preparation to study theta rhythm generation. In particular, knowing the cellular behaviour of PV and SOM interneurons during theta will be critical for understanding the effects of silencing their activity on the network rhythm. This is the topic that is explored in the optogenetic experiments described in the next chapter.

VI.5. Appendix 1

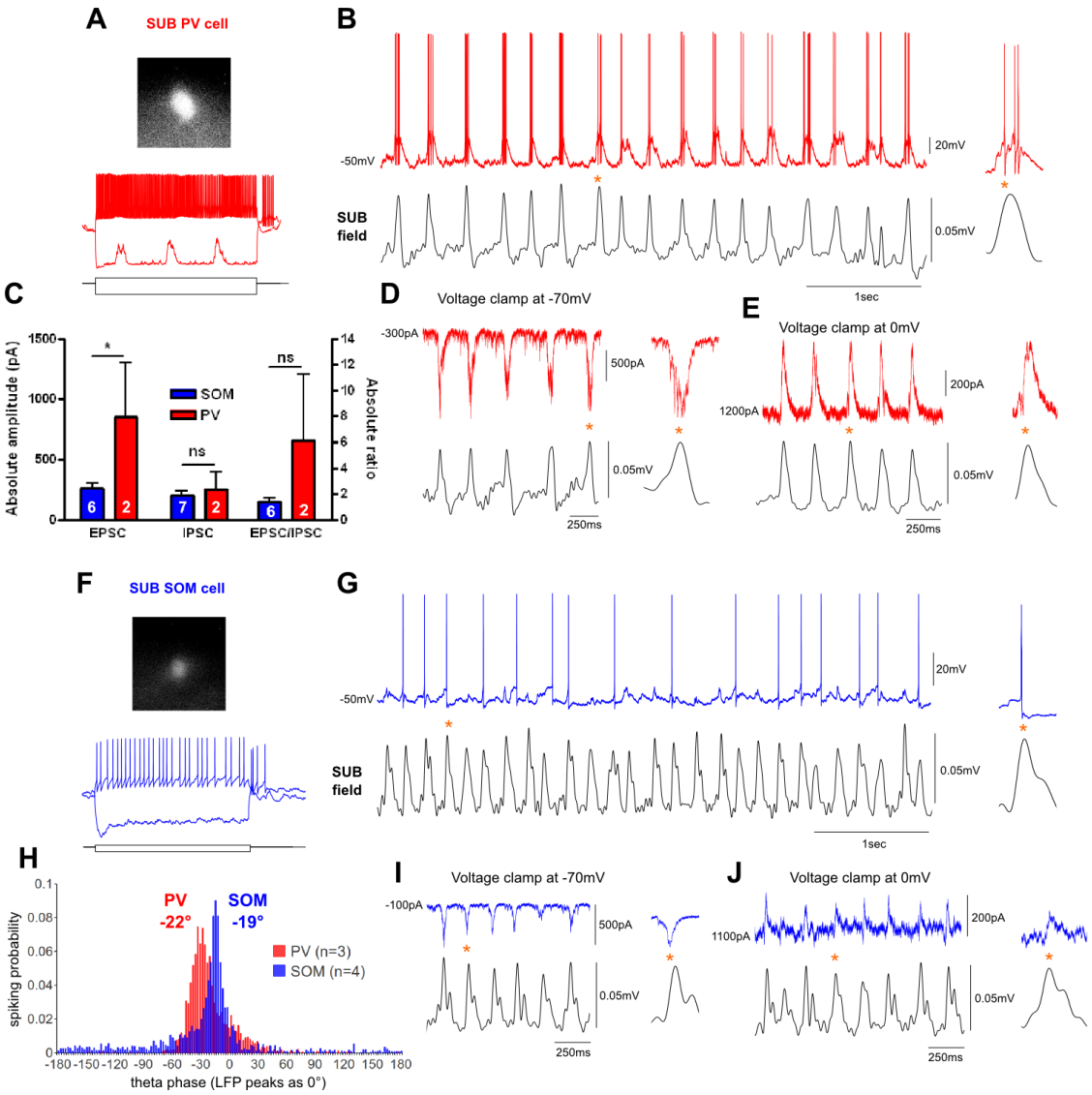

Figure 24. Appendix 1. Subiculum PV and SOM interneurons display distinct spontaneous firing patterns during CA1 theta rhythm. ***A,*** An example of a subiculum PV interneuron, expressing tdTomato in the soma and displaying the fast-firing pattern and small depolarizing sag, typical of PV neurons. ***B,*** The PV neuron exhibited spontaneous firing in the form of rhythmic bursts of spikes that were strongly phase-locked to the field theta rhythm. On average, the neuron fired ~4 spikes per burst. ***C,*** A graph illustrates the mean amplitude of EPSCs and IPSCs as well as the EPSC/IPSC ratio for PV and SOM interneurons, indicating that the PV cells received EPSCs that were ~3-fold greater compared to SOM cells, despite having similar-amplitude IPSCs. The white numbers inside the bars represent the number of cells recorded. ***D-E,*** The presence of EPSCs (***D***) and IPSCs (***E***) during theta rhythm was investigated in this PV neuron in voltage clamp at -70 and 0 mV, respectively. ***F,*** An example of a subiculum SOM interneuron, expressing tdTomato in the soma and showing a typical firing pattern that is slower in frequency compared to PV neurons and a larger-amplitude depolarizing sag. ***G,*** The SOM interneuron presented spontaneous firing that not as clearly synchronized to the ongoing theta rhythm as the PV neuron. The SOM neuron fired less than 1 spike per theta cycle on average. ***H,*** Averaged phase histograms of spontaneous spiking of phase-locked subiculum PV *vs.* SOM interneurons, with groups means of the spiking phase depicted, indicating that PV neurons fired at a slightly earlier phase compared to SOM neurons. ***I-J,*** The EPSCs (***I***) and IPSCs (***J***) during theta rhythm were examined in this SOM neuron in voltage clamp at -70 and 0 mV, respectively. * $p < 0.05$, ^{ns} $p > 0.05$.

VI.6. Appendix 2

Table 6. Appendix 2. Characterization of firing behaviour of subiculum PV and SOM interneurons during theta rhythm in intact hippocampal preparation

Intact preparation	**PV**	**SOM**	**p value**
n (number of neurons)	3	9	
Vrest (mV)	-52.67 ± 1.764	-51.11 ± 0.8889	0.4158
% spontaneously firing (% phase-locked neurons)	3/3= 100% (3/3 = 100%)	5/9 = 55.5% (4/5 = 80%)	
intraburst frequency (Hz)	261.1 ± 38.89	118.1 ± 6.945	0.0659
Interburst frequency (Hz)	4.378 ± 0.3621	6.119 ± 0.8560	0.2144
number of spikes per burst	3.000 ± 0.5774	1.640 ± 0.5913	0.179
spiking phase (°)	-21.67 ± 7.407	-19.38 ± 3.870	0.7781
EPSC amplitude (pA)	855.0 ± 449.0	261.7 ± 41.58	0.0386*
IPSC amplitude (pA)	255.5 ± 139.5	198.1 ± 36.61	0.559
EPSC/IPSC ratio	6.135 ± 5.107	1.351 ± 0.3140	0.1014

* $p < 0.05$. Mean value ± S.E.M.

Chapter VII: Optogenetic investigation into the role of CA1 PV and SOM interneurons in theta rhythm generation *in vitro*

VII.1. Introduction

The exact role of CA1 PV and SOM interneurons in hippocampal theta rhythm remains largely undefined despite years of *in vitro* and *in vivo* research. Considering that CA1 PV basket and axo-axonic cells provide predominantly perisomatic inhibition to CA1 pyramidal cells and they tend to fire at an opposite phase of theta from pyramidal cells during *in vivo* theta in anaesthetized animals (Klausberger et al., 2003), PV interneurons have been assumed to play a key role in pacing the firing of pyramidal cells during theta. On the other hand, SOM O-LM and bistratified cells inhibit pyramidal cells at the dendrites and they fire at a similar phase of theta as the pyramidal cells (Klausberger et al., 2003), thus SOM interneurons have been thought to play a coincidence detector role where their inhibition acts to select only the strongest excitatory inputs to be translated into pyramidal cell firing. Regarding the role of interneurons in controlling pyramidal cell firing, two recent studies employing optogenetic methods, one *in vitro* and one *in vivo*, have finally provided some evidence towards a clearer picture of how PV and SOM interneurons may contribute to this process (Lovett-Barron et al., 2012; Royer et al., 2012). Evidence from the *in vitro* study indicates that SOM interneurons, specifically bistratified cells, play a major role in controlling the output of CA1 pyramidal cells, by limiting spike bursts generated by sodium spikes in the dendrites in response to CA3 input (Lovett-Barron et al., 2012). The *in vivo* study demonstrated in awake, behaving mice that silencing PV interneurons shifts the theta phase preference of pyramidal cell firing whereas silencing SOM interneurons increases pyramidal cells' burst-firing without affecting their firing phase (Royer et al., 2012). Therefore, the new evidence points to the role of PV interneurons in controlling the exact timing of pyramidal cell firing during theta while SOM interneurons are involved in limiting the number of spikes fired by pyramidal cells upon strong activation.

Despite these recent advances, it still remains to be demonstrated how PV and SOM interneurons are involved in generating the network theta oscillations. Royer and colleagues (2012) reported that the optogenetic inhibition of PV or SOM interneurons within a small region of CA1 did not perturb the ongoing network theta rhythm *in vivo*, likely due to the extremely focal and relatively weak nature of the light stimulation (μm-scale optic fiber, 1-mW intensity) used in that study. *In vivo* hippocampal theta rhythm results from dynamic interactions between both the intrinsic hippocampal theta generators and rhythmic inputs originating from structures such as the medial septum and the entorhinal cortex, so it is perhaps not too surprising that effects on the rhythm were not detected. However, *in vitro* theta oscillations recordable from the intact hippocampal preparation arise solely out of the intrinsic hippocampal circuitry. The excitatory and inhibitory connections between the principal cells and the interneurons have been shown to be both necessary and sufficient for the generation of this form of *in vitro* CA1 theta rhythm (Goutagny et al., 2009). Given that the inhibition provided by interneurons to pyramidal cells is essential for the *in vitro* theta rhythm generation, it remains to be determined which interneuron subtype plays a key role in the generation of this rhythm.

Employing the latest optogenetic techniques to selectively inhibit specific interneuron subtypes, the aim here is to investigate the causal role of CA1 PV and SOM interneurons in network theta rhythm generation. From the results presented in the last Chapter, we know how CA1 PV and SOM interneurons behave during theta oscillations. Optogenetics will provide us with a way to selectively silence these interneurons with a millisecond-scale temporal resolution and examine the effects of the cell-type specific inhibition on the network rhythm.

VII.2. Materials and Methods

Animals

PV-Cre and SOM-Cre mice were mated with the reporter line, Ai9 mice, in order to generate PV-tdTomato and SOM-tdTomato offspring, which express the fluorescent protein tdTomato as well as the Cre recombinate under the control of the PV or SOM promoter, respectively. For more details on these mouse lines, see Chapter 5, Section 5.2. All animals were treated according to protocols and guidelines approved by McGill University and the Canadian Council of Animal Care.

Virus injection and intact hippocampal preparation

Optogenetic inhibition was achieved using a light-sensitive outward proton-pump protein, archaerhodopsin-T (ArchT), which supports robust membrane hyperpolarization and complete silencing of neuronal spiking activity when stimulated with yellow light (Han et al., 2011). Isolated from Halorubrum strain TP009, a type of halobacteria, ArchT has a >3-fold improved light sensitivity over the prototype, archaerhodopsin-3 (Arch) (Chow et al., 2010). A Cre-dependent adeno-associated virus, AAVdj-Flex-ArchT-eYFP (Vollum Viral Core, OHSU, Portland, Oregon), leads to the expression of a fusion protein ArchT-eYFP under the control of the Cre recombinase. The viral vector, abbreviated as AAVdj-ArchT, was injected into the CA1 region of the middle hippocampus of PV- and SOM-tdTomato mice at P15 (0.5-0.6 μL bilaterally). Animals of both sexes were used. As a control experiment, 0.6 μL phosphate buffer solution (PBS) was injected bilaterally into the middle hippocampus CA1 region of PV- and SOM-tdTomato mice at P15. The virus injection procedure was carried out by Drs. Bénédicte Amilhon and Frédériceric Manseau, both postdoctoral fellows in the lab. A preliminary quantification of the virus infection was performed by Dr. Bénédicte Amilhon and Stephanie Scodras.

The virally infected PV-tdTomato and SOM-tdTomato mice (P30-36) were used to prepare the intact hipppocampal preparation, 15-21 d after the

injection with the virus. The same procedures as those described in Chapter 5, Section 5.2 were used to dissect the intact hippocampal preparation. Each intact preparation was checked for ArchT-eYFP expression using a fluorescence flashlight (NighSea, Bedford, MA) and the location and spread of infection were noted.

Electrophysiology and light stimulation

All electrophysiological recordings were performed at 30 ± 2ºC, using modified aCSF (same composition as in Chapter 5, Section 5.2) which was perfused at a rate of 20 - 25 ml/min. The electrophysiology setup, fluorescence system and intrapipette solution were the same as those described in Chapter 6, Section 6.2. The following procedures described (recordings, light stimulation and data analysis) were performed in collaboration with Drs. Bénédicte Amilhon and Frédéric Manseau.

For local field potential (LFP) recordings, a borosilicate-glass field electrode (1 - 5 MΩ) was placed in the middle CA1 stratum radiatum to record CA1 theta oscillations, following a similar procedure as those described in Chapter 6, Section 6.2 with some modifications. As shown in **Figure 25*A***, the field electrode was placed as close to the centre of the ArchT-eYFP infection zone as possible. Only preparations that produced network oscillations of 3 Hz or higher were included in the analysis. Yellow light was delivered through a polymer light guide (diameter: 3 mm) coupled to a TTL-controlled LED with a dominant wavelength of 593 nm (Luxeon, Quadica Developments, Brantford, Canada). Light intensity at the tip of the light guide was measured before each experiment to ensure that it exceeded 30 mW. In order to maximize the intensity of light reaching the tissue, the light guide was positioned as close to the field electrode and the infection zone as possible. For control preparations injected with PBS, the field electrode was placed in the middle CA1 stratum radiatum and the light guide was positioned close to the field electrode.

Once stable theta rhythm emerged, the yellow light was used to selectively inhibit the firing of PV or SOM CA1 interneurons in intact preparations from virally infected PV-tdTomato or SOM-tdTomato mice, respectively. After baseline theta oscillations were recorded for 60 s, the yellow light was turned on for 30 s to inhibit the target interneurons, followed by 60 s of post-inhibition recording. This 150-s long sequence was repeated multiple times for each oscillating preparation, as long as the frequency of network rhythm remained above 3 Hz. The sequence was repeated every 5 - 10 mins. The theta-frequency oscillations typically began after the preparation had been placed in the recording chamber and perfused with aCSF for ~30 min and slowed down below 3 Hz after additional ~2 h, at which point recordings were terminated. Analysis was restricted to trials with oscillations in the frequency range of 5 - 9 Hz. Each segment of the LFP signal before, during and after the light administration (29 s each) was analyzed using custom software in Matlab and the Chronux toolbox (http://chronux.org; Mitra and Bokil, 2008). The power spectrum of the signal was generated for each of the 29-s segments of LFP signal and from this, the peak frequency ("theta peak frequency" in Hz), power measured at the baseline peak frequency ("theta power at baseline peak frequency" in mV^2) and total power over 2.5 - 12 Hz ("theta summed power" in mV^2) were measured. The power spectrogram of the signal over time was also produced for illustration purposes. The changes in frequency and power of CA1 theta oscillations due to light stimulation were expressed as % change, normalized to the baseline (before) segment. Values from multiple trials (range: 2 - 6 trials) were averaged to represent each preparation/animal.

For simultaneous LFP and whole-cell recordings, the hippocampal preparation was oriented in the recording chamber as shown in **Figure 27*A***. For CA1 recordings, the field electrode was positioned in middle CA1 at the centre of the infection zone and once a stable network theta rhythm began, whole-cell recordings were performed on ArchT-expressing PV or SOM interneurons in CA1

stratum oriens/alveus, located in the infection zone and close to the field electrode. For recordings in the subiculum, the field electrode was placed in the molecular layer at the centre of the infection zone, and ArchT-positive PV or SOM interneurons located within the infection zone and close to the field electrode were recorded in whole-cell mode. ArchT-expressing neurons were identified by the presence of eYFP in the soma. After the whole-cell mode was achieved successfully, the water-immersion objective was carefully lifted up in order to position the light guide directly above both the field and patch electrodes. For whole-cell recordings, pipette resistance of 2.5 - 4 MΩ was used. The junction potential estimated at -15.2 mV was not corrected. Once a stable whole-cell mode was achieved, access resistance and the neuron's resting membrane potential (Vrest) were noted. Then, the cell was recorded at Vrest to observe the neurons' spontaneous firing behaviour. If the neuron presented very few or no spontaneous spikes, it was depolarized slightly to initiate regular firing. The effect of the optogenetic inhibition was tested by recording the neuron's firing behaviour along with the LFP signal for 30 s, turning on the yellow light for 10 s and then recording for additional 30 s for post-inhibition interval. In some cases, the effects of longer light intervals (*e.g.*, 30 s) were also tested. If possible, the neuron's basic properties were quickly checked for (as described in Chapter 5, Section 5.2), including firing pattern, mean firing rate, sag amplitude and rebound firing. The neuron was also held at various potentials in voltage clamp during light administration in order to record the photocurrent. All throughout the recording of the cell, access resistance and resting membrane potential were checked every 5 - 10 min. An approximate location of the recorded cell in the preparation was noted. Recordings were kept for analysis only if the cell recordings met the following criteria; spikes overshot 0 mV and access resistance was <30 MΩ.

After each experiment, the hippocampal preparation used for recording was fixed in 4% paraformaldehyde and slice-mounted for histological verification of the infection zone.

Statistical analysis

Data are presented as mean ± standard error of the mean, unless otherwise stated. Data were plotted and analyzed using Clampfit (Molecular Devices, Sunnyvale, CA), Prism 4 (GraphPad Software, San Diego, CA) and custom software in Matlab (MathWorks, Natick, MA). Statistical method used was Student's t test. *p* values of <0.05 were considered to be statistically significant. Images were processed using Gimp (www.gimp.org) and figures were constructed using Inkscape (www.inkscape.org).

VII.3. Results

3.1. Experiment 1: Silencing PV interneurons decreases the frequency of CA1 theta rhythm but silencing SOM interneurons does not significantly affect the rhythm

In order to inhibit a specific interneuron subtype, we expressed ArchT-eYFP, the light-sensitive outward proton-pump tagged with a fluorescent protein, using a Cre-dependent viral vector, AAVdj-ArchT. When expressed in neurons, ArchT has been shown to mediate robust hyperpolarization and complete silencing of spiking activity upon stimulation with yellow light (Han et al., 2011). We found that injecting the virus into the middle CA1 in PV- or SOM-tdTomato mice led to reliable expressions of ArchT specifically in PV and SOM interneurons, respectively, 2-3 weeks after the injection. The eYFP tag allowed visualization of the extent of the ArchT expression. A preliminary quantification indicates that the virus injection led to ArchT expression in the majority (80 - 90 %) of Cre-positive neurons within 1 mm of the injection site. The extent of ArchT expression (the "infection zone") was often confined to the middle CA1 but in

some cases, the infection also spilled over to include a portion of subiculum, a closeby hippocampal structure. In order to increase the sample size, we decided to include both types of preparations in our analysis: those with CA1-only infection (4/8 PV and 3/10 SOM preps) and those with infection in both CA1 and subiculum (the remaining 4 PV and 7 SOM preps). The subiculum displays similar *in vitro* network rhythmic activities as the CA1 (Jackson et al., 2011), and PV and SOM interneurons in the subiculum display cellular behaviours during subiculum *in vitro* theta that are very similar to those shown by CA1 PV and SOM interneurons (**Appendices 1-2**). Therefore, we felt that including those preparations with ArchT expression in both CA1 and subiculum in the analysis was justified. Intact hippocampal preparations obtained from PV- and SOM-tdTomato mice injected with AAVdj-ArchT gave rise to stable CA1 theta oscillations with frequencies of 3 - 10 Hz. A total of 8 PV and 10 SOM ArchT-injected preparations were included in the analysis. In addition, preparations from PBS-injected mice (6 PV and 8 SOM) were used as "sham-injection" controls.

We found that silencing PV interneurons led to an instantaneous and reversible reduction in the peak frequency of the CA1 theta rhythm (**Fig. 25**). The average change in the peak frequency of the oscillation relative to baseline values was -15.1 ± 3.9 % (n = 8 preps) which was significantly different from the effect of the light on PBS-injected control preparations (1.5 ± 4.5 %, n = 6 preps, p = 0.0164). Inhibiting PV interneurons, however, did not significantly affect the summed theta power (combined power over theta frequencies) of the field signal (ArchT: 7.6 ± 4.3 % *vs.* control: 5.1 ± 1.5 %, p = 0.6412). When the power of the signal was measured at the baseline peak frequency, PV interneuron silencing caused a large decrease in theta power (ArchT: -50.1 ± 11.5 % *vs.* control: -6.1 ± 3.3 %, p = 0.0074), reflecting the clear shift in the dominant frequency of the oscillation during light stimulation.

Figure 25

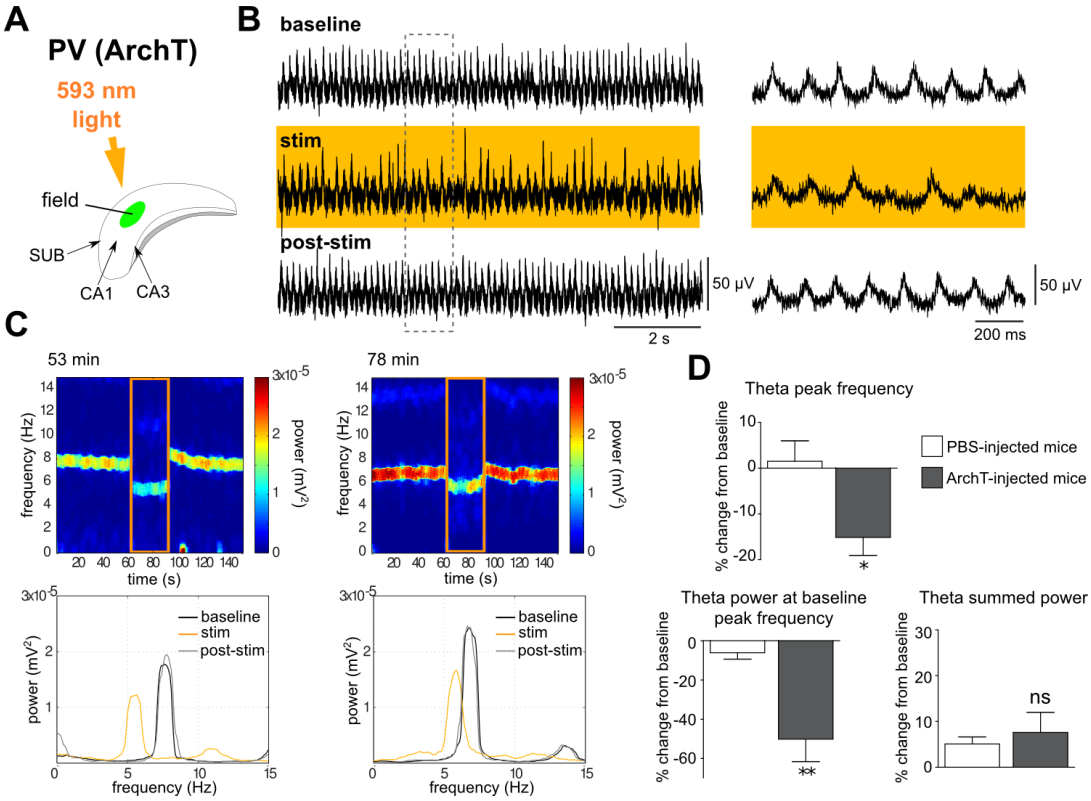
A
PV (ArchT)
593 nm
light
field
SUB
CA1
CA3
B
baseline
stim
post-stim
50 μV
2 s
50 μV
200 ms
C
53 min
78 min
frequency (Hz)
time (s)
power (mV²)
3x10-5
baseline
stim
post-stim
frequency (Hz)
D
Theta peak frequency
% change from baseline
PBS-injected mice
ArchT-injected mice
Theta power at baseline peak frequency
Theta summed power
ns

Figure 25. Silencing PV interneurons decreases CA1 theta rhythm frequency. ***A,*** A schematic shows an intact hippocampal preparation obtained from a PV-tdTomato mouse, 21 days after injection with AAVdj-ArchT. The infection zone (green) indicates that the ArchT-eYFP expression was restricted to the middle CA1 region. The field electrode was placed in the middle of the infection zone, in CA1 stratum radiatum. A light guide emitting 593-nm light was used for ArchT activation. ***B,*** Example traces of the CA1 field theta oscillations recorded from the PV preparation during baseline, light stim and post-stim periods. The segment outlined (dotted line) is expanded on the right. ***C,*** Power spectrograms (top) of two recordings from the same preparation taken at two different times (expressed in minutes in bath) are shown. PV interneuron silencing for 30 s (outlined with an orange rectangle) reversibly decreased the dominant frequency of the CA1 theta oscillation. Power spectra (bottom) of the same recordings clearly indicate a downward shift in the peak frequency of the oscillation during light stimulation compared to baseline. A small reduction in the peak power is also visible. ***D,*** Bar graphs illustrate the quantification of data collected from 8 PV-ArchT preps and 6 PBS control preps, expressed as % change from baseline values before light stimulation. PV interneuron silencing caused significant reductions in the peak frequency and power of the rhythm measured at the baseline peak frequency but no significant effect on the total theta power. ** $p < 0.01$, * $p < 0.05$, ^{ns} $p > 0.05$. The figure was provided by Dr. Bénédicte Amilhon.

Figure 26

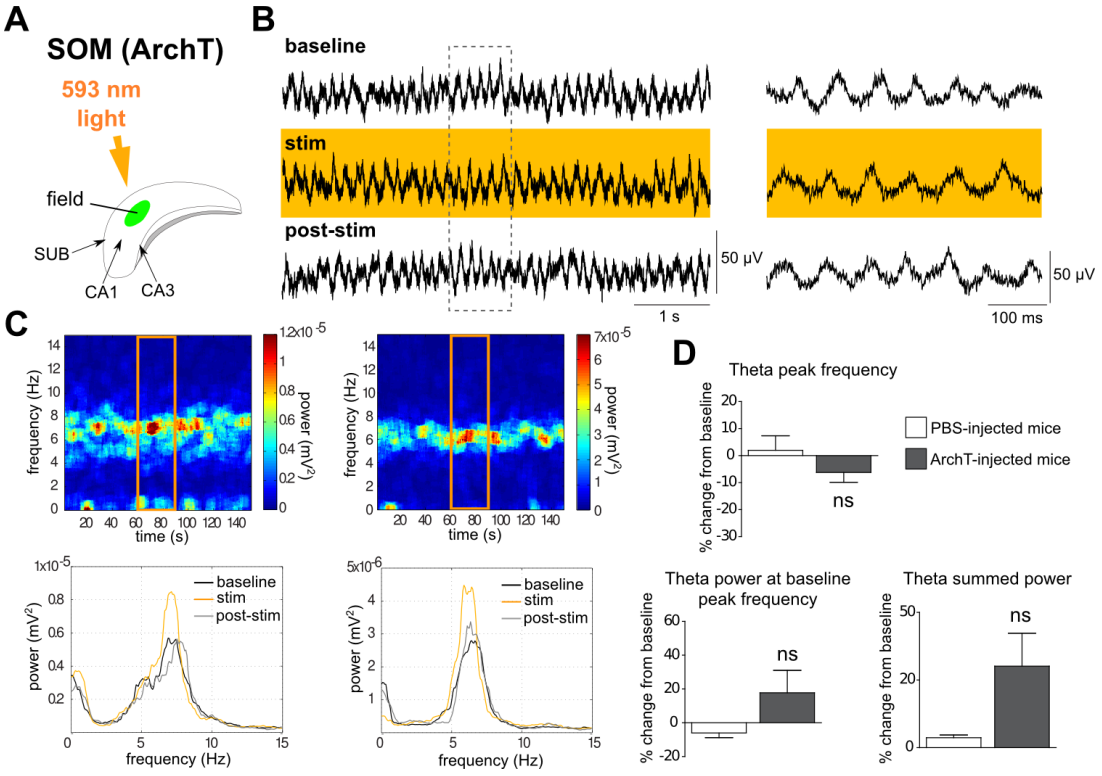
A
SOM (ArchT)
593 nm
light
field
SUB
CA1
CA3
B
baseline
stim
post-stim
50 µV
1 s
50 µV
100 ms
C
frequency (Hz)
time (s)
power (mV²)
baseline
stim
post-stim
frequency (Hz)
power (mV²)
D
Theta peak frequency
% change from baseline
PBS-injected mice
ArchT-injected mice
ns
Theta power at baseline peak frequency
Theta summed power
ns
ns

Figure 26. Silencing SOM interneurons has no significant effects on the frequency or power of CA1 theta rhythm. ***A,*** A schematic shows an intact hippocampal preparation obtained from a SOM-tdTomato mouse, 20 days after injection with AAVdj-ArchT. The infection zone (green) indicating the ArchT-eYFP expression was restricted to the middle CA1. The field electrode was placed in the middle of the infection zone, in CA1 stratum radiatum. A 593-nm light was used for ArchT activation. ***B,*** Example traces of the CA1 field theta oscillations recorded from the SOM preparation during baseline, light stim and post-stim periods. The segment outlined (dotted line) is expanded on the right. ***C,*** Power spectrograms (top) of two recordings from the same preparation taken at two different times are shown. SOM interneuron silencing for 30 s (outlined in orange) had little effect on the frequency or power of the CA1 theta oscillation. Power spectra (bottom) of the same recordings indicate the lack of change in the peak frequency of the oscillation during light stimulation compared to baseline. However, an increase in the peak power may be present. ***D,*** Bar graphs illustrate the quantification of data collected from 10 SOM-ArchT preps and 8 PBS control preps, expressed as % change from baseline values before light stimulation. SOM interneuron silencing had no significant effects on the peak frequency or power measured at the baseline peak frequency. There was a non-signficant trend towards an increase in total theta power ($p = 0.0723$). ^{ns} $p > 0.05$. The figure was provided by Dr. Bénédicte Amilhon.

In contrast, silencing SOM interneurons had no significant effects on the peak frequency or power of the CA1 theta oscillation (**Fig. 26**). The average changes in the peak frequency and power (measured at baseline peak frequency) were -6.2 ± 3.6 % and 17.8 ± 13.3 % (n = 10 preps), respectively, and these values were not significantly different from those observed in control preparations, 2.0 ± 5.4 % and -6.0 ± 2.7 % (n = 8 preps) (*p*s = 0.2073, 0.1345). However, there was a non-significant trend towards an increase in total theta power (ArchT: 30.1 ± 12.2 % *vs.* control: 3.7 ± 1.0 %; $p = 0.0723$).

Based on the data collected so far, these results indicate that the effect of PV interneuron silencing is primarily a downward shift in the frequency of the CA1 theta oscillation, whereas SOM interneuron inhibition has little effects on the frequency or power of the network rhythm.

3.2. Experiment 2: ArchT-expressing SOM interneurons are optogenetically inhibited in the intact hippocampal preparation

Given such an important role of SOM interneurons in controlling pyramidal cell firing demonstrated in recent studies (Lovett-Barron et al., 2012; Royer et al., 2012), it is somewhat surprising that inhibiting the activity of SOM interneurons has such minimal effects on CA1 theta rhythm. However, before weighing further on this apparent null effect, we must first ensure that SOM interneurons are indeed silenced during theta oscillations in the intact hippocampal preparation. ArchT-expressing PV and SOM interneurons have already been confirmed in our lab to respond to yellow light with robust hyperpolarization and inhibition of spiking in acute slices (not shown). Although our prediction is that the light stimulation should have the same effect on ArchT-expressing neurons in intact preparations, we decided to test this directly.

In order to address this issue, we carried out simultaneous LFP and whole-

cell recordings in the intact preparations. Theta oscillations were recorded by placing the field electrode in the middle of the infection zone and whole-cell recordings were performed on ArchT-expressing SOM interneurons located close to the field electrode. To ensure that light was able to reach both the field electrode and the neuron equally with high intensity, the water-immersion objective was lifted up carefully after achieving the whole-cell mode and the light guide was positioned directly above both the field and patch electrodes. This was very challenging because small movements can easily disrupt whole-cell recordings.

We were able to successfully record from one ArchT-expressing SOM interneuron in this configuration (**Fig. 27**). The intact preparation in this case had the ArchT-eYFP expression concentrated in the temporal subiculum bordering CA1. The field recording was done in the subiculum molecular layer and an ArchT-expressing SOM interneuron nearby was recorded. The SOM neuron expressed eYFP in the soma and its firing properties were similar to those of CA1 SOM interneurons, displaying tonic firing and a large depolarizing sag when hyperpolarized. **Figure 27*E*** shows that before light illumination, this neuron exhibited spontaneous firing that was synchronized to the field theta oscillation. At the light onset, the neuron stopped firing instantaneously and was silenced for the full duration of the 30-s stimulation. The voltage trace of the neuron shows that its membrane potential began to slowly recover from the hyperpolarization with time as the light stimulation continued. This is expected as Arch photocurrent has been shown to decline steadily over time under continuous light illumination and this is a common property among many opsins (Chow et al., 2010). Interestingly, silencing of the cell's spiking behaviour clearly revealed the presence of rhythmic EPSPs that were phase-locked to the ongoing theta rhythm. At the light offset, the neuron immediately resumed firing but initially at a higher frequency compared to the before-light baseline firing rate (a "rebound" effect). We noticed that this rebound effect appeared after long periods of continuous

Figure 27

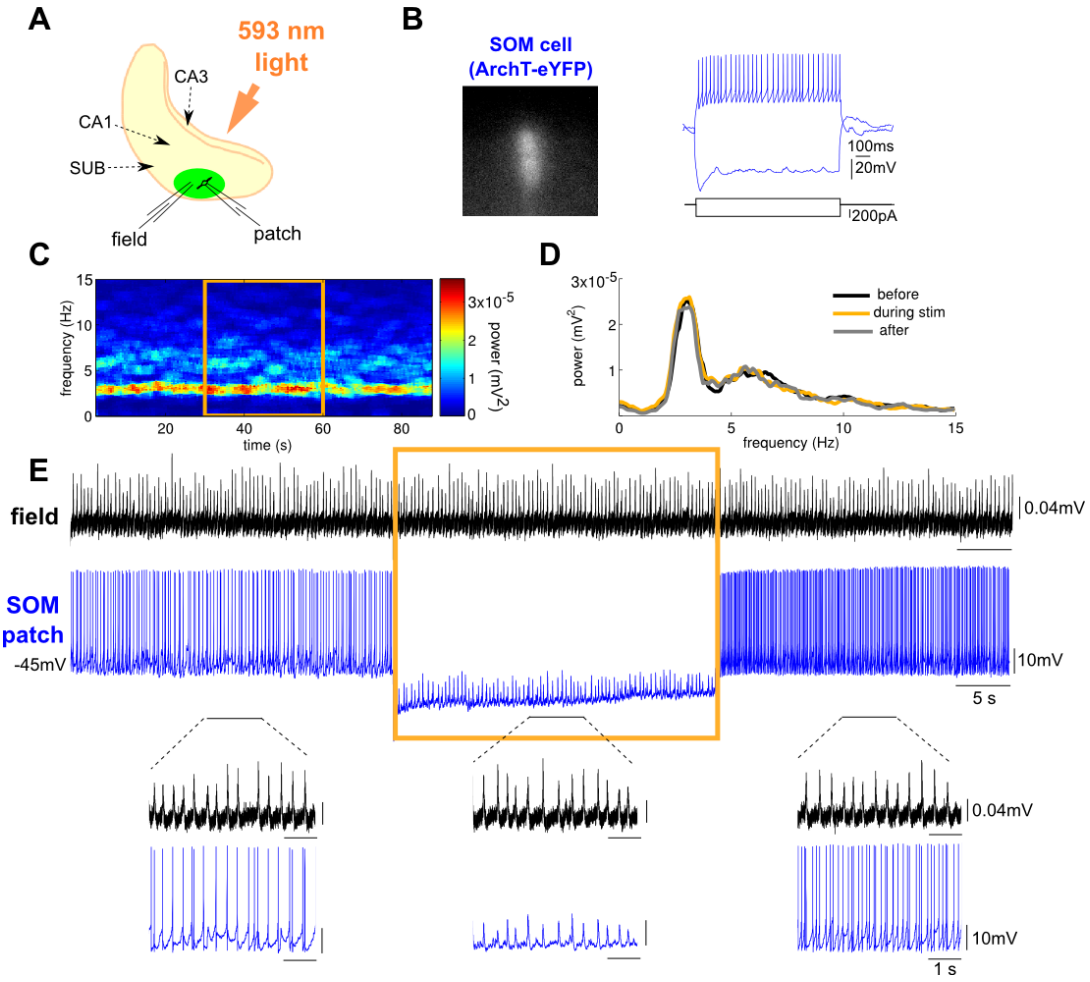
A
593 nm
light
CA3
CA1
SUB
field
patch
B
SOM cell
(ArchT-eYFP)
100ms
20mV
200pA
C
frequency (Hz)
time (s)
power (mV2)
3x10-5
D
power (mV2)
frequency (Hz)
before
during stim
after
E
field
0.04mV
SOM
patch
-45mV
10mV
5 s
1 s

Figure 27. An ArchT-expressing SOM interneuron is optogenetically inhibited in the intact hippocampal preparation. ***A,*** A schematic shows an intact hippocampal preparation obtained from a SOM-tdTomato mouse, 20 days after the injection with AAVdj-ArchT. The infection zone (green) indicates that the ArchT-eYFP expression was concentrated near the temporal subiculum (SUB) bordering CA1. The field electrode was placed in the middle of infection zone, in SUB molecular layer. An ArchT-expressing SOM interneuron located within the infection zone was recorded in whole-cell mode. A 593-nm light was used to activate ArchT. ***B,*** The ArchT-expressing SOM neuron was identified by the presence of eYFP in the soma. The neuron exhibited a tonic firing pattern and a large depolarizing sag when hypoerpolarized, characteristic of SOM interneurons. ***C,*** Power spectrogram of the field recording shown in ***E***. SOM interneuron silencing for 30 s (outlined in orange) had little effect on the SUB theta oscillation. ***D,*** Power spectrum of the same recording indicates maintenance of the same oscillation before, during and after light stimulation. ***E,*** The raw trace of spontaneous firing of the SUB SOM interneuron, simultaneously recorded with the SUB field theta oscillation. While the field oscillation was unaffected, the SOM neuron was strongly silenced during the 30-s light stimulation (outlined in orange). The 5-s segments of the recording before, during and after the stim are expanded at the bottom for clarity.

light stimulation but not with shorter illumination intervals (*e.g.*, 10 s). The rebound effect was transient and the neuron's firing rate was eventually restored to baseline. Consistent with Experiment 1, the light did not cause any significant changes in the frequency or power of the field theta rhythm in this SOM preparation. Although very preliminary, these results indicate that the yellow light is indeed able to silence ArchT-expressing SOM interneurons in the intact preparation during a spontaneously occurring theta rhythm.

VII.4. Discussion

The mechanisms underlying the generation of hippocampal theta rhythm have largely remained a mystery. With the recent development of optogenetic tools that enable selective silencing and activation of specific cell types *in vitro* and *in vivo*, we are finally beginning to understand the role of distinct interneuron subtypes in this process. The results presented here provide the first experimental evidence that PV interneurons are causally involved in setting the frequency of CA1 theta oscillations. Silencing PV interneurons led to a marked decrease in the peak frequency of the rhythm with no significant effect on the power of the oscillation. On the contrary, silencing SOM interneurons led to more subtle effects; there was no detectable change in the frequency of the oscillation and only a non-significant trend towards a small increase in the power. This result is in clear opposition to the view that SOM interneurons, specifically O-LM cells, are intrinsic theta rhythm generators (Maccaferri and McBain, 1996b). Rather than pacing the rhythm, the activity of SOM interneurons appears to contribute very little to the network oscillation and if anything, slightly dampen the power of the rhythm. The latter view should be taken with caution, however, since the result is still inconclusive.

If PV interneurons are indeed the pacemaker of intrinsic theta oscillations,

how do they accomplish this role? First of all, this is not a small feat, considering that PV interneurons account for only ~20 % of the entire CA1 interneuron population (Jinno and Kosaka, 2006). Although small in number, our results from Chapter 6 demonstrate that their firing behaviour is remarkably homogeneous with virtually every PV neuron firing with a high degree of phase-locking to the network theta rhythm. Therefore, it is likely that they produce a highly synchronous, clock-like output as a group. We also saw that each PV neuron's output is powerful, firing high-frequency bursts of multiple action potentials in each theta cycle. With such a rapid rate of burst-firing (> 200 Hz), the functional impact of their inhibitory signal is likely to be amplified through temporal summation. In addition, PV interneurons primarily target the perisomatic region of pyramidal cells. Anatomical evidence suggests that perisomatic inhibitory synapses on pyramidal cells may be more effective compared to dendritic ones because perisomatic terminals are larger in size and contain more synaptic vesicles and mitochondria, indicative of higher release probability (Miles et al., 1996). The perisomatic domain of pyramidal cells is also highly specialized for inhibition, since only inhibitory inputs have been found to innervate the somata and axon initial segments (Megías et al., 2001). Furthermore, a PV interneuron can synchronize the firing of a large network of pyramidal cells (Cobb et al., 1995; Miles et al., 1996), as it has been estimated that each PV basket cell makes synaptic contacts with more than 1000 pyramidal cells (Sik et al., 1995; Halasy et al., 1996). PV interneurons can also synchronize each other's activity through mutual synaptic connections and gap-junction mediated electrical coupling (Sik et al., 1995; Meyer et al., 2002). Therefore, due to highly synchronous, effective and divergent nature of their output, PV interneurons are able to provide the powerful inhibitory inputs necessary to synchronize subtheshold oscillations and firing of the large number of pyramidal cells contained in the local network during theta rhythm.

Then the question arises: when PV interneurons are silenced, why do we

observe a decrease in the frequency of theta rather than a complete abolition of the rhythm? In other words, if PV interneurons are responsible for providing the clock-like synchronizing input to the network, what is causing the emergence and maintenance of the slower rhythm when they are inhibited? Although the answer to this question is not entirely clear at this point, it is important to consider the fact that the optogenetic inhibition in these experiments was restricted to small portions of the intact preparation rather than the entire hippocampal network. As shown in **Figures 25-27**, the ArchT-eYFP expression was most often localized to a part of the middle section of the hippocampus. One possibility is that the native rhythm in the small infected network is completely abolished by PV neuron silencing and that the lower-frequency signal appears due to volume conduction of a slower oscillation from a neighbouring unaffected network. This is certainly possible because oscillators of distinct frequencies have been shown to co-exist simultaneously in the intact preparation (Goutagny et al., 2009). Although not shown here, we have also observed that when two distinct theta frequencies (*e.g.*, 4 and 7 Hz) exist within a given oscillation that is not explainable by harmonics, PV interneuron silencing eliminates the high-frequency rhythm but not the slower rhythm. Alternatively, it is also possible that the lower-frequency oscillation is supported by the activity of other interneuron subtypes and/or the pyramidal cells themselves within the affected network. The last and the least probable scenario is that PV interneurons are not sufficiently inhibited by the light so the slower rhythm reflects the result of a reduced firing rate of PV neurons. We believe that this is highly unlikely because we have tested many ArchT-expressing PV interneurons in acute slices and confirmed that all infected neurons are strongly silenced by the light stimulation (not shown). However, whether the light has the same effect on PV interneurons during theta rhythm in the intact preparation, where they are strongly driven by excitatory inputs, remains to be tested directly. A similar experiment as Experiment 2 should be performed on PV interneurons to answer this question.

We must now address the effect (or the lack thereof) of SOM interneuron silencing on the network rhythm. How can we explain the result that SOM interneuron inhibition led to no significant change in the frequency of the oscillation but that it may induce a small increase in the power of the signal? First of all, SOM interneurons account for ~14 % of the total CA1 interneuron population (Jinno and Kosaka, 2006). As demonstrated in Chapter 6, SOM interneurons display a wide variety of different firing behaviours during theta rhythm, ranging from silence (18%), irregular firing (27%) to highly phase-locked tonic or burst firing (55%). While the output of the highly phase-locked SOM neurons is likely to be rhythmic, the non-phase-locked subset probably produces noisy inhibitory inputs on postsynaptic pyramidal cells. It is possible that the rhythmic and non-rhythmic SOM interneurons normally have opposing effects on the network rhythm (amplifying and dampening) so when the two groups are both silenced, there is no detectable change in the field oscillation. Alternatively, the slight increase in theta power when SOM interneurons are silenced may have resulted because SOM interneurons normally attenuate theta rhythm through the release of somatostatin, which has been shown to reduce the power of hippocampal theta oscillations when injected into the MS-DBB (Bassant et al., 2005). Lastly, before completely ruling out SOM interneurons as potential theta generators, it should be noted that silencing them could potentially lead to more dramatic effects on network oscillations if the opsin could be expressed in all SOM interneurons across the entire septotemporal extent of the intact hippocampal preparation. This could be achieved by employing transgenic mice with a constitutive opsin expression instead of using viral vectors.

In summary, our results provide the first piece of evidence demonstrating that CA1 PV interneurons, recently shown to control the timing of pyramidal cell firing during *in vivo* theta (Royer et al., 2012), also play a causal role in generating the network rhythm itself. We hope that this work, along with several recent studies employing optogenetic techniques, signal the beginning of many

illuminating findings to come that will unravel the mechanisms of theta rhythm generation in the hippocampus.

Summary, conclusions and originality

Synchronized neural oscillations are hypothesized to mediate various cognitive functions ranging from attention, memory to conscious awareness (Ward, 2003). Thus, investigating the mechanisms with which neural oscillations are generated may provide new and important insights into how the brain carries out cognitive processes. In the preceding chapters, I have presented results from two projects that deal with the identification and exploration of potential rhythm generators in the septohippocampal network, the neural circuitry responsible for producing hippocampal theta rhythm. Hippocampal theta rhythm is an oscillation that is tightly associated with episodic memory and spatial learning in both humans and animals. Here, I will briefly summarize the results I obtained and discuss how they make distinct and original contributions to the existing knowledge.

For the first project, I investigated the intrinsic properties of the newly described glutamatergic MS-DBB neurons and examined their functional role in the septohippocampal network. Prior to this work, the MS-DBB was well-known to play an important role in hippocampal theta rhythm *in vivo*, by providing the hippocampal formation with cholinergic and GABAergic inputs. Recent evidence indicated that a considerable number of neurons in the MS-DBB may be glutamatergic (VGLUT2-positive) and that some of these neurons send projections to the hippocampus. However, very little was known about their characteristics and how they may influence hippocampal activity. Here, I showed that VGLUT2-positive MS-DBB neurons can functionally release glutamate (Chapter 2) and that as a population, the glutamatergic neurons exhibit a highly heterogeneous set of firing patterns, with a significant proportion displaying fast-firing properties and a prominent I_h, characteristics that were traditionally

attributed to GABAergic MS-DBB neurons (Chapter 3). I also found that some glutamatergic MS-DBB neurons fire in clusters, interspersed with rhythmic subthreshold oscillations, an electrophysiological characteristic that is unique for glutamatergic neurons. Subsets of both glutamatergic and GABAergic neurons show highly rhythmic spontaneous firing patterns in theta frequencies that are not driven by synaptic inputs, suggesting that some glutamatergic and GABAergic MS-DBB neurons may be intrinsic theta rhythm generators. Furthermore, I demonstrated that glutamatergic MS-DBB neurons provide a functional excitatory synaptic input to CA3 pyramidal cells, mediated by a monosynaptic AMPA-receptor-mediated glutamatergic response (Chapter 4).

These findings indicate a new and unique role for glutamatergic MS-DBB neurons in the septohippocampal network. Unlike the slow, tonic excitation provided by cholinergic neurons, glutamatergic MS-DBB neurons can induce fast, rhythmic depolarizations on target cells. Thus, the role of the glutamatergic neurons may be to contribute a rhythmic excitatory drive to the local network as well as to the hippocampus. Therefore, along with GABAergic MS-DBB neurons whose rhythmic inhibitory inputs are thought to pace the firing of hippocampal interneurons, glutamatergic MS-DBB neurons may provide rhythmic excitatory inputs to pyramidal cells that affect their firing patterns and contribute to the hippocampal field theta rhythm. This study is the first to demonstrate the intrinsic rhythmic properties of glutamatergic MS-DBB neurons and their direct, excitatory effect on postsynaptic hippocampal neurons. Results from this project have since been reported in an article published in the Journal of Neuroscience (Huh et al., 2010).

For the second project, I explored the cellular behaviour of two CA1 interneuron classes, PV- and SOM-expressing interneurons, during intrinsically generated *in vitro* CA1 theta rhythm and tested their respective roles as theta rhythm generators. Previous studies indicated that PV interneurons control and synchronize the timing of pyramidal cell firing via perisomatic innervation, and

their fast-firing properties have been linked to gamma-frequency rhythms. In contrast, SOM interneurons were hypothesized to be theta generators because of their spontaneous firing patterns in theta frequencies, and their inhibitory inputs targeting pyramidal cell dendrites have been associated with dendritic electrogenesis regulation. During *in vivo* theta, both PV and SOM interneurons fire strongly phase-locked to theta but with different phase preferences. It was largely unknown which factors determine the interneurons' distinct firing behaviours during theta and whether their activities play a causal role in the generation of the field rhythm. Here, I showed that SOM interneurons exhibit rhythmic intrinsic properties such as I_h and a tendency to fire rhythmically at theta-range frequencies at rest, while PV interneurons possess clearly very different properties, showing little I_h or spontaneous firing but displaying fast firing rates and membrane kinetics, suitable for gamma rhythms (Chapter 5). During the *in vitro* CA1 theta rhythm, I demonstrated that as a group, PV interneurons fire in a strikingly uniform manner, firing bursts of multiple action potentials that are strongly phase-locked to field theta, in comparison to SOM interneurons whose firing patterns are more heterogeneous (Chapter 6). The degree of phase-locking appears to depend on the level of excitatory drive from the network, as PV interneurons receive EPSCs that are several-fold greater in amplitude compared to SOM interneurons. Once phase-locked, both PV and SOM interneurons fire near the peak of theta, and the firing frequencies within theta cycles (intraburst frequencies) are consistent with the interneurons' intrinsic firing rates and membrane kinetics. Finally, using optogenetic inhibition, I showed that silencing PV interneurons had a significant effect on the frequency of field theta oscillations whereas silencing SOM interneurons had no appreciable effect on either the frequency or power of the field theta signal, demonstrating that PV interneurons set the frequency of the network theta oscillations (Chapter 7).

These findings add a new and interesting twist on the mechanisms of rhythm generation in the hippocampal formation. SOM interneurons are thought

to be intrinsic rhythm generators due to their theta-frequency spontaneous firing and I_h expression but when embedded in a network rhythm, external factors such as excitatory inputs appear to determine the extent of their phase-locking. The optogenetic result also argues against the notion of SOM interneurons as theta generators because silencing them had no significant effect on the field theta rhythm. It is possible that SOM interneurons act instead as theta resonators, effectively transmitting theta-patterned inputs into theta-frequency spiking outputs, as previously demonstrated for O-LM cells in slices (Kispersky et al., 2012). It remains to be determined whether SOM interneurons can act as rhythm generators in some cases and rhythm resonators in others, depending on the network state or the specific SOM interneuron subtype involved. On the other hand, PV interneurons are driven strongly by excitatory inputs to fire synchronously in a phase-locked manner. Even though PV interneurons do not display properties of an intrinsic theta generator at the cellular level, their highly synchronous and powerful inhibitory inputs appear to play a key role in generating theta oscillations at the network level, as suggested by our optogenetic results. In that sense, the excitatory inputs that drive PV interneuron spiking and the feedback inhibitory inputs provided by PV interneurons onto pyramidal cells should be considered together as the network-level theta rhythm generators. This study reveals previously unidentified synaptic and intrinsic mechanisms underlying interneurons' firing behaviour during theta rhythm. It is also the first study to examine the causal role of specific CA1 interneuron classes in generating field theta oscillations.

In conclusion, the results gained through these projects provide new information about the potential role of several different neuron types in the septohippocampal network in relation to theta rhythm generation. Because the hippocampal theta rhythm recorded *in vivo* most likely reflects a product of several intrinsic and extrinsic theta generators working in concert, it remains to be elucidated exactly how they interact together to generate, modulate and

synchronize theta oscillations across neural circuits. Hopefully, a greater understanding of this matter will bring new insights into the mechanisms with which neural oscillations contribute to essential operations of the brain such as learning and memory.

Implications for brain disorders

An increasing number of interneuron-based hypotheses of pathogenesis are emerging in psychiatry, pointing to the involvement of inhibitory interneurons in the etiology of various neurological disorders. In Alzheimer's disease (AD), GABA hypofunction is a well-known biomarker and reductions in SOM expression in neocortex and hippocampus have been reported by studies examining post-mortem AD brains for decades (e.g., Davies et al., 1980). There is also a genetic association between SOM and Apolipoprotein E4 (apoE4) apsilon-4 allele, a major genetic risk factor for AD; AD patients display even lower cortical SOM levels if they carry the apoE4 epsilon-4 allele (Grouselle et al., 1998) and variations in the *Somatostatin* gene have been linked to an increased risk for AD in apoE4 epsilon-4 allele carriers (Vepsalainen et al., 2007). Studies using apoE4 or hAPP (human amyloid precursor protein) transgenic mouse models of AD also recently reported decreases in SOM interneuron densities in the dentate gyrus and CA1 (Andrews-Zwilling et al., 2010; Perez-Cruz et al., 2011) and aberrant spontaneous epileptiform activity in cortical and hippocampal networks, suggestive of overexcitation (Palop et al., 2007). Another recent study using hAPP mice has also linked abnormal rhythmic activities observed in the cortex and the hippocampus of this AD model with dysfunction of PV interneurons (Verret et al., 2012). Therefore, the emerging interneuron hypothesis of AD is that, heightened levels of apoE4 or beta-amyloid can lead to interneuronal deficits, particularly involving PV and SOM neurons, leading to improper inhibition, network hyperexcitability, abnormal synaptic plasticity and ultimately cognitive impairments. Potential mechanisms for this process may include interneuron-specific taupathy (Andrews-Zwilling et al., 2010) and altered GABAergic synaptic plasticity (Yang et al., 2009).

In temporal lobe epilepsy, the dominant thinking has been that the function of PV interneurons is largely preserved while SOM interneurons are especially sensitive to seizure-associated damages (for reviews, see Cossart et al., 2005; Magloczky and Freund, 2005). However, a couple of recent studies have put forth a hypothesis that decreased activities of cortical PV interneurons may be causally linked to seizure susceptibility through mechanisms involving neuregulin 1 (NRG1), its receptor ErbB4 and a voltage-gated potassium channel, Kv1.1 (Li et al., 2011; Tan et al., 2011). Given that ErbB4 is preferentially expressed by PV interneurons (Yau et al., 2003), Li and colleagues (2011) found that ErbB4 deletion specifically in PV interneurons promotes seizure generation in mice that can be rescued with NRG1 infusion, and that ErbB4 is downregulated in cortical tissue from temporal lobe epilepsy patients. These lines of evidence suggest that interneurons, especially PV and SOM neurons, are involved in controlling network excitability and when these interneurons are dysfunctional, the overall effect is hyperactivity, desynchronization of pyramidal cells and epileptogenesis. In line with this idea, a recent study using *in vivo* unit recordings in epileptic patients revealed that cortical neurons in the epileptic zone indeed show increased heterogeneity in spiking at the onset of seizure, indicating heightened desynchronization (Truccolo et al., 2011).

Another disorder for which desynchronized neural networks may be involved is schizophrenia. Intriguingly, *Nrg1* and *Erbb4* are well-known susceptibility genes for schizophrenia and much evidence exists to support the role of PV interneurons in this disease. Post-mortem brain tissue from schizophrenic patients display a reduced density of hippocampal PV interneurons (Zhang and Reynolds, 2002), lower mRNA levels of GAD67 in PV neurons in the prefrontal cortex (Hashimoto et al., 2003) as well as a decreased number of synaptic terminals from cortical chandelier cells, a subtype of PV interneurons (Woo et al., 1998). Reminiscent of the latter anatomic deficit in humans, conditional deletion of ErbB4 in PV interneurons in mice leads to fewer synapses

formed by hippocampal chandelier cells onto pyramidal cells (Fazzari et al., 2010). Recent evidence from our laboratory also illustrates that prenatal infection, a known risk factor for schizophrenia, leads to reductions in the density of PV but not SOM interneurons, deficits in inhibitory drive and altered *in vitro* theta oscillations in the mouse CA1 (Ducharme et al., 2012). In addition, abnormalities in neural oscillations and synchrony are commonly reported in schizophrenic patients (for review, see Uhlhaas and Singer, 2010). These lines of evidence are consistent with the current hypothesis that in all of these disorders, dysfunctional inhibitory circuits can lead pyramidal cells to become less synchronized, resulting in abnormal network oscillations, impaired neural computations and cognitive deficits. Perhaps not coincidentally, associations among these neurological disorders are known to exist; people with a history of epilepsy have a greater risk of developing schizophrenia (Qin et al., 2005) and individuals with early-onset AD have a higher risk of having unprovoked seizures (Amatniek et al., 2006).

The role of glutamatergic MS-DBB neurons in brain disorders is almost completely unknown. Some evidence suggests that glutamatergic septal neurons may be as sensitive to damage by beta-amyloid accumulation as are cholinergic septal neurons, which are well-known to be severely affected in AD brains (Colom et al., 2010). Previously, we have also shown that nerve growth factor (NGF), the signalling of which is impaired from the early stages of AD, not only affects acetylcholine but also glutamate release from MS-DBB neurons that can co-release both neurotransmitters *in vitro* (Huh et al., 2008). Because beta-amyloid and NGF are both targets of emerging new treatment strategies for AD (Tuszynski et al., 2005; Benilova et al., 2012), it will be important to determine how glutamatergic MS-DBB neurons are affected in AD and the potential effects of the drugs on their function. Taking into account the new evidence that glutamatergic MS-DBB neurons innervate locally and send functional projections to the hippocampus (Manseau et al., 2005; Huh et al., 2010), it remains to be worked out in detail how the glutamatergic neurons participate in hippocampal

theta rhythm generation/modulation and how this process may be affected in various disease states.

Future directions

There are still many aspects of theta rhythm generation in the septohippocampal network that remain to be explored. First, it remains to be identified how glutamatergic MS-DBB neurons behave during both *in vitro* and *in vivo* hippocampal theta oscillations. Knowing whether they are active during hippocampal theta rhythm and if so, whether they fire tonically or rhythmically in a phase-locked fashion will be important in order to better understand their role in rhythm generation. Secondly, with the help of the latest optogenetic techniques, it is now possible to directly test the contribution of glutamatergic MS-DBB neurons in theta rhythm and hippocampus-related functions. Thirdly, it remains to be determined whether the heterogeneity in firing pattern and phase-locking observed among SOM interneurons during the *in vitro* theta rhythm was a result of sampling many different interneuron subtypes. Performing morphological reconstructions of recorded cells will be required to identify the exact interneuron subtypes recorded, based on axodendritic distributions (O-LM, bistratified or septally projecting cells). Lastly, it will be interesting to test the effects of silencing PV or SOM interneurons across the entire septotemporal extent of the intact hippocampal preparation, in order to see if the effects differ from those we have observed using local-circuit opsin expressions. This could be achieved by employing transgenic mice with a constitutive opsin expression instead of using viral vectors. In addition, there are many more interesting avenues to explore in the future, for example investigating the role of these neurons in hippocampal theta rhythm *in vivo* and in spatial and episodic learning and memory tasks. With the advent of many new optogenetic tools, we are at the cusp of finally being able to understand the nature of rhythm generation in the septohippocapmal network. It is indeed a very exciting time in the field of memory research.

Contribution of co-authors

Manuscript 1:

Huh, C.Y.L., Goutagny, R., & Williams, S. (2010). Glutamatergic neurons of the mouse medial septum and diagonal band of Broca synaptically drive hippocampal pyramidal cells: relevance for hippocampal theta rhythm. Journal of Neuroscience, 30, 15951-15961.

- Contribution of student (C.Y.L.H.): Carried out data collection and analysis. Study design and manuscript writing were also done by the student with the help of the supervisor (S.W.) and a postdoctoral fellow (R.G.).

Manuscript 2:

Huh, C.Y.L., Amilhon, B., Ferguson, K.A., Scodras, S., Skinner, F.K., & Williams S. (in preparation). Mechanisms underlying distinct firing patterns of parvalbumin- *vs.* somatostatin-expressing CA1 interneurons during *in vitro* hippocampal theta rhythm.

- Contribution of student (C.Y.L.H.): Carried out most of data collection and analysis. Experimental design and manuscript writing are also being done by the student with the help of the supervisor (S.W.). A postdoctoral fellow (B.A.) carried out the anatomical characterization of transgenic mouse lines with the help of a research assistant (S.S.). Collaborators (K.A.F. and F.K.S.) designed and carried out Matlab analyses of some of the electrophysiological data.

Manuscript 3:

Amilhon, B., Huh, C.Y.L., Manseau, F., Goutagny, R., Adamantidis, A., & Williams S. (in preparation). Optogenetic study of the role of parvalbumin

and somatostatin interneurons in theta oscillations in the hippocampus.

- Contribution of student (C.Y.L.H.): Carried out some of the field and patch recordings using optogenetic inhibition and performed some of the data analysis; both tasks were done in collaboration with postdoctoral fellows (B.A. and F.M.). B.A. did most of the data collection, analysis and experimental design, performed virus injections, anatomical characterizations of transgenic mouse lines and virus infection quantifications. A postdoctoral fellow (R.G.), a collaborator (A.A.) and the supervisor (S.W.) contributed to study design.

Bibliography

Acsady L, Gorcs TJ, Freund TF, Görcs T (1996) Different populations of vasoactive intestinal polypeptide-immunoreactive interneurons are specialized to control pyramidal cells or interneurons in the hippocampus. Neuroscience 73:317–334.

Acsady L, Halasy K, Freund T (1993) Calretinin is present in non-pyramidal cells of the rat hippocampus—III. Their inputs from the median raphe and medial septal nuclei. Neuroscience 52:829–841.

Aika Y, Ren JQ, Kosaka K, Kosaka T (1994) Quantitative analysis of GABA-like-immunoreactive and parvalbumin-containing neurons in the CA1 region of the rat hippocampus using a stereological method, the disector. Experimental Brain Research 99:267–276.

Ali AB, Deuchars J, Pawelzik H, Thomson AM (1998) CA1 pyramidal to basket and bistratified cell EPSPs: dual intracellular recordings in rat hippocampal slices. Journal of Physiology 507:201–217.

Ali AB, Thomson AM (1998) Facilitating pyramid to horizontal oriens-alveus interneurone inputs: dual intracellular recordings in slices of rat hippocampus. Journal of Physiology 507:185–199.

Allen TG, Abogadie FC, Brown DA (2006) Simultaneous release of glutamate and acetylcholine from single magnocellular "cholinergic" basal forebrain neurons. Journal of Neuroscience 26:1588–1595.

Alonso A, Köhler C (1982) Evidence for separate projections of hippocampal pyramidal and non-pyramidal neurons to different parts of the septum in the rat brain. NeurosciLett 31:209–214.

Alonso A, Köhler C (1984) A study of the reciprocal connections between the

septum and the entorhinal area using anterograde and retrograde axonal transport methods in the rat brain. The Journal of comparative neurology 225:327–343.

Amatniek JC, Hauser WA, DelCastillo-Castaneda C, Jacobs DM, Marder K, Bell K, Albert M, Brandt J, Stern Y (2006) Incidence and Predictors of Seizures in Patients with Alzheimer's Disease. Epilepsia 47:867–872.

Andrews-Zwilling Y, Bien-Ly N, Xu Q, Li G, Bernardo A, Yoon SY, Zwilling D, Yan TX, Chen L, Huang Y (2010) Apolipoprotein E4 causes age- and Tau-dependent impairment of GABAergic interneurons, leading to learning and memory deficits in mice. JNeurosci 30:13707–13717.

Ascoli G, Gasparini S, Medinilla V, Migliore M (2010) Local control of postinhibitory rebound spiking in CA1 pyramidal neuron dendrites. The Journal of neuroscience 30:6434–6442.

Bartus RT, Dean III RL, Beer B, Lippa AS (1982) The cholinergic hypothesis of geriatric memory dysfunction. Science 217:408–414.

Bassant M-H, Simon A, Poindessous-Jazat F, Csaba Z, Epelbaum J, Dournaud P (2005) Medial septal GABAergic neurons express the somatostatin sst2A receptor: functional consequences on unit firing and hippocampal theta. JNeurosci 25:2032–2041.

Bassant MH, Apartis E, Jazat-Poindessous FR, Wiley RG, Lamour YA (1995) Selective immunolesion of the basal forebrain cholinergic neurons: effects on hippocampal activity during sleep and wakefulness in the rat. Neurodegeneration 4:61–70.

Baude A, Bleasdale C, Dalezios Y, Somogyi P, Klausberger T (2007) Immunoreactivity for the GABAA receptor alpha1 subunit, somatostatin and Connexin36 distinguishes axoaxonic, basket, and bistratified interneurons of the rat hippocampus. Cerebral cortex 17:2094–2107.

Benilova I, Karran E, De Strooper B (2012) The toxic Aβ oligomer and Alzheimer's disease: an emperor in need of clothes. Nature neuroscience 15:349–357.

Berens P (2009) CircStat: A MATLAB Toolbox for Circular Statistics. Journal of Statistical Software 31:1–21.

Bigl V, Woolf NJ, Butcher LL (1982) Cholinergic projections from the basal forebrain to frontal, parietal, temporal, occipital, and cingulate cortices: a combined fluorescent tracer and acetylcholinesterase analysis. Brain ResBull 8:727–749.

Bland BH, Colom L V (1993) Extrinsic and intrinsic properties underlying oscillation and synchrony in limbic cortex. ProgNeurobiol 41:157–208.

Bland BH, Declerck S, Jackson J, Glasgow S, Oddie S (2007) Septohippocampal properties of N-methyl-D-aspartate-induced theta-band oscillation and synchrony. Synapse 61:185–197.

Bland BH, Konopacki J, Kirk IJ, Oddie SD, Dickson CT (1995) Discharge patterns of hippocampal theta-related cells in the caudal diencephalon of the urethan-anesthetized rat. JNeurophysiol 74:322–333.

Blasco-Ibáñez JM, Freund TF (1995) Synaptic input of horizontal interneurons in stratum oriens of the hippocampal CA1 subfield: structural basis of feed-back activation. EurJNeurosci 7:2170–2180.

Borhegyi Z, Varga V, Szilagyi N, Fabo D, Freund TF (2004) Phase segregation of medial septal GABAergic neurons during hippocampal theta activity. JNeurosci 24:8470–8479.

Bostock E, Muller RU, Kubie JL (1991) Experience-dependent modifications of hippocampal place cell firing. Hippocampus 1:193–205.

Bourque MJ, Trudeau LE (2000) GDNF enhances the synaptic efficacy of dopaminergic neurons in culture. EurJNeurosci 12:3172–3180.

Bowen DM, Smith CB, White P, Davison AN (1976) Neurotransmitter-related enzymes and indices of hypoxia in senile dementia and other abiotrophies. Brain 99:459–496.

Brashear HR, Zaborszky L, Heimer L (1986) Distribution of GABAergic and cholinergic neurons in the rat diagonal band. Neuroscience 17:439–451.

Brauer K, Holzer M, Bruckner G, Tremere L, Rasmusson DD, Poethke R, Arendt T, Hartig W (1999) Two distinct populations of cholinergic neurons in the septum of raccoon (Procyon lotor): evidence for a separate subset in the lateral septum. JComp Neurol 412:112–122.

Buhl EH, Szilágyi T, Halasy K, Somogyi P, Szilagyi T (1996) Physiological properties of anatomically identified basket and bistratified cells in the CA1 area of the rat hippocampus in vitro. Hippocampus 6:294–305.

Burwell RD, Amaral DG (1998a) Perirhinal and postrhinal cortices of the rat: interconnectivity and connections with the entorhinal cortex. Journal of Comparative Neurology 391:293–321.

Burwell RD, Amaral DG (1998b) Cortical afferents of the perirhinal, postrhinal, and entorhinal cortices of the rat. The Journal of Comparative Neurology 398:179–205.

Buzsaki G (2002) Theta oscillations in the hippocampus. Neuron 33:325–340.

Castañeda MT, Sanabria ERG, Hernandez S, Ayala A, Reyna TA, Wu J-Y, Colom L V (2005) Glutamic acid decarboxylase isoforms are differentially distributed in the septal region of the rat. Neuroscience research 52:107–119.

Chow BY, Han X, Dobry AS, Qian X, Chuong AS, Li M, Henninger MA, Belfort

GM, Lin Y, Monahan PE, Boyden ES (2010) High-performance genetically targetable optical neural silencing by light-driven proton pumps. Nature 463:98–102.

Cobb SR, Buhl EH, Halasy K, Paulsen O, Somogyi P (1995) Synchronization of neuronal activity in hippocampus by individual GABAergic interneurons. Nature 378:75–78.

Cobb SR, Halasy K, Vida I, Nyiri G, Tamas G, Buhl EH, Somogyi P (1997) Synaptic effects of identified interneurons innervating both interneurons and pyramidal cells in the rat hippocampus. Neuroscience 79:629–648.

Cole AE, Nicoll RA (1983) Acetylcholine mediates a slow synaptic potential in hippocampal pyramidal cells. Science 221:1299–1301.

Colom L V, Castaneda MT, Banuelos C, Puras G, Garcia-Hernandez A, Hernandez S, Mounsey S, Benavidez J, Lehker C (2010) Medial septal beta-amyloid 1-40 injections alter septo-hippocampal anatomy and function. NeurobiolAging 31:46–57.

Colom L V, Castaneda MT, Reyna T, Hernandez S, Garrido-Sanabria E (2005) Characterization of medial septal glutamatergic neurons and their projection to the hippocampus. Synapse 58:151–164.

Corkin S (1968) Acquisition of motor skill after bilateral medial temporal-lobe excision. Neuropsychologia 6:255–265.

Cornwell BR, Johnson LL, Holroyd T, Carver FW, Grillon C (2008) Human hippocampal and parahippocampal theta during goal-directed spatial navigation predicts performance on a virtual Morris water maze. JNeurosci 28:5983–5990.

Cossart R, Bernard C, Ben-Ari Y (2005) Multiple facets of GABAergic neurons and synapses: multiple fates of GABA signalling in epilepsies. Trends in

neurosciences 28:108–115.

Coyle JT, Price DL, DeLong MR (1983) Alzheimer's disease: a disorder of cortical cholinergic innervation. Science 219:1184–1190.

Csicsvari J, Hirase H, Czurko A, Mamiya A, Buzsaki G (1999) Oscillatory coupling of hippocampal pyramidal cells and interneurons in the behaving Rat. JNeurosci 19:274–287.

Czurko A, Huxter J, Li Y, Hangya B, Muller RU (2011) Theta phase classification of interneurons in the hippocampal formation of freely moving rats. JNeurosci 31:2938–2947.

Danik M, Cassoly E, Manseau F, Sotty F, Mouginot D, Williams S (2005) Frequent coexpression of the vesicular glutamate transporter 1 and 2 genes, as well as coexpression with genes for choline acetyltransferase or glutamic acid decarboxylase in neurons of rat brain. JNeurosciRes 81:506–521.

Danik M, Puma C, Quirion R, Williams S (2003) Widely expressed transcripts for chemokine receptor CXCR1 in identified glutamatergic, gamma-aminobutyric acidergic, and cholinergic neurons and astrocytes of the rat brain: a single-cell reverse transcription-multiplex polymerase chain reaction study. JNeurosciRes 74:286–295.

Davies P, Katzman R, Terry R (1980) Reduced somatostatin-like immunoreactivity in cerebral cortex from cases of Alzheimer disease and Alzheimer senile dementa. Nature 288:279–280.

Debiec J, LeDoux J (2002) Cellular and systems reconsolidation in the hippocampus. Neuron 36:527–538.

Ducharme G, Lowe GC, Goutagny R, Williams S (2012) Early alterations in hippocampal circuitry and theta rhythm generation in a mouse model of prenatal infection: implications for schizophrenia. PloS one 7:e29754.

Dumalska I, Wu M, Morozova E, Liu R, Van den PA, Alreja M (2008) Excitatory effects of the puberty-initiating peptide kisspeptin and group I metabotropic glutamate receptor agonists differentiate two distinct subpopulations of gonadotropin-releasing hormone neurons. JNeurosci 28:8003–8013.

Fazzari P, Paternain A V, Valiente M, Pla R, Luján R, Lloyd K, Lerma J, Marín O, Rico B (2010) Control of cortical GABA circuitry development by Nrg1 and ErbB4 signalling. Nature 464:1376–1380.

Fell J, Ludowig E, Staresina BP, Wagner T, Kranz T, Elger CE, Axmacher N (2011) Medial temporal theta/alpha power enhancement precedes successful memory encoding: evidence based on intracranial EEG. The Journal of neuroscience 31:5392–5397.

Fellous JM, Sejnowski TJ (2000) Cholinergic induction of oscillations in the hippocampal slice in the slow (0.5-2 Hz), theta (5-12 Hz), and gamma (35-70 Hz) bands. Hippocampus 10:187–197.

Fox S (1989) Membrane potential and impedance changes in hippocampal pyramidal cells during theta rhythm. Experimental Brain Research 77:283–294.

Fox SE, Wolfson S, Ranck Jr. JB (1986) Hippocampal theta rhythm and the firing of neurons in walking and urethane anesthetized rats. ExpBrain Res 62:495–508.

Franken P, Malafosse A, Tafti M (1998) Genetic variation in EEG activity during sleep in inbred mice. Am J Physiol Regul Integr Comp Physiol 275:R1127–R1137.

Fremeau RT, Troyer MD, Pahner I, Nygaard GO, Tran CH, Reimer RJ, Bellocchio EE, Fortin D, Storm-Mathisen J, Edwards RH, Fremeau Jr. RT (2001) The expression of vesicular glutamate transporters defines two classes of excitatory synapse. Neuron 31:247–260.

Freund TF (1989) GABAergic septohippocampal neurons contain parvalbumin. Brain Res 478:375–381.

Freund TF, Buzsáki G (1996) Interneurons of the hippocampus. Hippocampus 6:347–470.

Freund TFF, Antal M (1988) GABA-containing neurons in the septum control inhibitory interneurons in the hippocampus. Nature 336:170–173.

Frotscher M, Leranth C (1985) Cholinergic innervation of the rat hippocampus as revealed by choline acetyltransferase immunocytochemistry: a combined light and electron microscopic study. JComp Neurol 239:237–246.

Frotscher M, Soriano E, Leranth C (1992) Cholinergic and GABAergic neurotransmission in the fascia dentata: electron microscopic immunocytochemical studies in rodents and primates. Epilepsy ResSuppl 7:65–78.

Fuentealba P, Begum R, Capogna M, Jinno S, Marton LF, Csicsvari J, Thomson A, Somogyi P, Klausberger T, Márton LF (2008) Ivy cells: a population of nitric-oxide-producing, slow-spiking GABAergic neurons and their involvement in hippocampal network activity. Neuron 57:917–929.

Fukuda T, Kosaka T (2000) Gap junctions linking the dendritic network of GABAergic interneurons in the hippocampus. JNeurosci 20:1519–1528.

Gaykema RP, Luiten PG, Nyakas C, Traber J (1990) Cortical projection patterns of the medial septum-diagonal band complex. The Journal of comparative neurology 293:103–124.

Gerashchenko D, Salin-Pascual R, Shiromani PJ (2001) Effects of hypocretin-saporin injections into the medial septum on sleep and hippocampal theta. Brain Res 913:106–115.

Gillies MJ, Traub RD, LeBeau FEN, Davies CH, Gloveli T, Buhl EH, Whittington MA (2002) A model of atropine-resistant theta oscillations in rat hippocampal area CA1. The Journal of Physiology 543:779–793.

Gloveli T, Dugladze T, Saha S, Monyer H, Heinemann U, Traub RD, Whittington M a, Buhl EH (2005) Differential involvement of oriens/pyramidale interneurones in hippocampal network oscillations in vitro. JPhysiol 562:131–147.

Gogolak G, Stumpf C, Petsche H, Sterc J (1968) The firing pattern of septal neurons and the form of the hippocampal theta wave. Brain Res 7:201–207.

Goldin M, Epsztein J, Jorquera I, Represa A, Ben-Ari Y, Crépel V, Cossart R (2007) Synaptic kainate receptors tune oriens-lacunosum moleculare interneurons to operate at theta frequency. JNeurosci 27:9560–9572.

Gong S, Zheng C, Doughty ML, Losos K, Didkovsky N, Schambra UB, Nowak NJ, Joyner A, Leblanc G, Hatten ME, Heintz N (2003) A gene expression atlas of the central nervous system based on bacterial artificial chromosomes. Nature 425:917–925.

Gonzalo-Ruiz A, Morte L (2000) Localization of amino acids, neuropeptides and cholinergic markers in neurons of the septum-diagonal band complex projecting to the retrosplenial granular cortex of the rat. Brain ResBull 52:499–510.

Gorelova N, Reiner PB (1996) Role of the afterhyperpolarization in control of discharge properties of septal cholinergic neurons in vitro. JNeurophysiol 75:695–706.

Goutagny R, Jackson J, Williams S (2009) Self-generated theta oscillations in the hippocampus. Nature neuroscience 12:1491–1493.

Goutagny R, Manseau F, Jackson J, Danik M, Williams S (2008) In vitro

activation of the medial septum-diagonal band complex generates atropine-sensitive and atropine-resistant hippocampal theta rhythm: an investigation using a complete septohippocampal preparation. Hippocampus 18:531–535.

Green JD, Arduini AA (1954) Hippocampal electrical activity in arousal. JNeurophysiol 17:533–557.

Griffith WH (1988) Membrane properties of cell types within guinea pig basal forebrain nuclei in vitro. JNeurophysiol 59:1590–1612.

Griffith WH, Matthews RT (1986) Electrophysiology of AChE-positive neurons in basal forebrain slices. NeurosciLett 71:169–174.

Griguoli M, Cherubini E (2012) Regulation of hippocampal inhibitory circuits by nicotinic acetylcholine receptors. The Journal of physiology 590:655–666.

Griguoli M, Maul A, Nguyen C, Giorgetti A, Carloni P, Cherubini E (2010) Nicotine blocks the hyperpolarization-activated current Ih and severely impairs the oscillatory behavior of oriens-lacunosum moleculare interneurons. JNeurosci 30:10773–10783.

Gritti I, Henny P, Galloni F, Mainville L, Mariotti M, Jones BE (2006) Stereological estimates of the basal forebrain cell population in the rat, including neurons containing choline acetyltransferase, glutamic acid decarboxylase or phosphate-activated glutaminase and colocalizing vesicular glutamate transporters. Neuroscience 143:1051–1064.

Gritti I, Mainville L, Mancia M, Jones BE (1997) GABAergic and other noncholinergic basal forebrain neurons, together with cholinergic neurons, project to the mesocortex and isocortex in the rat. JComp Neurol 383:163–177.

Gritti I, Manns ID, Mainville L, Jones BE (2003) Parvalbumin, calbindin, or calretinin in cortically projecting and GABAergic, cholinergic, or

glutamatergic basal forebrain neurons of the rat. JComp Neurol 458:11–31.

Grouselle D, Winsky-Sommerer R, David JP, Delacourte A, Dournaud P, Epelbaum J (1998) Loss of somatostatin-like immunoreactivity in the frontal cortex of Alzheimer patients carrying the apolipoprotein epsilon 4 allele. Neuroscience letters 255:21–24.

Gulyas A, Gorcs TJ, Freund T, Görcs T (1990) Innervation of different peptide-containing neurons in the hippocampus by GABAergic septal afferents. Neuroscience 37:31–44.

Gulyas AI, Hajos N, Katona I, Freund TF (2003) Interneurons are the local targets of hippocampal inhibitory cells which project to the medial septum. EurJNeurosci 17:1861–1872.

Gulyás AI, Megías M, Emri Z, Freund TF (1999) Total number and ratio of excitatory and inhibitory synapses converging onto single interneurons of different types in the CA1 area of the rat hippocampus. The Journal of neuroscience 19:10082–10097.

Gulyás AI, Miles R, Sík A, Tóth K, Tamamaki N, Freund TF, Gulyas AI, Miles R, Sik A, Toth K, Tamamaki N, Freund TF (1993) Hippocampal pyramidal cells excite inhibitory neurons through a single release site. Nature 366:683.

Gulyás AI, Szabó GG, Ulbert I, Holderith N, Monyer H, Erdélyi F, Szabó G, Freund TF, Hájos N (2010) Parvalbumin-containing fast-spiking basket cells generate the field potential oscillations induced by cholinergic receptor activation in the hippocampus. The Journal of neuroscience 30:15134–15145.

Hagan JJ, Salamone JD, Simpson J, Iversen SD, Morris RG (1988) Place navigation in rats is impaired by lesions of medial septum and diagonal band but not nucleus basalis magnocellularis. BehavBrain Res 27:9–20.

Hajszan T, Alreja M, Leranth C (2004) Intrinsic vesicular glutamate transporter 2-immunoreactive input to septohippocampal parvalbumin-containing neurons: novel glutamatergic local circuit cells. Hippocampus 14:499–509.

Halasy K, Buhl EH, Lorinczi Z, Tamas G, Somogyi P (1996) Synaptic target selectivity and input of GABAergic basket and bistratified interneurons in the CA1 area of the rat hippocampus. Hippocampus 6:306–329.

Han X, Chow BY, Zhou H, Klapoetke NC, Chuong A, Rajimehr R, Yang A, Baratta M V, Winkle J, Desimone R, Boyden ES (2011) A high-light sensitivity optical neural silencer: development and application to optogenetic control of non-human primate cortex. Frontiers in systems neuroscience 5:18.

Harkany T, De Jong GI, Soos K, Penke B, Luiten PG, Gulya K (1995) Beta-amyloid (1-42) affects cholinergic but not parvalbumin-containing neurons in the septal complex of the rat. Brain Res 698:270–274.

Harris KD, Csicsvari J, Hirase H, Dragoi G, Buzsaki G (2003) Organization of cell assemblies in the hippocampus. Nature 424:552–556.

Harvey CD, Collman F, Dombeck DA, Tank DW (2009) Intracellular dynamics of hippocampal place cells during virtual navigation. Nature 461:941–946.

Hashimoto T, Volk DW, Eggan SM, Mirnics K, Pierri JN, Sun Z, Sampson AR, Lewis DA (2003) Gene expression deficits in a subclass of GABA neurons in the prefrontal cortex of subjects with schizophrenia. The Journal of neuroscience 23:6315–6326.

Henderson Z, Lu CB, Janzso G, Matto N, McKinley CE, Yanagawa Y, Halasy K (2010) Distribution and role of Kv3.1b in neurons in the medial septum diagonal band complex. Neuroscience 166:952–969.

Henderson Z, Morris NP, Grimwood P, Fiddler G, Yang HW, Appenteng K

(2001) Morphology of local axon collaterals of electrophysiologically characterised neurons in the rat medial septal/ diagonal band complex. JComp Neurol 430:410–432.

Henke H, Lang W (1983) Cholinergic enzymes in neocortex, hippocampus and basal forebrain of non-neurological and senile dementia of Alzheimer-type patients. Brain Res 267:281–291.

Herkenham M (1978) The connections of the nucleus reuniens thalami: Evidence for a direct thalamo-hippocampal pathway in the rat. The Journal of Comparative Neurology 177:589–609.

Hernandez SG, Colom L V, Banuelos C (2009) Glutamatergic septal axons innervate somas and proximal dendrites of CA1-CA3 hippocampal neurons. Society for Neuroscience Abstracts.

Herzog E, Bellenchi GC, Gras C, Bernard V, Ravassard P, Bedet C, Gasnier B, Giros B, El Mestikawy S (2001) The existence of a second vesicular glutamate transporter specifies subpopulations of glutamatergic neurons. JNeurosci 21:RC181.

Herzog E, Takamori S, Jahn R, Brose N, Wojcik SM (2006) Synaptic and vesicular co-localization of the glutamate transporters VGLUT1 and VGLUT2 in the mouse hippocampus. JNeurochem 99:1011–1018.

Hisano S, Hoshi K, Ikeda Y, Maruyama D, Kanemoto M, Ichijo H, Kojima I, Takeda J, Nogami H (2000) Regional expression of a gene encoding a neuron-specific Na(+)-dependent inorganic phosphate cotransporter (DNPI) in the rat forebrain. Brain Res 83:34–43.

Huerta PT, Lisman JE (1993) Heightened synaptic plasticity of hippocampal CA1 neurons during a cholinergically induced rhythmic state. Nature 364:723–725.

Huerta PT, Lisman JE (1995) Bidirectional synaptic plasticity induced by a single burst during cholinergic theta oscillation in CA1 in vitro. Neuron 15:1053–1063.

Huh CYL, Danik M, Manseau F, Trudeau L-E, Williams S (2008) Chronic exposure to nerve growth factor increases acetylcholine and glutamate release from cholinergic neurons of the rat medial septum and diagonal band of Broca via mechanisms mediated by p75NTR. The Journal of neuroscience 28:1404–1409.

Huh CYL, Goutagny R, Williams S (2010) Glutamatergic neurons of the mouse medial septum and diagonal band of Broca synaptically drive hippocampal pyramidal cells: relevance for hippocampal theta rhythm. The Journal of neuroscience 30:15951–15961.

Hölscher C, Anwyl R, Rowan MJ, Holscher C (1997) Stimulation on the positive phase of hippocampal theta rhythm induces long-term potentiation that can be depotentiated by stimulation on the negative phase in area CA1 in vivo. JNeurosci 17:6470.

Ishizuka N, Weber J, Amaral DG (1990) Organization of intrahippocampal projections originating from CA3 pyramidal cells in the rat. JComp Neurol 295:580–623.

Jackson J, Goutagny R, Williams S (2011) Fast and Slow Gamma Rhythms Are Intrinsically and Independently Generated in the Subiculum. JNeurosci 31:12104–12117.

Jansen R, Linkenkaer-Hansen K, Heistek T, Timmerman J, Mansvelder HD, Brussaard AB, De Gunst M, Van Ooyen A (2009) Inbred mouse strains differ in multiple hippocampal activity traits. The European journal of neuroscience 30:1092–1100.

Jinno S, Klausberger T, Marton LF, Dalezios Y, Roberts JD, Fuentealba P,

Bushong EA, Henze D, Buzsaki G, Somogyi P (2007) Neuronal diversity in GABAergic long-range projections from the hippocampus. JNeurosci 27:8790–8804.

Jinno S, Kosaka T (2000) Colocalization of parvalbumin and somatostatin-like immunoreactivity in the mouse hippocampus: quantitative analysis with optical dissector. The Journal of comparative neurology 428:377–388.

Jinno S, Kosaka T (2002) Immunocytochemical characterization of hippocamposeptal projecting GABAergic nonprincipal neurons in the mouse brain: a retrograde labeling study. Brain Res 945:219–231.

Jinno S, Kosaka T (2006) Cellular architecture of the mouse hippocampus: a quantitative aspect of chemically defined GABAergic neurons with stereology. Neuroscience Research 56:229–245.

Jones G, Norris S, Henderson Z (1999) Conduction velocities and membrane properties of different classes of rat septohippocampal neurons recorded in vitro. JPhysiol 517:867–877.

Kahana MJ, Sekuler R, Caplan JB, Kirschen M, Madsen JR (1999) Human theta oscillations exhibit task dependence during virtual maze navigation. Nature 399:781–784.

Katona I, Acsády L, Freund TF (1999) Postsynaptic targets of somatostatin-immunoreactive interneurons in the rat hippocampus. Neuroscience 88:37–55.

Katsumaru H, Kosaka T, Heizmann CW, Hama K (1988) Immunocytochemical study of GABAergic neurons containing the calcium-binding protein parvalbumin in the rat hippocampus. Experimental brain research 72:347–362.

Kelsey JE, Vargas H (1993) Medial septal lesions disrupt spatial, but not

nonspatial, working memory in rats. BehavNeurosci 107:565–574.

Kentros C, Hargreaves E, Hawkins RD, Kandel ER, Shapiro M, Muller R V (1998) Abolition of long-term stability of new hippocampal place cell maps by NMDA receptor blockade. Science 280:2121–2126.

Kim J, Fanselow MS (1992) Modality-specific retrograde amnesia of fear. Science 256:675–677.

Kimura H, McGeer P, Peng F, McGeer EG (1980) Choline acetyltransferase-containing neurons in rodent brain demonstrated by immunohistochemistry. Science 208:1057–1059.

Kispersky TJ, Fernandez FR, Economo MN, White JA (2012) Spike Resonance Properties in Hippocampal O-LM Cells Are Dependent on Refractory Dynamics. Journal of Neuroscience 32:3637–3651.

Kiss J, Csaki A, Bokor H, Kocsis K, Kocsis B (2002) Possible glutamatergic/aspartatergic projections to the supramammillary nucleus and their origins in the rat studied by selective [(3)H]D-aspartate labelling and immunocytochemistry. Neuroscience 111:671–691.

Kiss J, Magloczky Z, Somogyi J, Freund TF (1997) Distribution of calretinin-containing neurons relative to other neurochemically identified cell types in the medial septum of the rat. Neuroscience 78:399–410.

Klausberger T, Magill PJ, Marton LF, Roberts JD, Cobden PM, Buzsaki G, Somogyi P (2003) Brain-state- and cell-type-specific firing of hippocampal interneurons in vivo. Nature 421:844–848.

Klausberger T, Marton LF, Baude A, Roberts JD, Magill PJ, Somogyi P (2004) Spike timing of dendrite-targeting bistratified cells during hippocampal network oscillations in vivo. NatNeurosci 7:41–47.

Klausberger T, Somogyi P (2008) Neuronal diversity and temporal dynamics: the unity of hippocampal circuit operations. Science 321:53–57.

Knapp JA, Morris NP, Henderson Z, Matthews RT (2000) Electrophysiological characteristics of non-bursting, glutamate decarboxylase messenger RNA-positive neurons of the medial septum/diagonal band nuclei of guinea-pig and rat. Neuroscience 98:661–668.

Kocsis B, Li S (2004) In vivo contribution of h-channels in the septal pacemaker to theta rhythm generation. EurJNeurosci 20:2149–2158.

Kocsis B, Vertes RP (1994) Characterization of neurons of the supramammillary nucleus and mammillary body that discharge rhythmically with the hippocampal theta rhythm in the rat. JNeurosci 14:7040–7052.

Koenig J, Linder AN, Leutgeb JK, Leutgeb S (2011) The spatial periodicity of grid cells is not sustained during reduced theta oscillations. Science 332:592–595.

Kogo N, Dalezios Y, Capogna M, Ferraguti F, Shigemoto R, Somogyi P (2004) Depression of GABAergic input to identified hippocampal neurons by group III metabotropic glutamate receptors in the rat. EurJNeurosci 19:2727–2740.

Konopacki J, Bland BH, Roth SH (1988) The development of carbachol-induced EEG “theta” examined in hippocampal formation slices. Brain Res 466:229–232.

Konopacki J, MacIver MB, Bland BH, Roth SH (1987) Carbachol-induced EEG “theta” activity in hippocampal brain slices. Brain Res 405:196–198.

Kramis R, Vanderwolf CH, Bland BH (1975) Two types of hippocampal rhythmical slow activity in both the rabbit and the rat: relations to behavior and effects of atropine, diethyl ether, urethane, and pentobarbital. ExpNeurol 49:58–85.

Kulik A, Vida I, Luján R, Haas C a, López-Bendito G, Shigemoto R, Frotscher M (2003) Subcellular localization of metabotropic GABA(B) receptor subunits GABA(B1a/b) and GABA(B2) in the rat hippocampus. The Journal of neuroscience 23:11026–11035.

Lacaille JC, Williams S (1990) Membrane properties of interneurons in stratum oriens-alveus of the CA1 region of rat hippocampus in vitro. Neuroscience 36:349–359.

Lasztoczi B, Tukker JJ, Somogyi P, Klausberger T (2011) Terminal Field and Firing Selectivity of Cholecystokinin-Expressing Interneurons in the Hippocampal CA3 Area. Journal of Neuroscience 31:18073–18093.

Lee MG, Chrobak JJ, Sik A, Wiley RG, Buzsaki G (1994) Hippocampal theta activity following selective lesion of the septal cholinergic system. Neuroscience 62:1033–1047.

Leranth C, Frotscher M (1989) Organization of the septal region in the rat brain: cholinergic-GABAergic interconnections and the termination of hippocampo-septal fibers. JComp Neurol 289:304–314.

Leranth C, Kiss J (1996) A population of supramammillary area calretinin neurons terminating on medial septal area cholinergic and lateral septal area calbindin-containing cells are aspartate/glutamatergic. JNeurosci 16:7699–7710.

Leung LS, Shen B (2004) Glutamatergic synaptic transmission participates in generating the hippocampal EEG. Hippocampus 14:510–525.

Leung LW, Yim CY (1991) Intrinsic membrane potential oscillations in hippocampal neurons in vitro. Brain research 553:261–274.

Leutgeb S, Mizumori SJ (1999) Excitotoxic septal lesions result in spatial memory deficits and altered flexibility of hippocampal single-unit

representations. The Journal of neuroscience 19:6661–6672.

Li K-X, Lu Y-M, Xu Z-H, Zhang J, Zhu J-M, Zhang J-M, Cao S-X, Chen X-J, Chen Z, Luo J-H, Duan S, Li X-M (2011) Neuregulin 1 regulates excitability of fast-spiking neurons through Kv1.1 and acts in epilepsy. Nature Neuroscience 15:267–273.

Lin W, McKinney K, Liu L, Lakhlani S, Jennes L (2003) Distribution of vesicular glutamate transporter-2 messenger ribonucleic Acid and protein in the septum-hypothalamus of the rat. Endocrinology 144:662–670.

Linke R, Pabst T, Frotscher M (1995) Development of the hippocamposeptal projection in the rat. JComp Neurol 351:602–616.

Losonczy A, Zhang L, Shigemoto R, Somogyi P, Nusser Z (2002) Cell type dependence and variability in the short-term plasticity of EPSCs in identified mouse hippocampal interneurones. The Journal of Physiology 542:193–210.

Lovett-Barron M, Turi GF, Kaifosh P, Lee PH, Bolze F, Sun X-H, Nicoud J-F, Zemelman B V, Sternson SM, Losonczy A (2012) Regulation of neuronal input transformations by tunable dendritic inhibition. Nature Neuroscience 15:423–430.

Lupica C, Bell J, Hoffman A, Watson P (2001) Contribution of the hyperpolarization-activated current (Ih) to membrane potential and GABA release in hippocampal interneurons. Journal of Neurophysiology 86:261–268.

Maccaferri G (2005) Stratum oriens horizontal interneurone diversity and hippocampal network dynamics. JPhysiol 562:73–80.

Maccaferri G, McBain CJ (1995) Passive propagation of LTD to stratum oriens-alveus inhibitory neurons modulates the temporoammonic input to the hippocampal CA1 region. Neuron 15:137–145.

Maccaferri G, McBain CJ (1996a) Long-term potentiation in distinct subtypes of hippocampal nonpyramidal neurons. JNeurosci 16:5334–5343.

Maccaferri G, McBain CJ (1996b) The hyperpolarization-activated current (Ih) and its contribution to pacemaker activity in rat CA1 hippocampal stratum oriens-alveus interneurones. JPhysiol 497:119–130.

MacVicar BA, Tse FW (1989) Local neuronal circuitry underlying cholinergic rhythmical slow activity in CA3 area of rat hippocampal slices. JPhysiol 417:197–212.

Magloczky Z, Freund TF (2005) Impaired and repaired inhibitory circuits in the epileptic human hippocampus. Trends in neurosciences 28:334–340.

Maglóczky Z, Acsády L, Freund TF (1994) Principal cells are the postsynaptic targets of supramammillary afferents in the hippocampus of the rat. Hippocampus 4:322–334.

Manns ID, Alonso A, Jones BE (2003) Rhythmically discharging basal forebrain units comprise cholinergic, GABAergic, and putative glutamatergic cells. JNeurophysiol 89:1057–1066.

Manns ID, Mainville L, Jones BE (2001) Evidence for glutamate, in addition to acetylcholine and GABA, neurotransmitter synthesis in basal forebrain neurons projecting to the entorhinal cortex. Neuroscience 107:249–263.

Manseau F, Danik M, Williams S (2005) A functional glutamatergic neurone network in the medial septum and diagonal band area. JPhysiol 566:865–884.

Manseau F, Goutagny R, Danik M, Williams S (2008) The hippocamposeptal pathway generates rhythmic firing of GABAergic neurons in the medial septum and diagonal bands: an investigation using a complete septohippocampal preparation in vitro. JNeurosci 28:4096–4107.

Markram H, Segal M (1990) Electrophysiological characteristics of cholinergic and non-cholinergic neurons in the rat medial septum-diagonal band complex. Brain Res 513:171–174.

McAlonan GM, Dawson GR, Wilkinson LO, Robbins TW, Everitt BJ (1995) The effects of AMPA-induced lesions of the medial septum and vertical limb nucleus of the diagonal band of Broca on spatial delayed non-matching to sample and spatial learning in the water maze. EurJNeurosci 7:1034–1049.

McGeer PL, McGeer EG, Suzuki J, Dolman CE, Nagai T (1984) Aging, Alzheimer's disease, and the cholinergic system of the basal forebrain. Neurology 34:741–745.

McHugh TJ, Blum KI, Tsien JZ, Tonegawa S, Wilson MA (1996) Impaired hippocampal representation of space in CA1-specific NMDAR1 knockout mice. Cell 87:1339–1349.

Megías M, Emri Z, Freund TF, Gulyás AI (2001) Total number and distribution of inhibitory and excitatory synapses on hippocampal CA1 pyramidal cells. Neuroscience 102:527–540.

Meibach RC, Siegel A (1977) Efferent connections of the septal area in the rat: an analysis utilizing retrograde and anterograde transport methods. Brain Res 119:1–20.

Mesulam MM, Mufson EJ, Wainer BH, Levey AI (1983) Central cholinergic pathways in the rat: an overview based on an alternative nomenclature (Ch1-Ch6). Neuroscience 10:1185–1201.

Meyer AH, Katona I, Blatow M, Rozov A, Monyer H (2002) In vivo labeling of parvalbumin-positive interneurons and analysis of electrical coupling in identified neurons. The Journal of neuroscience 22:7055–7064.

Miles R, Tóth K, Gulyás AI, Hájos N, Freund TF (1996) Differences between

somatic and dendritic inhibition in the hippocampus. Neuron 16:815–823.

Milner B, Corkin S, Teuber H-L (1968) Further analysis of the hippocampal amnesic syndrome: 14-year follow-up study of H.M. Neuropsychologia 6:215–234.

Mitchell S, Rawlins J, Steward O, Olton DS (1982) Medial septal area lesions disrupt theta rhythm and cholinergic staining in medial entorhinal cortex and produce impaired radial arm maze behavior in rats. JNeurosci 2:292–302.

Mitra P, Bokil H (2008) Observed brain dynamics. New York: Oxford university press.

Mizumori SJ, McNaughton BL, Barnes CA, Fox KB (1989) Preserved spatial coding in hippocampal CA1 pyramidal cells during reversible suppression of CA3c output: evidence for pattern completion in hippocampus. JNeurosci 9:3915–3928.

Montez T, Poil S-S, Jones BF, Manshanden I, Verbunt JPA, Van Dijk BW, Brussaard AB, Van Ooyen A, Stam CJ, Scheltens P, Linkenkaer-Hansen K (2009) Altered temporal correlations in parietal alpha and prefrontal theta oscillations in early-stage Alzheimer disease. Proceedings of the National Academy of Sciences of the United States of America 106:1614–1619.

Moore RY, Halaris AE, Jones BE (1978) Serotonin neurons of the midbrain raphe: ascending projections. The Journal of comparative neurology 180:417–438.

Morin F, Beaulieu C, Lacaille J (1996) Membrane properties and synaptic currents evoked in CA1 interneuron subtypes in rat hippocampal slices. Journal of neurophysiology 76:1–16.

Moriyama Y, Yamamoto A (2004) Glutamatergic chemical transmission: look! Here, there, and anywhere. JBiochem(Tokyo) 135:155–163.

Morris NP, Fyffe RE, Robertson B (2004) Characterisation of hyperpolarization-activated currents (I(h)) in the medial septum/diagonal band complex in the mouse. Brain Res 1006:74–86.

Morris NP, Harris SJ, Henderson Z (1999) Parvalbumin-immunoreactive, fast-spiking neurons in the medial septum/diagonal band complex of the rat: intracellular recordings in vitro. Neuroscience 92:589–600.

Morris R (1989) Synaptic plasticity and learning: selective impairment of learning rats and blockade of long-term potentiation in vivo by the N-methyl-D-aspartate receptor antagonist AP5. J Neurosci 9:3040–3057.

Morris RG, Garrud P, Rawlins JN, O'Keefe J (1982) Place navigation impaired in rats with hippocampal lesions. Nature 297:681–683.

Muller RU, Kubie JL (1987) The effects of changes in the environment on the spatial firing of hippocampal complex-spike cells. The Journal of Neuroscience 7:1951–1968.

Mátyás F, Freund TF, Gulyás AI (2004) Immunocytochemically defined interneuron populations in the hippocampus of mouse strains used in transgenic technology. Hippocampus 14:460–481.

Naber PA, Witter MP, Lopes da Silva FH (2001) Evidence for a direct projection from the postrhinal cortex to the subiculum in the rat. Hippocampus 11:105–117.

Nakazawa K, Sun LD, Quirk MC, Rondi-Reig L, Wilson MA, Tonegawa S (2003) Hippocampal CA3 NMDA receptors are crucial for memory acquisition of one-time experience. Neuron 38:305–315.

Nissen W, Szabo A, Somogyi J, Somogyi P, Lamsa KP (2010) Cell type-specific long-term plasticity at glutamatergic synapses onto hippocampal interneurons expressing either parvalbumin or CB1 cannabinoid receptor.

JNeurosci 30:1337–1347.

Nitsch R, Leranth C (1996) GABAergic neurons in the rat dentate gyrus are innervated by subcortical calretinin-containing afferents. JComp Neurol 364:425–438.

Oliva Jr AA, Jiang M, Lam T, Smith KL, Swann JW (2000) Novel hippocampal interneuronal subtypes identified using transgenic mice that express green fluorescent protein in GABAergic interneurons. JNeurosci 20:3354–3368.

Onteniente B, Geffard M, Campistron G, Calas A (1987) An ultrastructural study of GABA-immunoreactive neurons and terminals in the septum of the rat. JNeurosci 7:48–54.

O'Keefe J, Dostrovsky J (1971) The hippocampus as a spatial map. Preliminary evidence from unit activity in the freely-moving rat. Brain Res 34:171–175.

O'Keefe J, Recce ML (1993) Phase relationship between hippocampal place units and the EEG theta rhythm. Hippocampus 3:317–330.

Palop JJ, Chin J, Roberson ED, Wang J, Thwin MT, Bien-Ly N, Yoo J, Ho KO, Yu G-Q, Kreitzer A, Finkbeiner S, Noebels JL, Mucke L (2007) Aberrant excitatory neuronal activity and compensatory remodeling of inhibitory hippocampal circuits in mouse models of Alzheimer's disease. Neuron 55:697–711.

Panula P, Revuelta A V, Cheney DL, Wu JY, Costa E (1984) An immunohistochemical study on the location of GABAergic neurons in rat septum. JComp Neurol 222:69–80.

Pawelzik H, Hughes DI, Thomson AM (2002) Physiological and morphological diversity of immunocytochemically defined parvalbumin- and cholecystokinin-positive interneurones in CA1 of the adult rat hippocampus. JComp Neurol 443:346–367.

Perez-Cruz C, Nolte MW, Van Gaalen MM, Rustay NR, Termont A, Tanghe A, Kirchhoff F, Ebert U (2011) Reduced spine density in specific regions of CA1 pyramidal neurons in two transgenic mouse models of Alzheimer's disease. The Journal of neuroscience 31:3926–3934.

Perry EKK, Gibson PHH, Blessed G, Perry RHH, Tomlinson BEE (1977) Neurotransmitter enzyme abnormalities in senile dementia: Choline acetyltransferase and glutamic acid decarboxylase activities in necropsy brain tissue. Journal of the neurological sciences 34:247–265.

Petsche H, Stumpf C, Gogolak G (1962) The significance of the rabbit's septum as a relay station between the midbrain and the hippocampus. I. The control of hippocampus arousal activity by the septum cells. Electroencephalogr Clin Neurophysiol 14:202–211.

Pikkarainen M, Rönkkö S, Savander V, Insausti R, Pitkänen A (1999) Projections from the lateral, basal, and accessory basal nuclei of the amygdala to the hippocampal formation in rat. The Journal of Comparative Neurology 403:229–260.

Qin P, Xu H, Laursen TM, Vestergaard M, Mortensen PB (2005) Risk for schizophrenia and schizophrenia-like psychosis among patients with epilepsy: population based cohort study. BMJ (Clinical research ed) 331:1–6.

Rawlins JN, Feldon J, Gray JA (1979) Septo-hippocampal connections and the hippocampal theta rhythm. ExpBrain Res 37:49–63.

Rocamora N, Pascual M, Acsady L, De Lecea L, Freund TF, Soriano E (1996) Expression of NGF and NT3 mRNAs in hippocampal interneurons innervated by the GABAergic septohippocampal pathway. JNeurosci 16:3991–4004.

Rotenberg A, Mayford M, Hawkins RD, Kandel ER, Muller RU (1996) Mice expressing activated CaMKII lack low frequency LTP and do not form stable

place cells in the CA1 region of the hippocampus. Cell 87:1351–1361.

Royer S, Sirota A, Patel J, Buzsaki G (2010) Distinct representations and theta dynamics in dorsal and ventral hippocampus. JNeurosci 30:1777–1787.

Royer S, Zemelman B V, Losonczy A, Kim J, Chance F, Magee JC, Buzsáki G (2012) Control of timing, rate and bursts of hippocampal place cells by dendritic and somatic inhibition. Nature Neuroscience 15:769–775.

Rudy B, McBain CJ (2001) Kv3 channels: voltage-gated K+ channels designed for high-frequency repetitive firing. Trends Neurosci 24:517–526.

Rutishauser U, Ross IB, Mamelak AN, Schuman EM (2010) Human memory strength is predicted by theta-frequency phase-locking of single neurons. Nature 464:903–907.

Scoville WB, Milner B (1957) Loss of Recent Memory After Bilateral Hippocampal Lesions. Journal of Neurology, Neurosurgery & Psychiatry 20:11–21.

Segal M (1986) Properties of rat medial septal neurones recorded in vitro. The Journal of Physiology 379:309–330.

Sik A, Penttonen M, Ylinen A, Buzsáki G (1995) Hippocampal CA1 interneurons: an in vivo intracellular labeling study. JNeurosci 15:6651–6665.

Simon AP, Poindessous-Jazat F, Dutar P, Epelbaum J, Bassant MH (2006) Firing properties of anatomically identified neurons in the medial septum of anesthetized and unanesthetized restrained rats. JNeurosci 26:9038–9046.

Skaggs WE, McNaughton BL, Wilson MA, Barnes CA (1996) Theta phase precession in hippocampal neuronal populations and the compression of temporal sequences. Hippocampus 6:149–172.

Somogyi P, Klausberger T (2005) Defined types of cortical interneurone structure space and spike timing in the hippocampus. JPhysiol 562:9–26.

Sotty F, Danik M, Manseau F, Laplante F, Quirion R, Williams S (2003) Distinct electrophysiological properties of glutamatergic, cholinergic and GABAergic rat septohippocampal neurons: novel implications for hippocampal rhythmicity. The Journal of physiology 551:927–943.

Squire LR, Alvarez P (1995) Retrograde amnesia and memory consolidation: a neurobiological perspective. Current opinion in neurobiology 5:169–177.

Steward O, Scoville SA (1976) Cells of origin of entorhinal cortical afferents to the hippocampus and fascia dentata of the rat. The Journal of Comparative Neurology 169:347–370.

Stewart M, Fox SE (1989) Two populations of rhythmically bursting neurons in rat medial septum are revealed by atropine. JNeurophysiol 61:982–993.

Stewart M, Fox SE (1990) Do septal neurons pace the hippocampal theta rhythm? Trends Neurosci 13:163–168.

Van Strien NM, Cappaert NLM, Witter MP (2009) The anatomy of memory: an interactive overview of the parahippocampal-hippocampal network. NatRevNeurosci 10:272–282.

Swanson L, Cowan W (1975) Hippocampo-hypothalamic connections: origin in subicular cortex, not ammon's horn. Science 189:303–304.

Swanson L, Sawchenko P, Cowan W (1981) Evidence for collateral projections by neurons in Ammon's horn, the dentate gyrus, and the subiculum: a multiple retrograde labeling study in the rat. JNeurosci 1:548.

Swanson LW, Cowan WM (1977) An autoradiographic study of the organization of the efferent connections of the hippocampal formation in the rat. JComp

Neurol 172:49–84.

Swanson LW, Cowan WM (1979) The connections of the septal region in the rat. The Journal of comparative neurology 186:621–655.

Szabo A, Somogyi J, Cauli B, Lambolez B, Somogyi P, Lamsa KP (2012) Calcium-Permeable AMPA Receptors Provide a Common Mechanism for LTP in Glutamatergic Synapses of Distinct Hippocampal Interneuron Types. Journal of Neuroscience 32:6511–6516.

Takamori S, Rhee JSS, Rosenmund C, Jahn R (2000) Identification of a vesicular glutamate transporter that defines a glutamatergic phenotype in neurons. Nature 407:189–194.

Takács VT, Klausberger T, Somogyi P, Freund TF, Gulyás AI (2012) Extrinsic and local glutamatergic inputs of the rat hippocampal CA1 area differentially innervate pyramidal cells and interneurons. Hippocampus 22:1379–1391.

Tan G-H, Liu Y-Y, Hu X-L, Yin D-M, Mei L, Xiong Z-Q (2011) Neuregulin 1 represses limbic epileptogenesis through ErbB4 in parvalbumin-expressing interneurons. Nature Neuroscience 15:258–266.

Taniguchi H, He M, Wu P, Kim S, Paik R, Sugino K, Kvitsani D, Fu Y, Lu J, Lin Y, Miyoshi G, Shima Y, Fishell G, Nelson SB, Huang ZJ (2011) A Resource of Cre Driver Lines for Genetic Targeting of GABAergic Neurons in Cerebral Cortex. Neuron 71:995–1013.

Tesche CD, Karhu J (2000) Theta oscillations index human hippocampal activation during a working memory task. ProcNatlAcadSciUSA 97:919–924.

Thompson LT, Best PJ (1990) Long-term stability of the place-field activity of single units recorded from the dorsal hippocampus of freely behaving rats. Brain Res 509:299–308.

Toth K, Borhegyi Z, Freund TF (1993) Postsynaptic targets of GABAergic hippocampal neurons in the medial septum-diagonal band of broca complex. JNeurosci 13:3712–3724.

Truccolo W, Donoghue JA, Hochberg LR, Eskandar EN, Madsen JR, Anderson WS, Brown EN, Halgren E, Cash SS (2011) Single-neuron dynamics in human focal epilepsy. Nature neuroscience 14:635–641.

Tuszynski MH, Thal L, Pay M, Salmon DP, HS U, Bakay R, Patel P, Blesch A, Vahlsing HL, Ho G, Tong G, Potkin SG, Fallon J, Hansen L, Mufson EJ, Kordower JH, Gall C, Conner J (2005) A phase 1 clinical trial of nerve growth factor gene therapy for Alzheimer disease. NatMed 11:551–555.

Tóth K, Freund TF (1992) Calbindin D28k-containing nonpyramidal cells in the rat hippocampus: their immunoreactivity for GABA and projection to the medial septum. Neuroscience 49:793–805.

Tóth K, Freund TF, Miles R (1997) Disinhibition of rat hippocampal pyramidal cells by GABAergic afferents from the septum. JPhysiol 500:463–474.

Uhlhaas PJ, Singer W (2010) Abnormal neural oscillations and synchrony in schizophrenia. Nature reviews Neuroscience 11:100–113.

Vanderwolf CH (1969) Hippocampal electrical activity and voluntary movement in the rat. ElectroencephalogrClinNeurophysiol 26:407–418.

Vepsalainen S, Helisalmi S, Koivisto AM, Tapaninen T, Hiltunen M, Soininen H (2007) Somatostatin genetic variants modify the risk for Alzheimer's disease among Finnish patients. Journal of neurology 254:1504–1508.

Verret L, Mann EO, Hang GB, Barth AMI, Cobos I, Ho K, Devidze N, Masliah E, Kreitzer AC, Mody I, Mucke L, Palop JJ (2012) Inhibitory Interneuron Deficit Links Altered Network Activity and Cognitive Dysfunction in Alzheimer Model. Cell 149:708–721.

Vertes RP (1992) PHA-L analysis of projections from the supramammillary nucleus in the rat. JComp Neurol 326:595–622.

Vertes RP, Crane AM, Colom L V, Bland BH (1995) Ascending projections of the posterior nucleus of the hypothalamus: PHA-L analysis in the rat. JComp Neurol 359:90–116.

Ward LM (2003) Synchronous neural oscillations and cognitive processes. Trends in Cognitive Sciences 7:553–559.

Whitehouse PJ (1998) The cholinergic deficit in Alzheimer's disease. JClinPsychiatry 59 Suppl 13:19–22.

Widmer H, Ferrigan L, Davies CH, Cobb SR (2006) Evoked slow muscarinic acetylcholinergic synaptic potentials in rat hippocampal interneurons. Hippocampus 16:617–628.

Winocur G, Moscovitch M, Bontempi B (2010) Memory formation and long-term retention in humans and animals: convergence towards a transformation account of hippocampal-neocortical interactions. Neuropsychologia 48:2339–2356.

Winson J (1978) Loss of hippocampal theta rhythm results in spatial memory deficit in the rat. Science 201:160.

Witter M, Wouterlood F, Naber P, Van Haeften T (2006) Anatomical Organization of the Parahippocampal-Hippocampal Network. Annals of the New York Academy of Sciences 911:1–24.

Woo TU, Whitehead RE, Melchitzky DS, Lewis DA (1998) A subclass of prefrontal gamma-aminobutyric acid axon terminals are selectively altered in schizophrenia. Proceedings of the National Academy of Sciences of the United States of America 95:5341–5346.

Woodson W, Nitecka L, Ben-Ari Y (1989) Organization of the GABAergic system in the rat hippocampal formation: a quantitative immunocytochemical study. The Journal of comparative neurology 280:254–271.

Wu C, Shen H, Luk WP, Zhang L (2002) A fundamental oscillatory state of isolated rodent hippocampus. The Journal of Physiology 540:509–527.

Wu M, Hajszan T, Leranth C, Alreja M (2003) Nicotine recruits a local glutamatergic circuit to excite septohippocampal GABAergic neurons. EurJNeurosci 18:1155–1168.

Wyss JM, Swanson LW, Cowan WM (1979) A study of subcortical afferents to the hippocampal formation in the rat. Neuroscience 4:463–476.

Yamaguchi Y, Kawashima S (2001) Effects of amyloid-beta-(25-35) on passive avoidance, radial-arm maze learning and choline acetyltransferase activity in the rat. EurJPharmacol 412:265–272.

Yang L, Wang Z, Wang B, Justice NJ, Zheng H (2009) Amyloid precursor protein regulates Cav1.2 L-type calcium channel levels and function to influence GABAergic short-term plasticity. The Journal of neuroscience 29:15660–15668.

Yanovsky Y, Sergeeva OA, Freund TF, Haas HL (1997) Activation of interneurons at the stratum oriens/alveus border suppresses excitatory transmission to apical dendrites in the CA1 area of the mouse hippocampus. Neuroscience 77:87–96.

Yau H-J, Wang H-F, Lai C, Liu F-C (2003) Neural development of the neuregulin receptor ErbB4 in the cerebral cortex and the hippocampus: preferential expression by interneurons tangentially migrating from the ganglionic eminences. Cerebral cortex 13:252–264.

Ylinen A, Soltesz I, Bragin A, Penttonen M, Sik A, Buzsaki G (1995) Intracellular correlates of hippocampal theta rhythm in identified pyramidal cells, granule cells, and basket cells. Hippocampus 5:78–90.

Yoder RM, Pang KC (2005) Involvement of GABAergic and cholinergic medial septal neurons in hippocampal theta rhythm. Hippocampus 15:381–392.

Zemankovics R, Kali S, Paulsen O, Freund TF, Hajos N (2010) Differences in subthreshold resonance of hippocampal pyramidal cells and interneurons: the role of h-current and passive membrane characteristics. JPhysiol 588:2109–2132.

Zhang H, Lin SC, Nicolelis MA (2010) Spatiotemporal coupling between hippocampal acetylcholine release and theta oscillations in vivo. JNeurosci 30:13431–13440.

Zhang ZJ, Reynolds GP (2002) A selective decrease in the relative density of parvalbumin-immunoreactive neurons in the hippocampus in schizophrenia. Schizophrenia research 55:1–10.

Zola-Morgan S, Squire L (1990) The primate hippocampal formation: evidence for a time-limited role in memory storage. Science 250:288–290.

Zola-Morgan S, Squire LR, Amaral DG (1989) Lesions of the amygdala that spare adjacent cortical regions do not impair memory or exacerbate the impairment following lesions of the hippocampal formation. Journal of neuroscience 9:1922–1936.